2017

Effects of nanoparticles on the properties of cement-based materials

Xin Wang
Iowa State University

Effects of nanoparticles on the properties of cement-based materials

by

Xin Wang

A dissertation submitted to the graduate faculty

in partial fulfillment of the requirements for the degree of

DOCTOR OF PHILOSOPHY

Major: Civil Engineering (Civil Engineering Materials)

Program of Study Committee:
Kejin Wang, Major Professor
Fatih Bektas
Say Kee Ong
Emily Smith
Christopher R. Williams

The student author, whose presentation of the scholarship herein was approved by the program of study committee, is solely responsible for the content of this dissertation. The Graduate College will ensure this dissertation is globally accessible and will not permit alterations after a degree is conferred.

Iowa State University

Ames, Iowa

2017

DEDICATION

To my parents …

TABLE OF CONTENTS

LIST OF FIGURES

LIST OF TABLES

NOMENCLATURE

Abbreviations	Definition
Cement notation	
C	Calcium Oxide CaO
S	Silicon dioxide SiO_2
A	Aluminium oxide Al_2O_3
F	Iron oxide Fe_2O_3
H	Water H_2O
$	Sulfate SO_3
Cement phase	
C_3S	Tricalcium silicate
C_2S	Dicalcium silicate
C_3A	Tricalcium aluminate
C_4AF	Tetracalcium aluminoferrite
CH	Portlandite or Calcium hydroxide
C-S-H	Calcium silicate hydrate
AFt	Ettringite
AFm	Monosulfo/carboaluminate
Ms	Monosulfaluminate
Hc	Hemicarboaluminate
OPC or PC	Ordinary Portland Cement
SCM	Supplementary Cementitious Materials
FA	Fly Ash
MK	Metakaolin
α or doH	degree of hydration
w/c	water-to-cement ratio
w/cm	water-to-cementitous materials ratio
Methods	
XRD	X-Ray Diffraction
TGA	Thermogravimetry Analysis
NAD	Nitrogen Adsorption/Desorption
SEM	Scanning Electron Microscopy
Concrete	
SCC	Self-Consolidating Concrete
SFSCC	Semi-Flowable Self-Consolidating Concrete

ACKNOWLEDGEMENTS

This work would not be completed without the help of many people. I would like to express my deepest gratitude to my major professor, Dr. Wang, for her guidance and encouragement as I progressed. I am truly thankful for her patience and all the efforts she investigated to help me through the hard time. I would like to thank all my committee members, Dr. Ong, Dr. Williams, Dr. Bektas and Dr. Smith, for their helpful suggestions on this work.

I would also like to thank Robert Steffes, lab manager of the Portland cement Concrete Research Laboratory, for his technical support on my research and his friendship.

I am deeply grateful to all personnel at MARL, especially to Dr. Warren Straszheim, Dr. Scott Schlorholtz, and Dr. Jerry Amenson (retired April 2015), for helping me with samples' preparation and testing.

To my fellow research group members, thank you very much for your help with my research and most of all your friendship.

Last but not least, I would like to thank my parents, Tan Wang and Qizhi Bian, for their encouragement, patience, support and unconditional love as I pursue my degree in the United States. This dissertation is dedicated to them.

ABSTRACT

The addition of small amounts of nanoparticles can alter hydration and microstructure evolution of cement-based materials. The present study aimed at investigating the effects of nanoparticles on the properties of cement-based materials. The nanomaterials studied include nano-limestone, nano-silica, and nano-clay particles, and the cementitious materials studied are combinations of ordinary Portland cement (OPC), fly ash (FA) and metakaolin (MK).

Isothermal calorimetry and chemical shrinkage measurements were performed to follow the kinetics of hydration. Set times of the pastes were measured according to ASTM C191. Rheological behavior of cement pastes was characterized using a rotational rheometer. Thermogravimetric analysis (TGA), X-ray diffraction (XRD), and Nitrogen adsorption (NAD) were conducted to analyze the microstructural characteristics of the studied cement pastes. Stepwise drying-shrinkage tests were performed on thin disc paste samples (with a diameter of 25 mm and thickness of 0.80 mm). The disc samples were dried from the saturated condition (100% RH) to 30% RH and then re-saturated to 100% RH. Properties of fresh concrete mixtures, such as air content, slump flow, and J-ring flow, were tested. Properties of hardened concretes, including compressive strength, rapid chloride permeability, freezing-thawing resistance, and free drying shrinkage, were examined.

The experimental results indicate that the addition of nanoparticles, regardless the types, accelerated cement early hydration (the first 24 h), i.e., the maximum heat flow increased while the time to reach silicate and aluminate reaction peaks decreased, and reduced initial and final set times of cement pastes.

Addition of these nanomaterials generally increased yield stress and viscosity of the cement paste, especially after 60 min when cement hydration began to accelerate. Nano-clay greatly

affected the rheological behavior of cement pastes. Significantly higher shear stresses were required to initiate the flow.

Thermogravimetric analysis (TGA) results indicate the continuous hydration enhancing effects of nanomaterials up to 28 days. When 1% nanomaterials were added to the cement or cement-fly ash paste, the amounts of both calcium hydroxide and total chemically bound water contents increased at 3 days, indicating that the nanomaterials accelerated cement hydration. At 7 and 28 days, nanomaterial addition increased the amount of total chemically bound water content while tended to decrease the calcium hydroxide content, suggesting that calcium hydroxide reacted to formed hydration product. The reaction of calcium hydroxide to form C-S-H when nano-silica was added was more profound in the cement-fly ash pastes. XRD and TGA results indicated that a new hydration product, calcium hemicarboaluminate hydrate (Hc), was formed in the nano-limestone modified cement and cement-fly ash pastes. For the cement pastes, nanomaterial addition increased chemical shrinkage values, which confirmed the hydration acceleration effects of the nanomaterials. However, for the cement-fly ash blended paste, only nano-silica addition increased chemical shrinkage of the paste at all ages tested. At 28 days, the nano-limestone and nano-clay additions actually reduced chemical shrinkage value of the paste. This may imply that in these pastes, the permeation of water was inhibited, suggesting more research on the permeability and transport properties.

Regardless the types of nanomaterials, 1% nanomaterial addition improve the compressive strength of both cement and cement-fly ash pastes at all ages studied (up to 28 days). Among three nanomaterials studied, NS appeared to be the most effective one in the strength development, possibly due to its smallest particle size and highest reactivity.

The results indicate that additions of the nanomaterials increased the specific surface area and the amount of gel pores (2-10 nm) in the early age (7 days) cement pastes. At 28 days, the addition of nano-silica continued to increase the specific surface area and the volume of gel pores, especially in the fly ash blended paste. However, the addition of nano-limestone reduced the specific surface area and the total amount of pores (2-100 nm) at 28 days, especially in the Portland cement paste. An additional signature pore peak located around 18 nm was observed in the nano-silica modified and 28-days fly ash blended pastes. The addition of nano-silica generally increased the total shrinkage of cement pastes. However, the addition of nano-limestone sometimes reduced drying shrinkage, especially for the later age cement pastes. The shrinkage in each relative humidity range was found to be dependent on the volume of pores evaporate in the corresponding RH range and the resistance of the paste to deformation, especially at 7 days. Nanomaterial additions and extended curing increased reversible drying shrinkage, which suggests that the volume of gel (2-10 nm) pores appeared more closely related to reversible shrinkages. The 7-day OPCFA pastes were more prone to irreversible drying shrinkage, especially with the addition of nanomaterials.

Nano-limestone was applied to modify the fresh and hardened properties of self-consolidating concrete (SCC) and semi-flowable self-consolidating concrete (SFSCC). The results indicated that the addition nano-limestone further increased concrete strength and freezing-thawing resistance and reduced concrete permeability.

CHAPTER 1. GENERAL INTRODUCTION

1.1 Background

The development of modern cement and concrete industry calls for the improvement of the durability. Many approaches have been investigated to improve the durability properties of concrete, with a focus on modification of the paste binder.

Nanotechnology has been increasingly brought into the study of cement and concrete in the recent years, and it is driving concrete research into a new era. Various nanomaterials (including nanosized powders, tubes, and fibers) have been developed and incorporated into cement-based materials. Much of the work to date has been with nano-silica (nano-SiO_2) and nano-titanium oxide (nano-TiO_2) [1-10]; there are increasing studies on applying nano-limestone (nano-$CaCO_3$), nano-clay, nano-iron (nano-Fe_2O_3), nano-carbon, and nano-alumina (nano-Al_2O_3) [2, 6, 11-22]. Research has demonstrated that well-dispersed nanomaterials can accelerate cement hydration, further refine micro-pores in concrete, and modify the internal structure of C–S–H gel (such as increasing length of the silicate chains), thus significantly reducing concrete permeability and improving concrete mechanical properties and durability [2, 23]. However, one shortcoming of nanomaterials modified cement-based materials is that the nanomaterial can adversely affect the workability due to the high specific surface area.

The modern drive for more sustainable concrete stimulates the increasing use of supplementary cementitious materials (SCMs) such as fly ash (FA) from power plants or metakaolin (MK). The use of SCMs to partially substitute Portland cement (PC) significantly reduces the carbon footprint of cementitious materials and allows the utilization of waste products. Because of its small, smooth, and spherical shape, FA introduces the advantage of increasing the workability of

cementitious materials. However, delayed set and slow early hydration and early strength development often limit the use of FA to a low replacement level for structural use [24-28].

Ternary cement-based systems which incorporate PC, SCM, and nano-material have great potential because the deficiencies of each material could be compensated for by advantages of one or more of the others, and in-common advantages of these three materials will be further enhanced.

However, the blending of PC, SCM, and nano-material leads to a more complicated system where the hydration of the PC and hydraulic reaction of the SCM occur simultaneously, influencing the reactivity of each other, and are both influenced by the presence of nanoparticles. Therefore, it is critical that an engineering/scientific basis be established for concrete technology moving toward these more complex mix designs. This work is aimed to enrich this basis by characterizing the nano-material modified cement-based materials with respect to their kinetics, microstructure, and properties.

1.2 Objective of dissertation

This dissertation focused on effects of nanomaterials on the hydration and properties of cement-based systems containing supplementary cementitious materials. The long-term goal is to obtain a better understanding of the mechanisms of the interactions in a PC – SCM - nanomaterial system and to gain an insight into processing - microstructure - property relationships of such systems.

The main points that this work aims to clarify are:

1. How do the nanoparticles affect the hydration kinetics and rheological behavior of cement paste?
2. How are the hydration and strength development of blended cements modified by nanoparticles?

3. How is the pore structure of cement paste modified by nanoparticles and SCMs, and how is the drying shrinkage of cement paste influenced by the pore structure?
4. What are the effects of nano-limestone on the fresh and hardened properties of portland concretes containing high volume SCMs?

1.3 Dissertation organization

This dissertation is divided into seven chapters. Four papers will be included and each paper will appear as a separate chapter.

Chapter 1 gives a general introduction to this dissertation and includes background, research objectives, and dissertation organization.

Chapter 2 contains a literature review on the application of nano-materials in cement based systems, and the physical and chemical effects of nano-materials addition on the hydration and properties of cement-based materials.

The body of this dissertation is comprised of a series of journal papers. In Chapter 3, the effect of nanomaterials on the early hydration kinetics and rheological behavior of portland cement pastes will be discussed. The early hydration accelerating effects of nanomaterials will be illustrated, and it is examined in Chapter 4 how these nanomaterials affect the hydration and strength development of blended fly ash cement pastes through both physically and chemically. In chapter 5, the effects of nanomaterials, fly ash, and metakaolin on the pore structure and drying shrinkage of cement pastes will be examined. In chapter 6, nano-limestone is utilized to produce self-consolidating concrete (SCC) and its effects on the properties of SCC is studied.

Finally, chapter 7 provides a summary of this research, overall conclusions and recommendations for further research.

1.4 References

1. J. S. Belkowitz, W. B. Belkowitz, R. D. Moser, F. T. Fisher, and C. A. Weiss. Jr., "The influence of nano silica size and surface area on phase development, chemical chrinkage and compressive ctrength of cement composites," in Nanotechnology in Construction Proceedings of NICOM5, K. Sobolev and S. P. Shah, Eds., ed: Springer International Publishing, 2015, pp. 207-212.
2. K. Sobolev, "Nanotechnology and nanoengineering of construction materials," in Nanotechnology in Construction Proceedings of NICOM5, K. Sobolev and S. P. Shah, Eds., ed: Springer International Publishing, 2015, pp. 3-13.
3. G. Li, "Properties of high-volume fly ash concrete incorporating nano-SiO_2," Cement and Concrete Research, vol. 34, pp. 1043-1049, 2004.
4. D. Kong, Y. Su, X. Du, Y. Yang, S. Wei, and S. P. Shah, "Influence of nano-silica agglomeration on fresh properties of cement pastes," Construction and Building Materials, vol. 43, pp. 557–562, 2013.
5. Q. Ye, Z. Zhang, D. Kong, and R. Chen, " Influence of nano-SiO_2 addition on properties of hardened cement paste as compared with silica fume," Construction and building materials, vol. 21, pp. 539-545, 2007.
6. W. Li, Z. Huang, F. Cao, Z. Sun, and S. P. Shah, "Effects of nano-silica and nano-limestone on flowability and mechanical properties of ultra-high-performance concrete matrix," Construction and Building Materials, vol. 95, pp. 366–374, 2015.
7. P. Hou, S. Kawashima, K. Wang, D. J. Corr, J. Qian, and S. P. Shah, "Effects of colloidal nanosilica on rheological and mechanical properties of fly ash–cement mortar," Cement and Concrete Composites, vol. 35, pp. 12–22, 2013.
8. H. Madani, A. Bagheri, and T. Parhizkar, "The pozzolanic reactivity of monodispersed nanosilica hydrosols and their influence on the hydration characteristics of Portland cement," Cement and Concrete Research, vol. 42, pp. 1563–1570, 2012.
9. M. Berra, F. Carassiti, T. Mangialardi, A. Paolini, and M. Sebastiani, "Effects of nanosilica addition on workability and compressive strength of Portland cement pastes," Construction and Building Materials, vol. 35, pp. 666–675, 2012.
10. B. Y. Lee and K. E. Kurtis, "Influence of TiO2 nanoparticles on early C_3S hydration," Journal of the American Ceramic Society, vol. 93, pp. 3399–3405, 2010.
11. L. P. Singh, S. R. Karade, S. K. Bhattacharyya, M. M. Yousuf, and S. Ahalawat, "Beneficial role of nanosilica in cement based materials – A review," Construction and Building Materials, vol. 47, pp. 1069–1077, 2013.
12. A. R. Jayapalan, B. Y. Lee, and K. E. Kurtis, "Can nanotechnology be 'green'? Comparing efficacy of nano and microparticles," Cement and concrete composites, vol. 36, pp. 16-24, 2013.
13. K. Sobolev, I. Flores, R. Hermosillo, and L. M. Torres-Martínez, "Nanomaterials and nanotechnology for high-performance cement composites," in Proceedings of ACI Session on

"Nanotechnology of Concrete: Recent Developments and Future Perspectives", Denver, 2006.

14. X. Wang, K. Wang, J. Li, N. Garg, and S. P. Shah, "Properties of self-consolidating concrete containing high volume supplementary cementitious materials and nano-limestone," Journal of Sustainable Cement-Based Materials, vol. 3, pp. 245-255, 2014.
15. A. Hakamy, F. U. A. Shaikh, and I. M. Low, "Characteristics of nanoclay and calcined nanoclay-cement nanocomposites," Composites Part B, vol. 78, pp. 174-184, 2015.
16. M. S. Morsy, Y. A. Al-Salloum, H. Abbas, and S. H. Alsayed, "Behavior of blended cement mortars containing nano-metakaolin at elevated temperatures," Construction and Building Materials, vol. 35, pp. 900–905, 2012.
17. T. S. M. Al-Saud, M. A. A. B. Hussain, E. I. Batyanovskii, S. A. Zhdanok, A. V. Krauklis, and P. P. Samtsou, "Influence of carbon nanomaterials on the properties of cement and concrete," Journal of Engineering Physics and Thermophysics, vol. 84, pp. 546-553, 2011.
18. N. Lewinski, V. Colvin, and R. Drezek, "Cytotoxicity of nanoparticles," Small, vol. 4, pp. 26-49, 2008.
19. M. S. Morsy, S. H. Alsayed, and M. Aqel, "Hybrid effect of carbon nanotube and nano-clay on physico-mechanical properties of cement mortar," Construction and Building Materials, vol. 25, pp. 145-149, 2011.
20. S. H. A. M.S. Morsy, M. Aqel, "Hybrid effect of carbon nanotube and nano-clay on physico-mechanical properties of cement mortar," Construction and Building Materials, vol. 25, pp. 145-149, 2011.
21. T. Matschei, B. Lothenbach, and F. P. Glasser, "The role of calcium carbonate in cement hydration," Cement and Concrete Research, vol. 37, pp. 551-558, 2007.
22. V. S. Ramachandran and C. Zhang, "Cement with calcium carbonate additions," in Proceeding of the 8th International Congress on the Chemistry of Cement, Río de Janeiro, Brasil, 1986, pp. 178–187.
23. F. Sanchez and K. Sobolev, "Nanotechnology in concrete – A review," Construction and Building Materials, vol. 24, pp. 2060-2071, 2010.
24. J. A.Vargas, "A designer's view of fly ash concrete," Concrete International, pp. 43-46, 2007.
25. P. K. Mehta, "Greening of the concrete industry for sustainable development," Concrete International, vol. 24, pp. 23-28, 2002.
26. B. Lothenbach, K. Scrivener, and R. D. Hooton, "Supplementary cementitious materials," Cement and Concrete Research, vol. 41, pp. 1244-1256, 2011.
27. A. Elahi, P. A. M. Basheer, S. V. Nanukuttan, and Q. U. Z. Khan, "Mechanical and durability properties of high performance concretes containing supplementary cementitious materials," Construction and Building Materials vol. 24, pp. 292–299, 2010.
28. C. Lee, R. Huang, W. Lin, and T. Weng, "Establishment of the durability indices for cement-based composite containing supplementary cementitious materials," Materials and Design, vol. 37, pp. 28-39, 2012.

CHAPTER 2. LITERATURE REVIEW

Nanoparticles are defined as particles with lengths ranging from 1 to 100 nanometers in two or three dimensions [1]. Nanoparticles have a high surface area to volume ratio (Figure 2.1), providing the potential for tremendous chemical reactivity.

This chapter summarizes a review of the effects of the addition of nanoparticles to cementitious systems, beginning with the basics of portland cement and supplementary cementitious materials and proceeding through the following subjects in order: early hydration kinetics, rheological behavior, methods to follow cement hydration after one day, microstructure, mechanical properties, and durability. Besides, a review of the dispersion of nanoparticles in aqueous suspension is also included.

2.1 Portland cement

Portland cement is a commonly used binder material to form the heterogenous mortar or concrete matrix. It is basically made by heating a mixture of limestone and clay, or other materials of similar bulk composition and sufficient reactivity, ultimately to a temperature of about 1450 ˚C. Partial fusion occurs, and nodules of clinker are produced. The clinker typically has a composition in the region of 67% CaO, 22% SiO_2, 5% Al_2O_3, 3% Fe_2O_3 and 3% other components, and normally contains four major phases, called alite, belite, aluminate, and ferrite [2]. Several other phases, such as alkali sulfates and calcium oxide, are normally present in minor amounts.

Alite is the most important constituent of all normal portland cement clinkers, of which it constitutes 50-70%. It is tricalcium silicate (Ca_3SiO_5) modified in composition and crystal structure by ionic substitutions [2]. It reacts relatively quickly with water, and in normal portland cements is the most important of the constituent phases for strength development; at ages up to 28 days, it is by far the most important.

Belite constitutes 15-30% of normal portland cement clinkers. It is dicalcium silicate (Ca_2SiO_4) modified by ionic substitutions and normally present wholly or largely as the β polymorph. It reacts slowly with water, thus contributing little to the strength during the first 28 days, but substantially to the further increase in strength that occurs at later ages. By one year, the strengths obtainable from pure alite and pure belite are about the same under comparable conditions.

Aluminate constitutes 5-10% of most normal portland cement clinkers. It is tricalcium aluminate ($Ca_3Al_2O_6$), substantially modified in composition and sometimes also in crystal structure by ionic substitutions. It reacts rapidly with water, and can cause considerably rapid setting unless a set-controlling agent, usually gypsum, is added.

Ferrite makes up 5-15% of normal portland cement clinkers. It is tetracalcium aluminoferrite (Ca_2AlFeO_5), substantially modified in composition by variation in Al/Fe ratio and ionic substitutions. The rate at which it reacts with water appears to be somewhat variable, perhaps due to differences in composition or other characteristics, but in general is high initially and low or very low at later ages.

Hardening results from reactions between the major phases and water. Gypsum is usually added to the clinker to control the setting process. The ASTM has designated five types of portland cement, designated Types I-V. Physically and chemically, these cement types differ primarily in their content of C_3A and in their fineness. In terms of performance, they differ primarily in the rate of early hydration and in their ability to resist sulfate attack. The physical properties and chemical composition of a general purpose Type I cement are shown in Table 2.1. Its particle size distribution is shown in Figure 2.2. Figure 2.3 shows the morphology of the cement. The small particles on the surface observed in Figure 2.3 are the result of the grinding process. Many of these particles disappeared after the initial hydration.

2.2 Supplementary cementitious materials

Since the development of portland cement over 175 years ago, it has become the dominant binder used in concrete for construction. Annual worldwide Portland cement production is approaching 3 Gt [3]. However, the environmental issue it brings is imminent. The manufacturing of portland cement consumes nearly 2-3 percent of global primary energy use and produces large amounts of carbon dioxide (approximately 1 ton per ton of clinker) [4]. The cement industry is under pressure to reduce both energy use and greenhouse gas emissions.

The most realistic solution is to use blended cement where cement is partially replaced with more sustainable materials. These alternatives must also develop adequate cementitious properties to maintain the mechanical properties of the cement-based materials, and are therefore called supplementary cementitious materials (SCMs). The chemistry of SCMs is generally characterized by lower calcium content than portland cement (Figure 2.4). Fly ash and metakaolin are studied in this work; they in themselves possess little or no reactivity in direct contact with water but can pozzolanically react with the CH released from cement hydration, forming hydration products and contributing to the strength development.

The use of fly ash as a SCM not only leads to a significant reduction in CO_2 emissions but also serves as a means to utilize by-products of industrial manufacturing processes. Fly ash is the residue produced by the burning of coal in power plants. Coal is pulverized in fine particles and burnt in a boiler. During the combustion, heat and a molten residue are generated. Heat is extracted on one side and the flue gas is cooled down. The residue hardens in spherical glassy particles. The lighter particles are collected and are the “fly ash”. It is a heterogeneous material mainly amorphous and containing small amount of crystalline phase. The crystalline phases are quartz, mullite, hematite, melilite or others. The characterization of the amorphous content is more

delicate but can be seen as an alumina-silica glass containing modifiers elements (Ca, Na, K, Mg, and Fe). The amount of CaO is limited but highly variable depending on the origin of the fly ash; the ASTM C618 standard differentiates high calcium Class C-fly ashes and low-calcium Class F fly ashes (Figure 2.4). Low-calcium Class F fly ash is studied here since it is the most abundant. The physical properties and chemical composition of a Class F fly ash are shown in Table 2.1. Figure 2.5 shows the morphology of the fly ash. By their spherical geometry, the fly-ash particles can act as "ball-bearing" to better the rheological properties of fresh pastes. The pozzolanic reaction of fly ash particles is much slower compared to cement grains and these particles continue to react with pore solution and cement hydrates for years after the hardening of pastes [2, 5, 6]. Accordingly, the microstructure of hardened cement pastes evolves substantially with the continuous formation of pozzolanic reaction products, C–S–H gel in cement chemistry terms, in the pore space enclosed by cement hydrates.

Metakaolin (MK) is manufactured from kaolinite ($[Al_2Si_2O_5(OH)_4]$), one of the most abundant natural clay minerals, by calcination at moderate temperatures (500-800 °C). This thermal treatment results in de-hydroxylation of the aluminate octahedral in the kaolinite layered structure, forming an amorphous or semi-amorphous material with a high specific surface area and chemical reactivity [7, 8]. Using metakaolin as a partial substitute for portland cement in concrete has been shown to increase long-term strength and durability compared with portland cement alone and reduce the quantity of cement required, thereby lowering concrete carbon dioxide footprint associated with cement manufacturing [9-11]. The physical properties and chemical composition of a metakaolin are shown in Table 2.1. Figure 2.6 shows the morphology of a metakaolin. Although it requires a higher quantity of water for given flowability, MK increases viscosity, yield

stress, and thixotrophy of concrete mixes, improving concrete shape-holding ability and finishing ability [7, 12].

2.3 Early hydration kinetics (first 24 h)

Hydration of cement is the combination of all chemical and physical processes taking place after contact of the anhydrous solid with water. The main reactions with cement notations are:

$$yC_3S + H_2O \rightarrow (3y\text{-}x)\ CH + C_x\text{-}S_y\text{-}H \quad 2.1$$

$$yC_2S + H_2O \rightarrow (2y\text{-}x)\ CH + C_x\text{-}S_y\text{-}H \quad 2.2$$

$$C_3A + 3\ C\$H_2 + 26\ H_2O \rightarrow C_6A\$H_{32} \quad 2.3$$

Most of these reactions are exothermic: the overall heat released can be thus recorded with a calorimetric device. A typical calorimetry curve of a modern portland cement is shown in Figure 2.7. The main reactions of hydration occur within the first 24 hours although the hydration will continue until exhaustion of reactants (> 1 year).

When discussing kinetic mechanisms, the hydration process is often divided into four periods indicated in the above calorimetry plot of hydration rate versus time: (1) initial reaction period of rapid heat generation (~ first few minutes), (2) period of slow reaction, (3) acceleration period, and (4) deceleration period [13]. The beginning and ending of these stages are still difficult to pinpoint precisely, but they provide a more accurate picture of the current state of knowledge.

2.3.1 Acceleration period

One of the most important periods is the so-called “acceleration period” which corresponds to period 3 in Figure 2.7 because high amounts of hydrates are formed during this period.

The main peak in the calorimetry curve is mainly attributed to the silicate reaction. The calcium silicate hydrate (C-S-H) is the main hydrate along with CH in hydrated cement paste. It forms connections between the cement grains leading to the setting and the strength development of the paste. C-S-H does not have a well-defined composition because of its amorphous structure.

Besides its composition, the morphology of the C-S-H gel is also changing during the hydration process.

C-S-H clusters are forming rapidly on the surface grains after the contact with water. In few hours, the clusters of C-S-H grow in number and size to become fibrillar clumps which form sea-anemone like structures (Figure 2.8). The shape observed with SEM is reported as fibrillar and several terms have been used in the past to describe it: type I from Diamond or needles radiating form grains [2].

The nucleation and growth process of C-S-H is now well supported as the rate controlling mechanism of the acceleration period [13-15]. Recent advances in both experiments and simulations [16] have brought new evidences to support this interpretation.

2.3.2 Second aluminate reaction during the deceleration period

During the deceleration period two main reactions overlap: the silicate reaction and the second aluminate dissolution. A small peak is visibly at about 16 hours from Figure 2.7 which corresponds to the second dissolution of the aluminate phase. XRD measurements indicates that the C_3A phase starts to dissolve right at the beginning of the contact with water and then stops for a certain period before restarting at the time of this small peak.

Several theories have been suggested to explain the retardation of the C_3A dissolution. The first hypothesis was that the C_3A is surrounded by a protective membrane, usually reported as ettringite [2, 15]. Many works have disproved this theory and suggested that the adsorption of sulfate on C_3A is rather the retardation mechanism [13, 15]. It is still not clear where the sulfate is adsorbed, probably on coordination sites which would be occupied by H or OH group in absence of sulfate [15].

The dosage of sulfate in the OPC is very important in practice. There is an optimum of sulfate with respect to the compressive strength which changes with the age of testing. Addition of gypsum beyond the optimum will also lead to a decrease in the strength at early ages, because the second aluminate reaction is delayed and the hydrates formed from this are not contributing to the strength [2, 13]. It is important that the aluminate reaction occurs during the deceleration period to contribute to the strength development by one day.

2.3.3 Effect of supplementary cementitious materials

In blended cements there is generally negligible reaction of the SCM in the first day or so [2, 15]. Nevertheless, the reaction of cement clinker is enhanced by SCM due to its physical presence; this is the so called filler effect and can be attributed to two main factors. First, when SCM grains substitute clinker grains, there is relatively more space available for the hydrates of the clinker phases to form in. Secondly, the surface of the SCM grains act as sites for the heterogeneous precipitation and growth of hydrates.

2.3.4 Effect of nanoparticles

The presence of nanoparticles in the cement system changes the hydration process from the beginning of hydration.

Research has demonstrated that the addition of chemically inert nanoparticle, such as TiO_2, accelerates the early hydration by providing additional nucleation sites; higher rate peaks and higher total heat of hydration were observed [17].

The conduction calorimetry results indicated that 10% nano-$CaCO_3$ replacement accelerated the hydration of C_3S and portand cement pastes; furthermore, the induction period of the C_3S hydration was significantly shortened (Figure 2.9). The formation of small fibrous C-S-H products around the nano-$CaCO_3$ particles was observed through scanning electron microscopy (SEM) [18].

Additionally, it was suggested that calcium carbonate can contribute CO_3^{2-} anions to the pore solution, which can subsequently be incorporated within the C-S-H gel. OH- anions released from C-S-H to preserve charge neutrality would elevate the pH and hence the driving force for continuing hydrate growth [19].

The hydration-accelerating effect of nano-silica (Figure 2.10) is generally attributed to the nucleation seeding effect provided by C-S-H particles that formed on the nano-silica surface [20, 21]. These C-S-H particles were formed from the early pozzolanic reaction of nano-silica with calcium ions released by the dissolving cement; they spread in the capillary pore space between cement or C_3S particles and serve as seeds for the formation of more compact C-S-H phase. Directly adding synthesized C-S-H seeds to portland cement and pure C_3S can cause a significant acceleration of the early hydration kinetics and even eliminate the induction period (Figure 2.11).

^{29}Si MAS NMR spectra demonstrated that the addition of micro- or nano-sized layer silicates to portland cements accelerated the cement hydration by increasing the degrees of hydration for both alite and belite [22].

2.4 Rheological behavior

Cement pastes set during the acceleration period, during which hydration products that form on the surfaces of clinker particles intersect, leading to the formation of clusters that eventually join into a continuous elastic network [23].

2.4.1 Bingham equation

In the period before setting, the fluid properties of cement pastes dominate. The rheology of cement-based materials is a quantitative property that describes the fluids' deformation and flow [24]. The rheological behavior of a fluid such as cement paste, mortar, or concrete is often

characterized by two parameters: yield stress τ_0 and plastic viscosity μ, as defined by the Bingham equation:

$$\tau = \tau_0 + u\dot{\gamma} \quad 2.4$$

where τ is the shear stress applied to the material (in Pa), τ_0 is the yield stress (in Pa), μ is the plastic viscosity (in Pa·s), and $\dot{\gamma}$ is the shear strain rate (also called the strain gradient) (in s^{-1}). Unlike in the Newtonian model, cement paste has a yield stress that reflects the minimum stress needed to initiate a flow. The plastic viscosity measures the resistance of cement paste against increase in speed of movement [24, 25].

2.4.2 Key parameters

Key parameters influencing the rheology of cement pastes include: particle size distribution, volume fraction of particles, colloidal forces (van der Waals forces, electrostatic forces, etc.), hydrodynamic effects, and hydration progress [26, 27].

Before the acceleration period of cement hydration, cement paste rheology is primarily controlled by attractive-particle interactions. The replacement of cement by fly ash generally decreases the yield stress and viscosity [28, 29]. When water content is kept constant, the addition of nanomaterials can adversely affect the flowability of cement pastes and increase the yield stress: (1) the high surface area of nanoparticles to be wet and their tendency to agglomerate may decrease the amount of free water; and (2) nanoparticles can fill the gaps between cement particles and increase the connectivity of the network structure [6, 30]. On the other hand, the addition of nanoparticles in cement pastes can theoretically increase particle-packing density, decrease the void ratio of solid particles, and increase the amount of free water for lubrication [6, 31]. Thus, the plastic viscosity could increase or decrease depending on these competing effects. Research has shown that the addition of nano-silica in cement pastes usually increased water demand and the

yield stress and viscosity [21]. Small additions of clay have been shown to increase the floc size, flocculation strength, and shear-yield stress of cement pastes [30, 32, 33].

2.5 Methods to follow cement hydration after one day

Cement hydration beyond one day, especially the period 1-28 days is of great practical importance, as 75% of the design strength may develop during this period.

The general hydration kinetics of cement is often represented by the rate of change of the overall degree of hydration α, which is defined as the total weight fraction of cement reacted. As a composite material consisting mainly of four compounds, or clinker phases (C_3S, C_2S, C_3A, and C_4AF), the overall degree of hydration of cement is typically written as [34]:

$$\alpha(t) = f_{C_3S}\,\alpha_{C_3S}(t) + f_{C_2S}\,\alpha_{C_2S}(t) + f_{C_3A}\,\alpha_{C_3A}(t) + f_{C_4AF}\,\alpha_{C_4AF}(t) \qquad 2.5$$

where f_i is the original weight fraction of phase i in the anhydrous cement and $\alpha_i(t)$ is the degree of hydration of phase i at time t. The direct determination of $\alpha_i(t)$ may be performed by means of, for example, optical microscopy or quantitative X-ray diffraction analysis (QXDA) [34] by measuring the fraction of unreacted phase i, , though it is difficult to obtain accurate results.

Some properties of a hydrating cement paste, such as the non-evaporable water content, the cumulative heat evolution, and the total chemical shrinkage have been shown to have approximately linear relationships with the overall degree of hydration [2, 34, 35]. As a matter of fact, α is more easily and commonly determined indirectly by tracking the time dependence of one or more of these properties:

$$\alpha(t) = \frac{\boldsymbol{W_n}(\boldsymbol{t})}{\boldsymbol{W_n^0}} = \frac{\boldsymbol{H(t)}}{\boldsymbol{H^0}} = \frac{\boldsymbol{CS}(\boldsymbol{t})}{\boldsymbol{CS^0}} \qquad 2.6$$

where $\boldsymbol{W_n}(\boldsymbol{t})$ and $\boldsymbol{W_n^0}$ are the non-evaporable water content at time *t* and at complete hydration, respectively (typically in g/g cement); $\boldsymbol{H(t)}$ and $\boldsymbol{H^0}$ are the cumulative heat evolution at time t and

at complete hydration, respectively (typically in J/g cement); and $\boldsymbol{CS}$ ($\boldsymbol{t}$) and $\boldsymbol{CS^0}$ are the total chemical shrinkage at time *t* and at complete hydration, respectively (typically in mL/g cement).

2.5.1 Sample preparation

Reliable analytics is impossible when the sample preparation is inappropriate. Before discussing the above mentioned methods for following cement hydration, this section gives general information related to sampling, grinding, and storage of anhydrous powder materials and preparation and curing of pastes as well as stoppage of hydration, focusing on the experimental work done in this dissertation.

2.5.1.1 Storage of anhydrate powder materials

One should start the experiments already from a sample as fresh as possible; besides, when using a cementitious material within a research project, usually it is not desired to change the batch of the material, as the results might not be comparable and the characterization of chemical-mineralogical and physical properties needs to be repeated for the new batch of material, creating extra work. However, a comprehensive study completing the dissertation research may take two years or more; therefore, it is important to store the powder materials properly. It is preferable to fill the powder material in barrels or buckets, which can be closed watertight and water vapor tight, and to store them in a room with low relative humidity.

Three nanomaterials, nano-limestone, nano-silica, and nano-clay are used in this study. They are stored in air-tight dark containers, which themselves are stored in an air-tight container with silica gel as the drier.

2.5.1.2 Sampling

Before using powders for, e.g. chemical-mineralogical analysis of particle properties, or before preparing samples of cementitious pastes, generally, representative samples need to be taken out

of a bigger quantity of granular material. To achieve this, the ‘golden rules of sampling’ [36] should be applied, namely, (1) powder should be sampled while in motion and (2) several small samples should be taken at different intervals or at different positions rather than taking one larger sample. The different samples can be homogenized afterwards to obtain a single sample.

Luckily, cement and similar materials, such as fly ash, are fine powders and the very high number of particles already in a few grams of the material (e.g. 1 g of ‘monosized’ cement with a particle size of 5 um and a density of 3.15 g/cm^3 contains 2.5 * 10^9 particles) helps greatly to reduce sampling errors. Thus, it is generally sufficient and frequently done in the case of finely powdered cementitious materials to sample using the scoop method. The cement is mixed in the bucket by using a spatula, and then a sample is taken from the middle.

2.5.1.3 Preparing a cement paste sample

Generally, when producing a paste sample, the different raw powder materials (cement, fly ash, etc.) are blended first to achieve a homogeneous mix, which is later mixed with water to form a homogeneous paste. Hand mixing can be suitable for hydration studies, since only a small batch of paste sample is required (< 200 g); however, if rheological measurements are done afterwards, a high shear mixer according to ASTM C1738 [37] is used.

If nanomaterials are to be used, the above described procedure would be inappropriate. To achieve a homogeneous cement paste, the nano-material is first dispersed in the mixing water to form a nanoparticle suspension, and this nano-suspension will then be used as the “virtual mixing water” for the mixing of cementitious materials.

2.5.1.4 Dispersion of nanomaterials

Nanoparticles are very difficult to deagglomerate and disperse in a cement paste due to their strong inter-particle attraction (i.e. van der Waals forces). As agglomerates, they behave in the

same way as particles of a similar size. Clusters of nanoparticles due to any improper dispersion may introduce air through vapor-gas nuclei trapped in crevices [38] and form unreacted pockets in the cement matrix, thus resulting in weak zones in concrete. Therefore, it is important to disperse nanoparticles properly to exploit the advantages of nanoparticles.

There are three major strategies for dispersing and stabilizing nanoparticles: (1) use of dispersant, (2) surface modification, and (3) mechanical dispersion.

There are several commonly used dispersants. Potential-determining ions (i.e. pH) and electrolytes (inorganic slats) work by providing an electrostatic repulsion when in a polar medium, such as water. Stably dispersion may arise also from the adsorption of surface active compounds or polymers, which provide a steric hindrance. They can be associated to electrical charge and form charged polymers, thus providing an electro- steric stabilization. Finally, non-adsorbing polymers could maintain the nanoparticles apart by means of a depletion mechanism. A recent study has shown that a good dispersion of nano-limestone can be achieved with polycarboxylate superplasticizer [39].

High intensity ultrasound has been widely used to disperse nanoparticles in a liquid. Ultrasonication generates intense shock waves by collapsing cavitation, which then leads to collisions among particles. The agglomerated particles are thus agitated and split by the collisions [40].

Ultrasonic waves are generated in a liquid suspension either by immersing an ultrasound probe or “horn” into the suspension (direct sonication), or by introducing the sample container with the suspension into a bath containing a liquid through which ultrasonic waves are propagated (indirect sonication). Direct sonication is recommended over indirect sonication for the purpose of dispersing dry powders, as it yields a higher effective energy output into the suspension.

For a given system, optimal sonication conditions must be determined by assessing the effect of a variety of sonication parameters on the dispersion state of the suspension under a broad range of relevant conditions. Moreover, the total effective acoustic energy utilized in fragmenting powder clusters is influenced by a number of instrument- and system-specific parameters. Factors affect the ultrasonication may include: temperature, sonication time and operation mode, sample volume and concentration, and sonicator probe, container geometry and tip immersion [41].

Temperature: During sonication, the extreme local heating cycles that take place at the micro-scale bubble interface due to cavitation will result in a bulk heating of the liquid over time. Excessive bulk heating can cause substantial liquid evaporation, resulting in changes to the sonicated volume, or the degradation of the material or medium components. A simple approach to minimize temperature driven side effects is to avoid substantial high-temperature excursions by immersing the suspension container in a cooling bath (e.g. ice-water bath, ice-salt bath, etc.). Besides, working with containers made of materials (e.g. aluminum, stainless steel, glass, plastic, etc.) with high thermal conductivities helps ensure a rapid release of heat from the suspension.

Sonication time and operation mode: The total amount of energy (E) delivered to a suspension not only depends on the applied power (P) but also on the total amount of time (t) that the suspension is subject to the ultrasonic treatment: $E = P * t$. Ultrasonic disruptors can typically operate in either continuous or pulsed mode. In pulsed mode, ultrasonic intervals are alternated with static (sonication off) intervals. The duration of on and off intervals can be regulated. Operating in pulsed mode retards the rate of temperature increase in the medium, minimizing unwanted side effects and allowing for better temperature control than continuous mode operation. Pulse mode operation is therefore generally recommended.

Sample volume and concentration: While sonication power and time describe the amount of energy delivered to the suspension, samples of different volumes and particle concentrations can respond differently to the same amount of delivered energy. The effect of concentration is thus dependent on both the energy delivered into the suspension and the physiochemical properties of the suspension. The effect of suspension volume (at equal particle concentrations) is measured as energy density (W·s/mL). This magnitude expresses the amount of delivered energy per unit of suspension volume. In principle, at equal power and particle concentration, higher energy densities (i.e., lower suspension volumes) will result in a greater disruptive effect. When working with small volumes the temperature of the suspension will rise more rapidly; therefore, more intense cooling conditions may be required.

Sonicator probe, container geometry and tip immersion: The amount of acoustic energy transferred to the suspension will depend on the shape and diameter of the probe and its immersion depth in the suspension. At equivalent instrumental power settings, microtip probes vibrate with larger amplitudes than conventional flat tip probes. However, microtips are less mechanically robust and are limited in terms of the maximum power setting at which they can be used. The manufacturer will typically specify a maximum power setting (based on a percentage of the maximum power output) for use with microtips. Microtips are appropriate for small suspension volumes (e.g., 25 mL or less). The way in which the ultrasonic energy is distributed within the suspension is also heavily influenced by the container geometry. When possible, it is recommended to use the smallest diameter vessel that allows for the probe to be inserted without touching the container walls. Using smaller container diameters raises the height of the liquid and maximizes the liquid-surface area exposed to the acoustic waves, as well as the container wall surface/volume ratio for dissipation of heat by the cooling bath. Conical bottom, flat bottom and

round bottom flasks will show different energy maxima and minima distribution profiles, which will in turn vary significantly for different probe tapers and probe tip immersion depths. Cylindrical, flat bottom beakers are recommended, especially for small volumes. Probe immersion depths between (2 to 5) cm are recommended when operating with standard ½" probes having flat tips or with microtips. Probes should be placed no closer than about 1 cm from the bottom of the sample container and contact between the probe and the container walls should be avoided.

The goal of the optimization procedure is to achieve the desired degree of dispersion with the least possible energy input, in order to minimize unwanted side effects. The process to determine such conditions is based on a trial-and-error approach.

2.5.1.5 Grinding of hydrated pastes

Some analytical methods, such as TGA, XRD or NAD used in this study, require the use of grounded samples. However, cement hydrate phases are very sensitive to grinding, as the increased temperatures and the friction during intense grinding processes may cause loss of crystal water and changes in the phase assemblage. For example, gypsum loses 1.5 mol of its crystal water above 40 ˚C, and ettringite is unstable in portland cement pastes above 50 ˚C [35]. Thus, hydrated pastes should be ground after hydration stoppage gently by hand in an agate mortar other than ground mechanically.

2.5.1.6 Hydration stoppage

Generally, the hydration of cements is stopped before analysis. At early hydration times hydration stoppage is necessary to suppress the further progress of hydration. At hydration times of 1 month or longer, where the further progress of hydration is very slow, stoppage procedures are used to remove free pore solution. For some techniques, such as XRD and NMR, hydration stoppage is not strictly necessary but is generally done, as it enables sample storage, and the low

relative humidity after stoppage helps to minimize carbonation and the characterization of the same sample at an identical degree of hydration by different techniques. Slightly different stopping procedures are optimal for the different characterization techniques.

The primary aim of the various available methods of hydration stoppage is to remove water present in the pores without removing the water present in the hydration products to avoid alteration of the hydrates and to preserve the microstructure. Zhang and Scherer compared the effects of the most common drying techniques (Table 2.2), including direct drying (oven, microwave, D-drying, P-drying, and freeze drying) and solvent exchange on the preservation of the hydrate assemblage and the microstructure [42], and they summarized the results as follows (where ">" means "better"):

1. To preserve microstructure: solvent replacement > freeze drying > oven drying.
2. To preserve composition: freeze drying > oven drying > solvent replacement.
3. To save time: oven drying > freeze drying > solvent replacement.
4. All the techniques more or less dehydrate C–S–H and ettringite.
5. Solvent replacement creates chemical artifacts in the specimens by reaction with hydration products or by strong adsorption.
6. D-drying, P-drying, and vacuum drying are similar processes. They cannot arrest the hydration effectively, owing to slow water removal. They are better for microstructural preservation than oven drying, but not as good as solvent replacement.

2.5.2 Isothermal calorimetry

Heat of hydration measured by isothermal calorimetry is a well-established method to provide continuous data suitable for measuring overall cement hydration progress [2]. This technique records the heat released from the sample and compares it to a reference sample. The reference

sample should have a constant heat capacity similar to the measured sample. Typical commercial instruments of this type used in the cement field in the U.S. are TAM Air (TA Instruments, U.S.) and I-Cal (Calmetrix, U.S.). For this technique (TAM Air), the average absolute difference between replicate specimens of cement paste is 2.4×10^{-5} W/g (cement), with a maximum absolute difference of 0.00011 W/g (cement), for measurements conducted between 1 h and 7 d after mixing [43].

The work of Berodier [44] highlights the importance of the water to cement ratio in the 1-28 days period of hydration and indicates that there are perhaps two later regimes (Figure 2.12). From 1 to 6 days the amount of hydration seems to be mainly determined by the water to cement ratio or the space available for the cement hydrates. After about 6 days all the systems seem to have very similar kinetics.

2.5.3 Chemical shrinkage

Chemical shrinkage is related to the volume changes during the hydration process [45]. The volume of the hydrates is lower than the initial volume of the reactants i.e. water, cement, SCM. Not only hydration of the main clinker minerals but also the secondary reactions, including formation of ettringite, result in chemical shrinkage. Determination of the degree of hydration requires knowledge of the ultimate value of chemical shrinkage, which depends on both binder composition and temperature. This technique is more convenient than isothermal calorimetry for long term hydration as the shrinkage measurement is cumulative; furthermore, the equipment is relatively inexpensive and making the measurements requires only limited training.

The primary objective of any chemical shrinkage test is to quantify the change in volume that occurs due to the hydration reactions, so the sample has to be kept water saturated and that the water needed to replace the volume decrease is measured. ASTM Standard Test Method C1608

[46] is based on the one developed by Geiker. The setup is shown in Figure 2.13. It consists of a cylindrical vial (50 mm height by 25 mm of diameter) that contains the paste, on top of which a pipette is connected. The vial is tapped to avoid the presence of entrapped air bubbles. Water is added on top of the paste until it fills also the pipette. The system is sealed at the interface between the pipette and the vial with rubber lids and on top of the pipette with a colored oil drop. This colored oil drop is used as an indicator of the level of water in the pipette. As the hydration proceeds and the paste shrinks, the level of water in the pipette decreases. This level is recorded every 30 min in the first day and every day thereafter until 28 days. The vials are maintained in a water bath at 23 °C to avoid effects of heat release on volumetric changes of the paste.

Despite the apparently simple principle of chemical shrinkage measurement, there are experimental difficulties that can yield spurious results. For example, the sample dimensions are critical when measuring chemical shrinkage for longer periods and on dense pastes. The size should be sufficiently large to provide accurate measurements and sufficiently small to reduce sources of as possible temperature effects and self-desiccation due to de-percolation of the capillary porosity. It is recommended that [46] a 5-10 mm introduced to the vial at a w/c of 0.4. Besides, air bubbles in paste should be limited by vacuum mixing or using freshly boiled water and carefully cast and compact samples; otherwise, a reduction in measured chemical shrinkage will be observed.

An example of the accuracy of chemical shrinkage measurement following the ASTM C1608 procedure conducted at the PCC lab on two replicate samples of a portland cement paste is shown in Figure 2.14.

2.5.4 Thermogravimetric analysis

Thermogravimetric analysis (TGA) is a widely applied technique in the field of cement science. Measurements of chemically bound water and portlandite contents by TGA are often used to follow the reaction of portland cement or to evaluate the reactivity of supplementary cementitious materials (SCMs), such as fly ash and blast furnace slags. TGA is able to identify X-ray amorphous hydrates, such as C-S-H or AH_3 [35].

Thermogravimetric analysis depends on measuring the dynamic weight loss from a sample as it is heated. The corresponding derivative thermogravimetric (DTG) curve is often calculated to better identify the changes. The results of thermal analysis are strongly influenced by the architecture of the measuring device, the kind of vessel used, the heating rate, the amount of solids, the particle size, gas flow rate and kind of purging gas, and the pretreatment of samples. The main rule of performing reliable TG analysis is to use the same procedure for all measurements. Figure 2.15 shows an example of TGA and DTG curves of a cement paste.

1. From 25 to 400 °C: loss of evaporable water and chemically bound water in C-S-H and calcium sulfate components. The mass loss for these phases overlap.
2. From 400 to 500 °C: the dehydration of calcium hydroxide and the chemical reaction is

$$Ca(OH)_2 \rightarrow CaO + H_2O \qquad 2.7$$

3. From 600 to 750 °C: the de-carbonation of calcium carbonate and the chemical reaction is

$$CaCO3 \rightarrow CaO + CO2 \qquad 2.8$$

A widely used technique to assess the degree of reaction of portland cements is to obtain the bound water content from the difference between the weight losses of samples dried to 105 and at 1000 °C. This procedure assumes that only pore water is removed until 105 °C.

Portlandite decomposes generally between 400 and 500 °C to CaO and H_2O, as shown in Figure 2.15. This weight loss ($WL_{Ca(OH)_2}$) due to the evaporation of water can be used to calculate the amount of portlandite present, using the molecular masses of portlandite ($m_{C_a(OH)_2}$= 74 g/mol) and water (m_{H_2o} = 18 g/mol):

$$C_a(OH)_{2,measured} = WL_{Ca(OH)_2} * m_{C_a(OH)_2}/m_{H_2o} = WL_{Ca(OH)_2} * \frac{74}{18} \quad 2.9$$

2.5.5 X-ray diffraction

X-ray diffraction is a powerful technique which allows crystalline phases to be studied in cement systems, including both the anhydrous clinker phases (C_3S, C_2S, C_3A, C_4AF, and other minor crystalline phases), and the main hydration products (mainly CH and ettringite). The diffraction of X-rays by a crystalline phase produces an XRD pattern consisting of peaks of varying intensities at characteristic diffraction angles. The diffraction angle or position of the peaks is determined by the symmetry and the size of the unit cell through Bragg's law:

$$n\lambda = 2d\sin\Theta \quad 2.10$$

where n is an integer, λ is the wavelength of the radiation used, d the spacing of the crystal planes, and θ the angle of the diffraction peak. The intensity of the peaks is determined by the types and positions of the atoms in the crystal lattice according to the structure factor:

$$F(hkl) = \sum_1^N \boldsymbol{f_n exp 2\pi i(hx_n + ky_n + lz_n)} \quad 2.11$$

where *hkl* are the Miller indices of the reflecting planes, f_n the atomic structure factor, and x_n, y_n, and z_n, the coordinates of the *n*th atom in the unit cell containing N atoms. So it is possible to distinguish the particular phases from the XRD pattern.

Qualitative phase analysis is based on a comparison of the peaks in a measured XRD pattern to a databased containing peak patterns of known phases. Usually a general-purpose database, such as the powder diffraction file (PDF) published by the International Centre for Diffraction Data is

used, often in combination with chemical or categorical filters, to restrict the number of candidate patterns. XRD scan of a hydrated cement paste is shown in Figure 2.16.

2.6 Microstructure

The hardened cement paste produced by the interaction of portland or blended cement with water is composed of anhydrous phases (unreacted clinker minerals, mineral additions), hydrate phases modified by foreign ions incorporation and adsorption (C–S–H, ettringite, portlandite, AFm), minor phases such as hydrotalkite, pore solution, and pores. The hydrate phase most abundant in hardened cement paste is calcium silicate hydrate.

Figure 2.17 presented modelled changes during hydration of a) OPC and b) blended cement with fly ash replacement. The majors changes in the presence of fly ash are related to the C-S-H composition which tends to have lower Ca/Si and higher Al/Si ratios than in OPC paste.

2.6.1 Phase assemblage

Accelerated hydration of cement paste and faster formation of calcium hydroxide at initial period was observed in the nanoparticles added cement paste [47, 48]. Nanoparticles were reported to favor the formation of small-sized crystals (such as $Ca(OH)_2$ and AFm) and small sized uniform clusters of C-S-H [49, 50].

Besides the physical effects, nanoparticles may react chemically in the cement hydration process. Limestone is now well acknowledged to interact with AFm and AFt phases. In an ordinary portland cement without limestone powder, the C_3A and at a slower rate also the C_4AF will react with the calcium sulfate to form ettringite ($C_3(A,F)\cdot 3CaSO_4\cdot 32H_2O$). Upon depletion of the sulfates, the remaining C_3A and C_4AF will react with the ettringite to form monosulphate ($C_3(A,F)\cdot CaSO_4\cdot 12H_2O$) or hydroxy-AFm solid solution [51, 52]. In the presence of limestone, the AFm-carbonate equivalents such as monocarbonate ($C_3(A,F)\cdot CaCO_3\cdot 11H_2O$) are formed

rather than the sulfate containing AFm phases. The AFt-carbonate equivalent has been observed by some researchers [53], but it is unlikely to form in a significant amount at ambient temperatures in a hydrating cement as it is less stable than the AFm phases. The decomposition of ettringite to monosulphate when reacting with the remaining C_3A and C_4AF upon sulfate depletion is prevented as monosulfate is less stable than monocarbonate in the presence of limestone. The stabilization of the voluminous, water rich ettringite instead of the less voluminous monosulphate, gives rise to an increase of the total volume of hydration products [51, 53]. However, there are many disagreements about the time when the hemicarbonate and monocarbonate phases are formed and in which order.

Nano-silica participates in the pozzolanic reactions, resulting in the consumption of $Ca(OH)_2$ and formation of C-S-H. Dense and compact microstructure with lesser amount of calcium hydroxide crystals was observed (Figure 2.18) [21, 54]. Gaitero and his co-authors reported that nano-silica particles increase the average length of the silicate chains of C-S-H gel [55]. SEM analysis results showed that the cement paste containing 2% nano-montmorillonite addition was denser and more uniform [56].

2.6.2 Pore structure

When cement powder and water are mixed, reactions begin to consume the cement particles and to produce solid products. This is accompanied by a net decrease in volume, called chemical shrinkage, because the volume of the solid products of hydration is less than the initial volume of solids and water from which they form. However, the solid hydration products have greater volume than the initial solids alone, so the water filled space is gradually replaced by solids during the reaction. The space not filled by solid products of hydration is traditionally called the capillary pore space. The principle hydration product, calcium silicate hydrate (C-S-H) gel, also contains a

significant volume of very small pores called gel pores. In this sense, the pore system naturally divides into two distinct populations of pores, one population becoming less numerous, and the other becoming more numerous, as the reactions proceed (Figure 2.19). The distinction between capillary pores and gel pores is somewhat arbitrary, with a cut-off of 10 nm being typically used (Table 2.3). It should be kept in mind that the sizes of capillary and gel pores overlap, and the spectrum of pore sizes in a cement paste is continuous. The capillary pore network remains fully connected until its volume fraction is reduced to about 18% [2].

The properties of porous materials are strongly affected by the characteristics of their pore system, such as porosity, pore size distribution, connectivity, etc. Thus, materials with the same total pore volume (porosity) may exhibit quite different mechanical and transport properties. In cement-based materials, compressive strength and elasticity primarily depend on the porosity, while transport properties, such as permeability and diffusivity, are influenced by the total volume, size distribution, shape and connectivity of the pores [57].

In general fly ash blended cements have a higher total porosity at early age compared to plain portland cement caused by the lower clinker content and the slow reaction of fly ash. At later ages fly ash could refine the pore structure of cement paste by the secondary pozzolanic reaction. The hydration products produced by the reaction of fly ash with calcium hydroxide (CH) fill in the pores, which does not only reduce the pore volume but also the pore size [58, 59]. Nevertheless, earlier studies indicate that there is an optimal replacement of SCM above which the refinement and the reduction of the pore volume are not occurring which, as a consequence, decreases the mechanical properties of the paste [60].

Acting as nano-reinforcement and as filler, nanoparticles can densify the microstructure and the interfacial transition zone (ITZ), and thereby lead to a reduced porosity [61]. Oil well cements

designed with nano-silica showed a decrease in porosity and permeability [62]. The addition of nano-silica refines the pore structure of designed concrete pavement and enhances the resistance to chloride penetration. However, for the concrete pavement containing polypropylene fibers and nano-silica, the pore structure is coarsened and the resistance to chloride penetration is reduced [63].

Through addition of ultrafine layer silicates, it was found that the C-S-H growth on the clay particles resulted in structures determined by the size and shape of the clay particles and the negative charge of some of the clay minerals [64]. Portland cements containing palygorskite and bentonite have a more open structure consisting of interconnected fine pores. In mortars with clays added the interfacial transition zone (ITZ) is connected to the system of interconnected fine pores.

2.7 Mechanical properties

Nano-SiO_2 has been found to be more efficient in enhancing strength than silica fume [65-68]. Addition of 10% nano-SiO_2 with dispersing agents increased the compressive strength of cement mortars at 28-day by as much as 26%, compared to only a 10% increase with the addition of 15% silica fume [69]. Even the addition of small amounts (0.25%) of nano-SiO_2 increased the strength, improving the 28-day compressive strength by 10% and flexural strength by 25% [70].

Flexural and compressive strength of hardened cement paste increased with the addition of nano-$CaCO_3$ at the ages of 7-day and 28-day, and the optimal content of nano-$CaCO_3$ addition was 1% [71]. Adding 1% nano-$CaCO_3$ increased the 7-day and 28-day compressive strength and decreased the free drying shrinkage of self-consolidating concrete [72].

The replacement of ordinary cement paste by 6 wt. % nano-metakaolin increased the compressive strength of blended mortar by 18% compared to control mix and the combination of 6 wt. % nano-metakaolin and 0.02 wt. % carbon nanotubes increased the compressive strength by

29% than control [73]. The composite with 0.60% of added nano-montmorillonite by weight of cement increased the compressive strength by 13.24% at the age of 56-day [74].

2.8 Drying shrinkage

Drying shrinkage is a characteristic property of hardened cement paste. Hardened cement paste is a highly porous material with a large specific surface area, primarily due to the porous microstructure of the main hydration product, $CaO–SiO_2–H_2O$ (C-S-H). Large quantities of water vapour are adsorbed on the internal surface of the hydration products. The volume of hardened cement paste is sensitive to its moisture content. When exposed to environmental humidity, which is less than 100% RH, a saturated paste begins to lose water and shrink. The shrinkage on first drying is partly irreversible.

Four primary mechanisms control the drying shrinkage of hardened cement paste. These are capillary stress, disjoining pressure, surface free energy, and movement of interlayer water [2]. Each has an effective range of relative humidity. There is no unified theory at present which adequately explains the reversible and irreversible drying shrinkage behavior over the entire relative humidity region.

Capillary pressure works at high relative humidity (RH) between 90% and 45%. Meniscus form in capillary pores once drying begins, and as the water evaporates, they proceed inward. The system contracts because tensile forces within the meniscus are balanced by forces in the pore walls. The relationship between the equilibrium vapor pressure above a meniscus and its radius of curvature is given by the Kelvin equation:

$$\ln (p/p_0) = (2\Upsilon V_m)/rRT \qquad 2.12$$

where p = vapor pressure over a curved meniscus, p_0 = vapor pressure over a planar surface, Υ = surface tension of water, R = gas constant, T = temperature, V_m = molar volume of water, and r =

the radius of curvature of the meniscus. The capillary pressure generated by a meniscus in a cylindrical pore is a function of the radius of curvature of the meniscus according to:

$$P_{cap} = 2\Upsilon/r \qquad 2.13$$

Combination of equations 2.12 and 2.13 gives:

$$P_{cap} = (RT/V_m) \ln (p/p_0) = K \ln (p/p_0) \qquad 2.14$$

where K= a materials constant. Thus, capillary pressure is a function of relative humidity. In cement paste, the strain resulting from a capillary stress must be a function of the pore structure, pore geometry, and the elastic modulus of the solid phase that the pressure is acting upon.

However, it is suggested that a liquid (capillary) can exist in the pores only if the capillary tension under the meniscus (which is given by the Kelvin Laplace equation) does not exceed the tensile strength of the liquid, which is often thought to be exhausted at no less than 45% of the saturation pressure, if not much higher. When the critical pressure (p/p_0) is reached, the meniscus collapses and this mechanism is ineffective.

Surface free energy is believed to operate over a large range of relative humidities. Water molecules adsorbed onto C-S-H particles reduce the surface free energy by satisfying bonds at the surface. When this water is removed during drying, the tensile forces build and shrinkage results. Since the surface free energy changes the most with adsorption of the first two monolayers, shrinkage by this mechanism is believed to have the most influence at low relative humidities (< 33% RH) [75].

Disjoining pressure is caused by the removal of adsorbed water from C-S-H particles. According to Powers [76], the forces surrounding C-S-H particles are balanced by an attractive van der Waals forces and repulsive forces from the adsorbed water layer. As relative humidity is decreased, the water layer surrounding C-S-H particles get thinner and the particles are drawn closer together. This mechanism is believed to be effective only above 11% RH because multilayer

adsorption of water is required for the film to exist. Movement of interlayer water operates below 11% relative humidity [77].

2.9 Durability

The durability of concrete is largely related to concrete permeability. The intrusions of gas, liquid and ions may cause harmful stresses and chemical changes in concrete that will affect its integrity. Nano-silica addition reduces concrete water permeability and rapid chloride penetration and help to control the leaching of calcium, which is closely associated with various types of concrete degradation [78-82]. 1% nano-$CaCO_3$ addition increased concrete freezing-thawing resistance and reduce concrete permeability [72]. The electromigration test showed that, for cement mortars of the same mix design, the incorporation of nanoparticles (Fe_2O_3, Al_2O_3, TiO_2, and SiO_2) and nano clays (nano-montmorillonite) improved the chloride penetration resistance of the mortar [83]. The nanomaterials also reduced the general ionic permeability of the mortar, as indicated by the reduced electric charge passing through.

2.10 References

[1] K. Sobolev, "Nanotechnology and nanoengineering of construction materials," in Nanotechnology in Construction Proceedings of NICOM5, K. Sobolev and S. P. Shah, Eds., ed: Springer International Publishing, 2015, pp. 3-13.

[2] H. F. W. Taylor, Cement Chemistry, 2 ed. London: Thomas Telford Publishing, 1997.

[3] "U.S. Geological Survey," Jannuary 2009.

[4] J. S. Damtoft, J. Lukasik, D. Herfort, D. Sorrentino, and E. M. Gartner, "Sustainable development and climate change initiatives," Cement and Concrete Research, vol. 38, pp. 115-127, 2008.

[5] Q. Zeng and K. Li, "Reaction and microstructure of cement–fly-ash system," Materials and Structures, vol. 48, pp. 1703-1716, 2015.

[6] K. Vance, A. Kumar, G. Sant, and N. Neithalath, "The rheological properties of ternary binders containing Portland cement, limestone, and metakaolin or fly ash," Cement and Concrete Research, vol. 52, pp. 196-207, 2013.

[7] B. B. Sabir, S. Wild, and J. Bai, "Metakaolin and calcined clays as pozzolans for concrete: a review," Cement and Concrete Composites, vol. 23, pp. 441–454, 2001.

[8] J. M. Justice and K. E. Kurtis, "Influence of metakaolin surface area on properties of cement-based materials," Journal of Materials in Civil Engineering, vol. 19, pp. 762-771, 2007.

[9] A. A. A. Hassan, M. Lachemi, and K. M. A. Hossain, "Effect of metakaolin and silica fume on the durability of self-consolidating concrete," Cement and Concrete Composites vol. 34, pp. 801–807, 2012.

[10] O. Karahan, K. M. A. Hossain, E. Ozbay, M. Lachemi, and E. Sancak, "Effect of metakaolin content on the properties self-Consolidating lightweight concrete," Construction and Building Materials, vol. 31, pp. 320–325, 2012.

[11] C.-S. Poon, S. C. K. L Lam, Y.-L. Wong, and R. Wong, "Rate of pozzolanic reaction of metakaolin in high-performance cement pastes," Cement and Concrete Research, vol. 31, pp. 1301-1306, 2001.

[12] N. Garg and K. Wang, "Comparing the performance of different commercial clays in fly ash-modified mortars," Journal of Sustainable Cement-Based Materials, vol. 1, pp. 111-125, 2012.

[13] J. W. Bullard, H. M. Jennings, R. A. Livingston, A. Nonat, G. W. Scherer, S. Schweitzer, et al., "Mechanisms of cement hydration," Cement and Concrete Research, vol. 41, pp. 1208–1223, 2011.

[14] B. Lothenbach and F. Winnefeld, "Thermodynamic modelling of the hydration of Portland cement," Cement and Concrete Research vol. 36, pp. 209 – 226, 2006.

[15] K. L. Scrivener, P. Juilland, and P. J. M. Monteiro, "Advances in understanding hydration of Portland cement," Cement and Concrete Research, vol. 78, pp. 38-56, 2015.

[16] J. Stark, "Recent advances in the field of cement hydration and microstructure analysis," Cement and Concrete Research, vol. 41, pp. 666-678, 2011.

[17] B. Y. Lee and K. E. Kurtis, "Influence of TiO_2 nanoparticles on early C_3S hydration," Journal of the American Ceramic Society, vol. 93, pp. 3399–3405, 2010.

[18] T. Sato and F. Diallo, "Seeding effect of nano-$CaCO_3$ on the hydration of tricalcium silicate," Journal of the Transportation Research Board, pp. 61-67, 2010.

[19] T. Oey, A. Kumar, J. W. Bullard, N. Neithalath, and G. Sant, "The filler effect: The influence of filler content and surface area on cementitious reaction rates," Journal of the American Ceramic Society, vol. 96, pp. 1978-1990, 2013.

[20] J. J. Thomas, H. M. Jennings, and J. J. Chen, "Influence of nucleation seeding on the hydration mechanisms of tricalcium Ssilicate and cement," The Journal of Physical Chemistry C, vol. 113, pp. 4327–4334, 2009.

[21] L. P. Singh, S. R. Karade, S. K. Bhattacharyya, M. M. Yousuf, and S. Ahalawat, "Beneficial role of nanosilica in cement based materials – A review," Construction and Building Materials, vol. 47, pp. 1069–1077, 2013.

[22] H. Krøyer, H. Lindgreen, H. J. Jakobsen, and J. Skibsted, "Hydration of Portland cement in the presence of clay minerals studied by ^{29}Si and ^{27}Al MAS NMR spectroscopy," Advances in Cement Research, vol. 15, pp. 103-112, 2003.

[23] G. W. Scherer, J. Zhang, J. A. Quintanilla, and S. Torquato, "Hydration and percolation at the setting point," Cement and Concrete Research, vol. 42, pp. 665–672, 2012.

[24] G. Sant, C. F. Ferraris, and J. Weiss, "Rheological properties of cement pastes: A discussion of structure formation and mechanical property development," Cement and Concrete Research, vol. 1286-1296, p. 38, 2008.

[25] V. A. Hackley and C. F. Ferraris, "The use of nomenclature in dispersion science and technology," NIST Recommended Practice Guide, SP 960-3, 2001.

[26] C. Rößler, A. Eberhardt, H. Kučerová, and B. Möser, "Influence of hydration on the fluidity of normal Portland cement pastes," Cement and Concrete Research, vol. 38 pp. 897–906, 2008.

[27] T. C. Powers, The Properties of Fresh Concrete. New York: Wiley, 1968.

[28] D. P. Bentz, C. F. Ferraris, M. A. Galler, A. S. Hansen, and J. M. Guynn, "Influence of particle size distributions on yield stress and viscosity of cement–fly ash pastes," Cement and Concrete Research, vol. 42, pp. 404–409, 2012.

[29] C. F. Ferraris, K. H. Obla, and R. Hill, "Influence of mineral admixtures on the rheology of cement paste and concrete," Cement and Concrete Research, vol. 31, pp. 245-255, 2001.

[30] R. D. Ferron, S. Shah, E. Fuente, and C. Negro, "Aggregation and breakage kinetics of fresh cement paste," Cement and Concrete Research, vol. 50, pp. 1-10, 2013.

[31] L. G. Li and A. K. H. Kwan, "Mortar design based on water film thickness," Construction and Building Materials, vol. 25, pp. 2381-2390, 2011.

[32] N. A. Tregger, M. E. Pakula, and S. P. Shah, "Influence of clays on the rheology of cement pastes," Cement and Concrete Research vol. 40, pp. 384-391, 2010.

[33] S. Amzian and C. F. Ferraris, "Cementitious paste setting using rheological and pressure measurements," ACI Materials Journal, vol. 104, pp. 137-145, 2007.

[34] L. J. Parrott, M. Geiker, W. A. Gutteridge, and D. Killoh, "Monitoring Portland cement hydration: Comparison of methods," Cement and Concrete Research, vol. 20, pp. 919-926, 1990.

[35] K. Scrivener, R. Snellings, and B. Lothenbach, A Practical Guide to Microstructural Analysis of Cementitious Materials: CRC Press 2015.

[36] T. Allen, Particle Size Measurement, 3 ed. London, UK: Chapman and Hall, 1981.

[37] ASTM C1738-11, "Standard practice for high-shear mixing of hydraulic cement paste," ASTM International, West Conshohocken, PA, 2011.

[38] C. Sauter, M.A. Emin, H.P. Schuchmann, and S. Tavman, "Influence of hydrostatic pressure and sound amplitude on the ultrasound induced dispersion and de-agglomeration of nanoparticles.," Ultrasonics Sonochemistry, vol. 15, pp. 517-523, 2008.

[39] S. Kawashima, J.-W. T. Seo, D. Corr, M. C. Hersam, and S. P. Shah, "Dispersion of $CaCO_3$ nanoparticles by sonication and surfactant treatment for application in fly ash–cement systems," Materials and Structures, vol. 47, pp. 1011-1023, 2014.

[40] K. Higashitani, K. Yoshida, N. Tanise, and H. Murata, "Dispersion of coagulated colloids by ultrasonication," Colloids and Surfaces A: Physicochemical and Engineering Aspects, vol. 81, pp. 167-175, 1993.

[41] J. S. Taurozzi and V. A. Hackley, "Preparation of nanoparticle dispersions from powdered material using ultrasonic disruption," National Institute of Standards and Technology Material Measurement Laboratory, Gaithersburg, MD 2012.

[42] J. Zhang and G. W. Scherer, "Comparison of methods for arresting hydration of cement," Cement and Concrete Research, vol. 41, pp. 1024-1036, 2011.

[43] D. P. Bentz and C. F. Ferraris, "Rheology and setting of high volume fly ash mixtures," Cement and Concrete Composites vol. 32, pp. 265–270, 2010.

[44] E. Berodier, "Impact of the supplementary cementitious materials on the kinetics and microstructural development of cement hydration," Doctor of Philosophy, EPFL, 2015.

[45] E.-i. Tazawa, S. Miyazawa, and T. Kasai, "Chemical shrinkage and autogenous shrinkage of hydrating cement paste," Cement and Concrete Research, vol. 25, pp. 288–292, 1995.

[46] ASTM C1608, " Standard Test Method for Chemical Shrinkage of Hydraulic Cement Paste," ASTM International, West Conshohocken, PA, 2012.

[47] L. Senff, J. A. Labrincha, V. M. Ferreira, D. Hotza, and W. L. Repette, "Effect of nano-silica on rheology and fresh properties of cement pastes and mortars," Construction and Building Materials, vol. 23, pp. 2487–2491, 2009.

[48] B. W. Jo, C. H. Kim, and J. H. Lim, "Investigations on the development of powder concrete with nano-SiO_2 Particles," Journal of Civil Engineering, vol. 11, pp. 37-42, 2007.

[49] L. Raki, J. Beaudoin, R. Alizadehl, J. Makar and T. Sato, "Cement and concrete nanoscience and nanotechnology," Materials, pp. 918-942, 2010.

[50] K. Sobolev, I. Flores, R. Hermosillo, and L.M. Torres-Martínez, "Nanomaterials and nanotechnology for high-performance cement composites," in Proceedings of ACI Session on “Nanotechnology of Concrete: Recent Developments and Future Perspectives”, Denver, 2006.

[51] V.L. Bonavetti, V. F. Rahhal, and E.F.Irassar, "Studies on the carboaluminate formation in limestone filler-blended cements," Cement and concrete research, vol. 31, pp. 853-859, 2001.

[52] G. Kakali, S. Tsivilis, E. Aggeli, and M. Bati, "Hydration products of C_3A, C_3S and Portland cement in the presence of $CaCO_3$," Cement and Concrete Research vol. 30, pp. 1073-1077, 2000.

[53] B. Lothenbach, G. L. Saout, E. Gallucci, and K. Scrivener, "Influence of limestone on the hydration of Portland cements," Cement and Concrete Research 38 (2008) 848–860, vol. 38, pp. 848-860, 2008.

[54] K. C. Jo BW, Lim JH, "Characteristics of cement mortar with nano-SiO_2 particles," ACI Materials Journal, vol. 104, pp. 404-407, 2007.

[55] J. J. Gaitero, I. Campillo, and A. Guerrero, "Reduction of the calcium leaching rate of cement paste by addition of silica nanoparticles," Cement and Concrete Research, vol. 38, pp. 1112-1118, 2008.

[56] M. Arabani, A. K. Haghib, A. M. Sanic, and N. Kamboozia, "Use of Nanoclay for Improvement the Microstructure and Mechanical Properties of Soil," in Proceedings of the 4th International Conference on Nanostructures, Kish Island, I.R.Iran, 2012.

[57] S. Mindess, J. F. Young, and D. Darwin, Concrete 2ed. Upper Saddle River, NJ 07458, U.S.A.: Pearson, 2002.

[58] R. L. Day and B. K. Marsh, "Measurement of porosity in blended cement pastes," Cement and Concrete Research, vol. 18, pp. 63-73, 1988.

[59] Z. Yu and G. Ye, "The pore structure of cement paste blended with fly ash," Construction and Building Materials vol. 45, pp. 30-35, 2013.

[60] E. Berodier and K. Scrivener, "Evolution of pore structure in blended systems," Cement and Concrete Research, vol. 73, pp. 25-35, 2015.

[61] F. Sanchez and K. Sobolev, "Nanotechnology in concrete – A review," Construction and Building Materials, vol. 24, pp. 2060-2071, 2010.

[62] M. Choolaei, A. M. Rashidi, M.Ardjmand, A. Yadegari, and Hamid Soltanian, "The effect of nano silica on the physical properties of oil well cement," Materials Science and Engineering A, vol. 538, pp. 288-294, 2012.

[63] M. Zhang and H. Li, "Pore structure and chloride permeability of concrete containing nano-particles for pavement," Construction and Building Materials, pp. 608-616, 2011.

[64] H. Lindgreen, M. Geiker, H. Krøyer, N. Springer, and J. Skibsted, "Microstructure engineering of Portland cement pastes and mortars through addition of ultrafine layer silicates," Cement and Concrete Composites, vol. 30, pp. 686-699, 2008.

[65] H. Li, H. Xiao, and J. Ou, "A study on mechanical and pressure-sensitive properties of cement mortar with nanophase materials," Cement and Concrete Research, vol. 34, pp. 435-438, 2004.

[66] H. Li, M. Zhang, and J. Ou, "Abrasion resistance of concrete containing nanoparticles for pavement," Wear vol. 260, pp. 1262-1266, 2006.

[67] B.W. Jo, K. C.H. Kim, G.H. Tae, and J.B. Park, "Characteristics of cement mortar with nano-SiO_2 particles," Construct Build Mater vol. 21, pp. 1351-1355, 2007.

[68] Q. Ye, Z. Zhang, D. Kong, and R. Chen, " Influence of nano-SiO_2 addition on properties of hardened cement paste as compared with silica fume," Construction and building materials, vol. 21, pp. 539-545, 2007.

[69] H. Li, H. Xiao, Y. Jie, and J. Ou, "Microstructure of cement mortar with nanoparticles," Compos B Eng vol. 35, pp. 185-189, 2004.

[70] I. F. K. Sobolev, L. M. Torres-Martinez, P. L. Valdez, E. Zarazua, and E. L. Cuellar, "Engineering of SiO_2 Nanoparticles for Optimal Performance in Nano Cement-Based Materials," Nanotechnology in Construction 3, pp. 139-148, 2009.

[71] X. Liu, L. Chen, A. Liu, and X. Wang, "Effect of Nano-$CaCO_3$ on Properties of Cement Paste," Energy Procedia, vol. 16, pp. 991-996, 2012.

[72] X. Wang, K. Wang, J. Li, N. Garg, S. P. Shah, "Properties of self-consolidating concrete containing high volume supplementary cementitious materials and nano-limestone," in Proceedings of the Fifth North American Conference on the Design and Use of Self-Consolidating Concrete, Chicago, Illinois, USA, 2013.

[73] M.S. Morsy, S. H. Alsayed, and M. Aqel, "Hybrid effect of carbon nanotube and nano-clay on physico-mechanical properties of cement mortar," Construction and Building Materials, vol. 25, pp. 145-149, 2011.

[74] T.P. Chang, J. Y. Shih, K.M. Yang, and T.C. Hsiao, "Material properties of portland cement paste with nanomontmorillonite," J Mater Sci vol. 42, pp. 7478-7487, 2007.

[75] R. P. Lohtia, B. D. Nautiyal, and O. P. Jain, "Creep af Fly Ash Concrete," ACI vol. 73, pp. 469-472, 1976.

[76] T. C. Powers, "The thermodynamics of volume change and creep," Matériaux et Construction, vol. 1, pp. 487-507, 1968.

[77] M. B. Pinson, E. Masoero, P. A. Bonnaud, H. Manzano, Q. Ji, S. Yip, et al., "Hysteresis from Multiscale Porosity: Modeling Water Sorption and Shrinkage in Cement Paste," Phys. Rev. Applied, vol. 3, pp. 1-17, 2015.

[78] M. Khanzadi, M. Tadayon, H. Sepehri, and M. Sepehri, "Influence of nano-silica Particles on Mechanical Properties and Permeability of Concrete," in Second international conference on sustainable construction materials and technologies, Italy, 2010.

[79] A. N. Givi, S. A. Rashid, F. N. A. Aziz, and M. A. M. Salleh, "Investigations on the development of the permeability properties of binary blended concrete with nano-SiO_2," Journal of Composite Materials, vol. 45, pp. 1931-1938, 2010.

[80] A. N. Givi, S. A. Rashid, F. N. A. Aziz, and M. A. M. Salleh, "The effects of lime solution on the properties of SiO_2 nanoparticles binary blended concrete," Composites: Part B, vol. 42, pp. 562-569, 2011.

[81] M. Zhang and H. Li, "Pore structure and chloride permeability of concrete containing nano-particles for pavement," Construction and Building Materials, vol. 25, pp. 608-616, 2011.

[82] A. Shamsai, S. Peroti, K.Rahmani and L. Rahemi, "Effect of Water-Cement Ratio on Abrasive Strength,Porosity and Permeability of Nano-Silica Concrete," World Applied Sciences Journal, vol. 17, pp. 929-933, 2012.

[83] X. He and X. Shi, "Chloride permeability and microstructure of Portland cement mortars incorporating nanomaterials," Journal of the Transportation Research Board, pp. 13-21, 2008.

Tables:

Table 2.1 Important characteristics of a Type I cement, a Class-F fly ash, and a metakaolin.

Chemical analysis	PC	FA	MK
SiO_2	20.20	46.00	53.00
Al_2O_3	4.70	17.80	43.80
Fe_2O_3	3.30	18.20	0.43
SO_3	3.30	2.59	0.03
CaO	62.90	8.40	0.02
MgO	2.70	0.95	0.03
Eq. Na_2O	0.54	2.01	0.35
P_2O_5	-	0.11	-
TiO_2	-	0.93	-
SrO	-	0.03	-
BaO	-	0.05	-
LOI	1.10	1.49	-
C_3S	58		
C_2S	7		
Physical Properties			
Specific gravity	3.15	2.51	2.56
Fineness by air permeability (m^2/kg)	391	310	13000

Table 2.2 Comparison of drying techniques [42].

Technique	Process	Pros	Cons
Oven drying	Atmospheric pressure, 35⩽T (˚C)⩽ 105	Fast	Microcracking, degrade C–S–H, ettringite
Microwave drying	Lower power, several minutes	fast	Destroy microstructure
D-drying	Vacuum < 4.2 Pa, solid CO_2 + alcohol at -79°C, 14 days	Definition of "non-evaporable" water	Remove some bound water
P-drying	1.1 Pa, room temperature		Contains residual pore water
Vacuum drying	Vacuum chamber 0.1 Pa		Degrade ettringite and monosulphate, increase pore volume, damage pore structure, Remove less water
Freeze drying	Submerge in liquid N_2 > 15 min, then place in a freeze dryer for > 1 day	Less damage to structure No hydration products change	Degrade ettringite and monosulphate
Supercritical drying	Replace pore water by solvent, then freon, supercritical drying of freon	Preserve pore structure	Expensive complex process
Solvent exchange	Solvent renewed regularly, then dried in a desiccator	Small damage to pore structure; gives finest pore size distribution; applies least stress Isopropanol is the best solvent	May partially dehydrate the C–S–H and ettringite; interaction with cement, could be sorbed into cement phases and not be removed without affecting microstructure

Table 2.3 Classification of pores and features in cement paste [2].

Type of pore	Size/nm	Description	Water	Properties
Capillary pores	50～10000	Large	Evaporable bulk water	Permeability, strength
	10～50	Medium	Evaporable moderate menisci	Permeability, strength, shrinkage (high RH)
Gel pores	2.5～10	Small	Evaporable strong menisci	Shrinkage (to 50% RH)
	0.5～2.5	Micropores	Non-evaporable -No menisci -Intermolecular interaction	Shrinkage, creep (35-11% RH)
	<0.5	Structural	Non-evaporable -Ionic/covalent bond	Shrinkage, creep (<11% RH)

Figures:

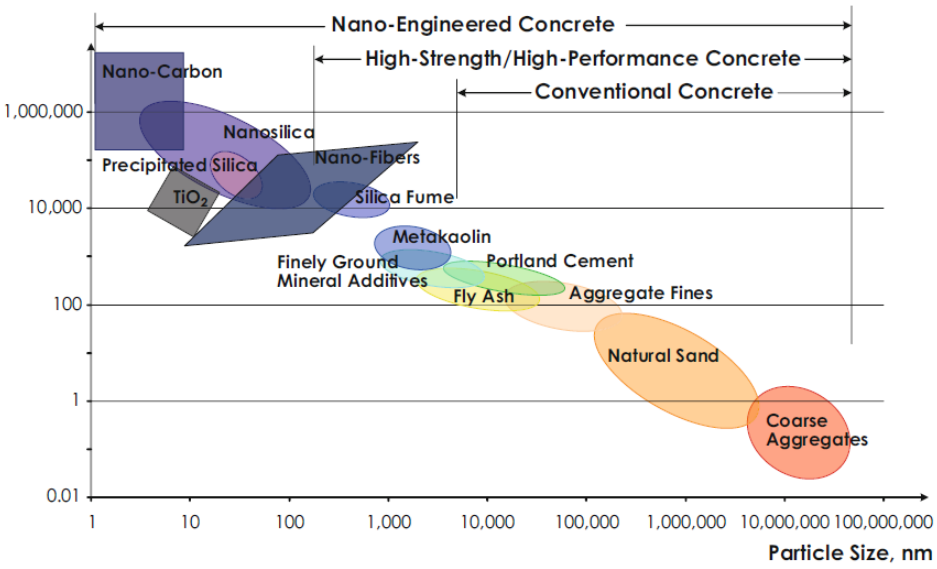

Figure 2.1. The particle size and specific surface area scale related to concrete materials [1].

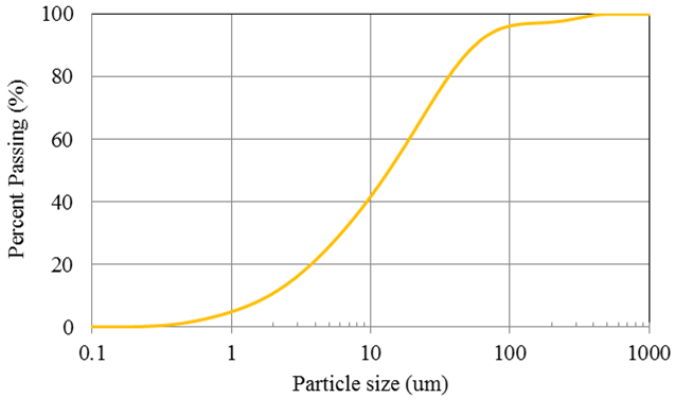

Figure 2.2. The particle size distribution of a Type I cement.

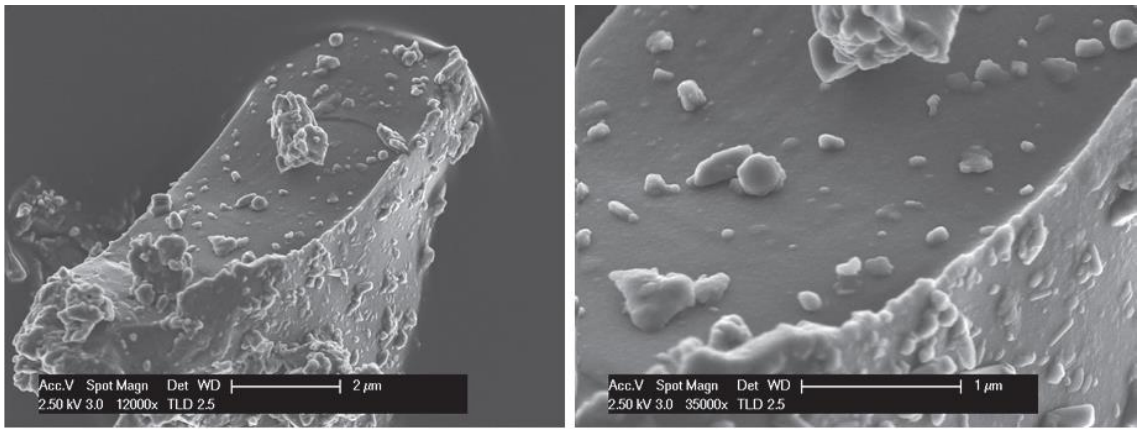

Figure 2.3. SEM images of cement grain and detail of the surface at 2.5kV [44].

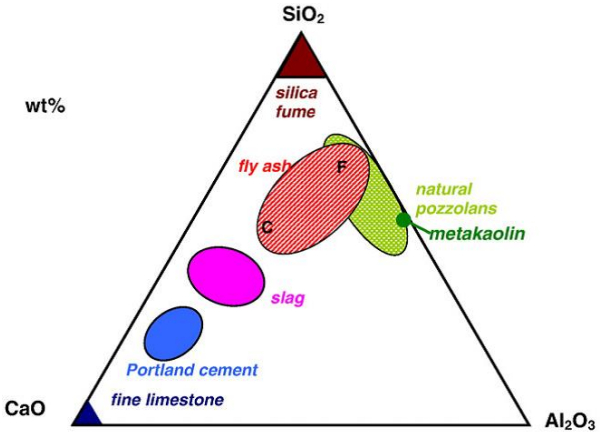

Figure 2.4. CaO-Al_2O_3-SiO_2 ternary diagram of cementitious materials [15].

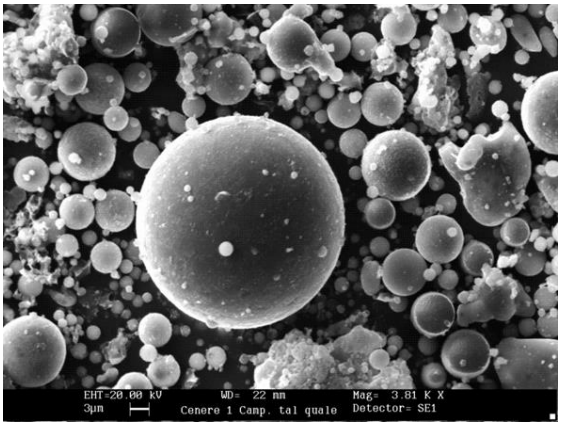

Figure 2.5. SEM image of typical fly ash particles at 20 kV with 20 mm working distance [44].

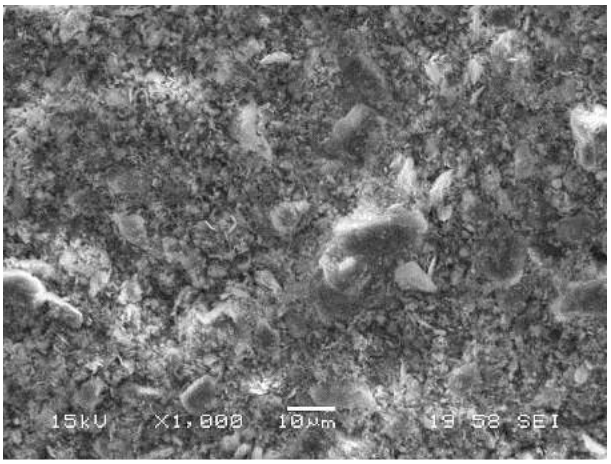

Figure 2.6. SEM micrograph of metakaolin particles at 1000X [35].

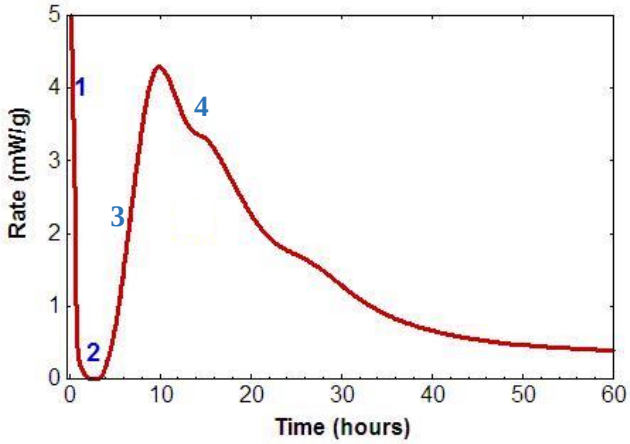

Figure 2.7. Typical isothermal calorimetry curve of cement hydration [35].

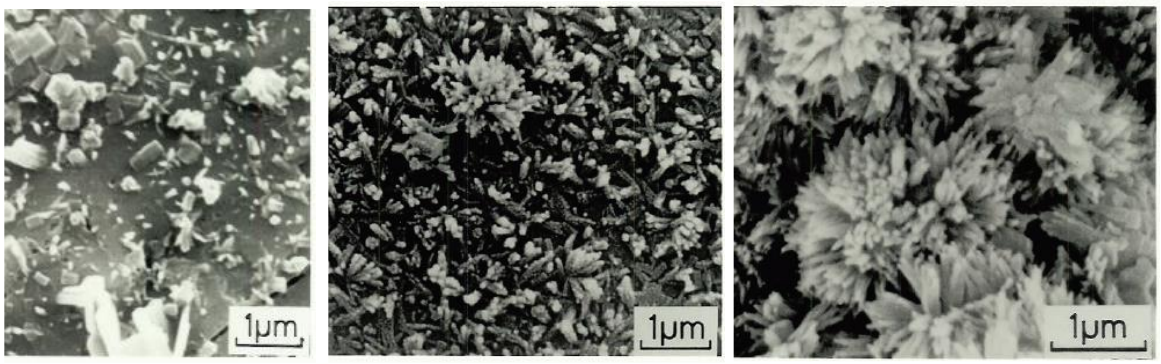

Figure 2.8. Cement hydrated for 3 hours, 6 hours and 10 hours [44].

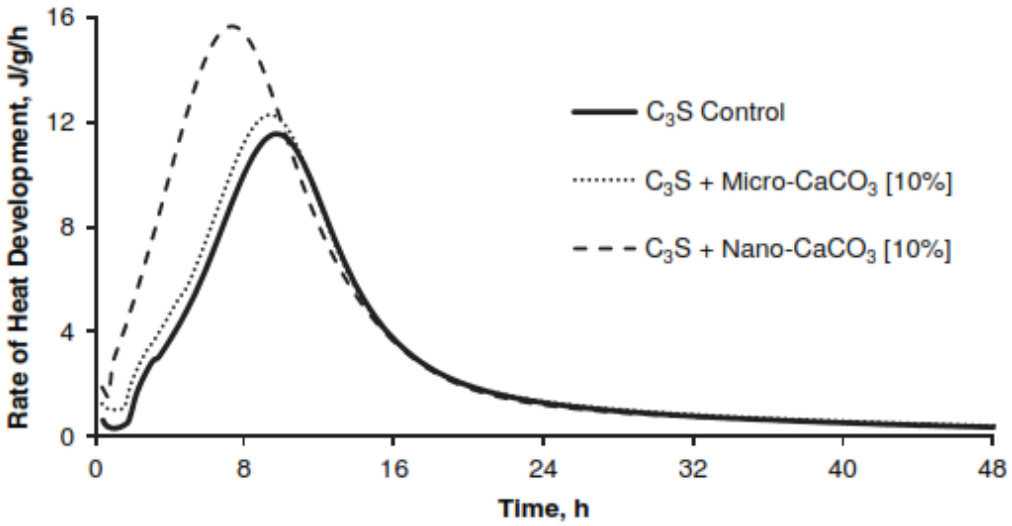

Figure 2.9. Conduction calorimetry results for C_3S control and C_3S with additions of 10% micro-$CaCO_3$ and nano- $CaCO_3$ [18].

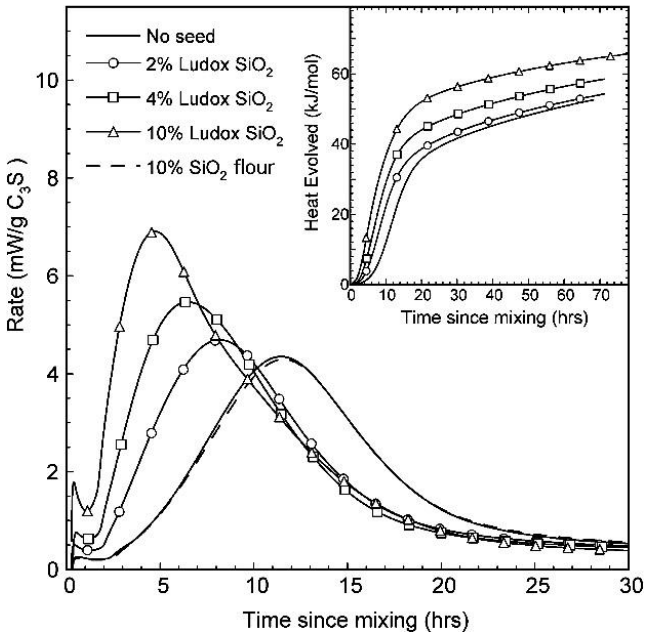

Figure 2.10. Effect of colloidal silica and silica flour (dashed line) on the hydration kinetics of C_3S [20].

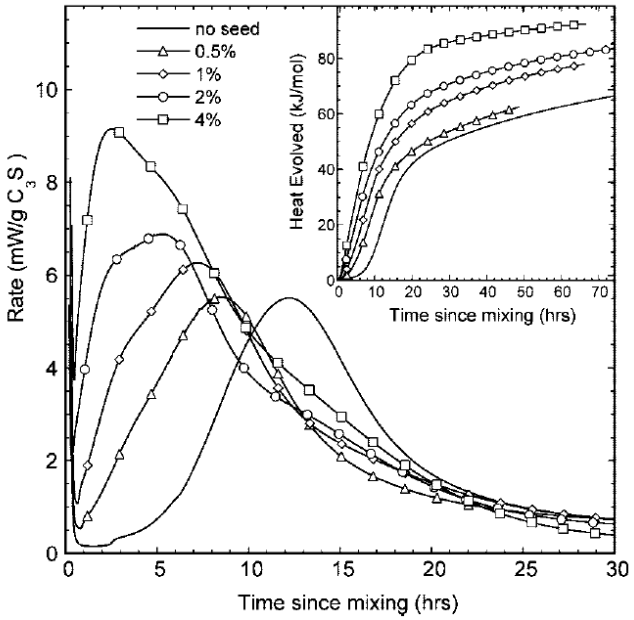

Figure 2.11. Effect of C-S-H seed made with a molar Ca/Si ratio of 1 on the early hydration kinetics of C_3S hydration. The seed amounts refer to the mass of solid C-S-H per mass of C_3S [20].

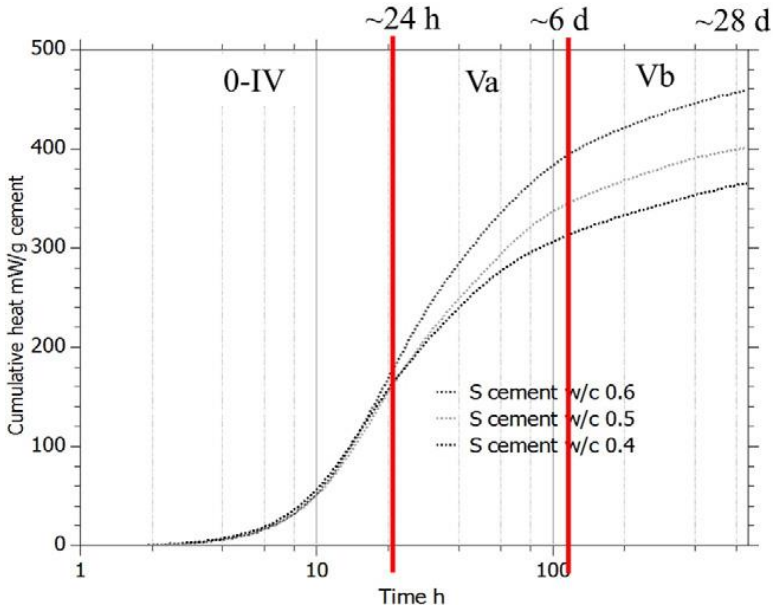

Figure 2.12. Cumulative heat of hydration for a plain portland cement at different water to cement ratios [15].

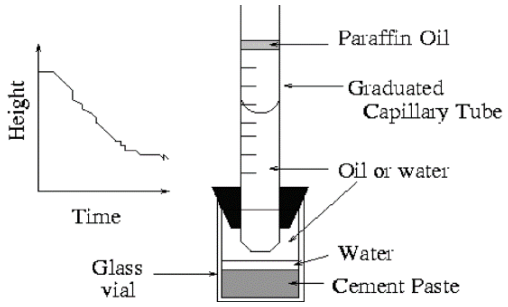

Figure 2.13. Illustration of experimental setup for chemical shrinkage test (ASTM C 1608).

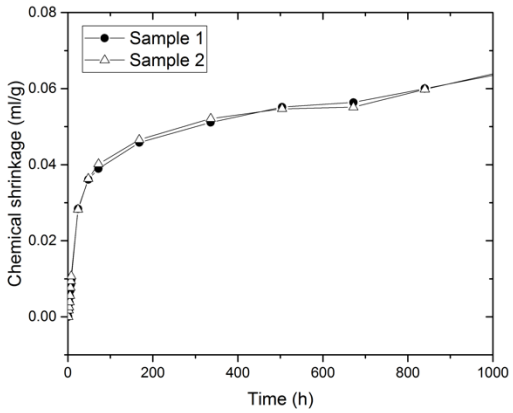

Figure 2.14. Chemical shrinkage measurement following the ASTM C1608 procedure conducted at the PCC lab on two replicate samples of a portland cement paste (w/c = 0.4, sample height = 10 mm).

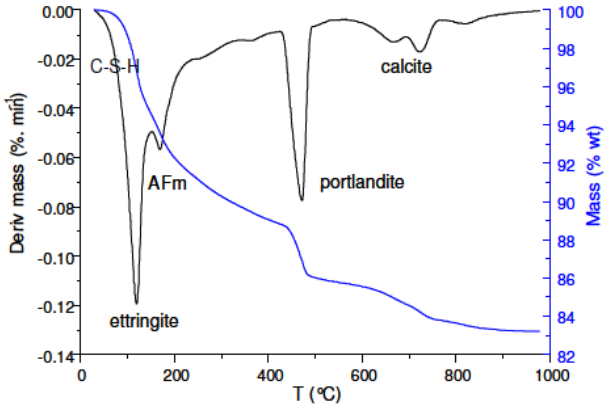

Figure 2.15. Typical TGA and DTG curves for a hydrated cement paste (4 days old). Adopted from [35].

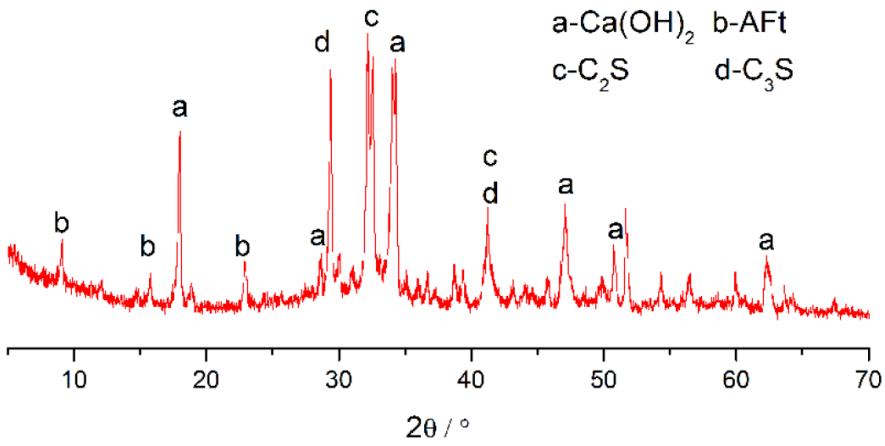

Figure 2.16. XRD scan of a hydrated cement paste.

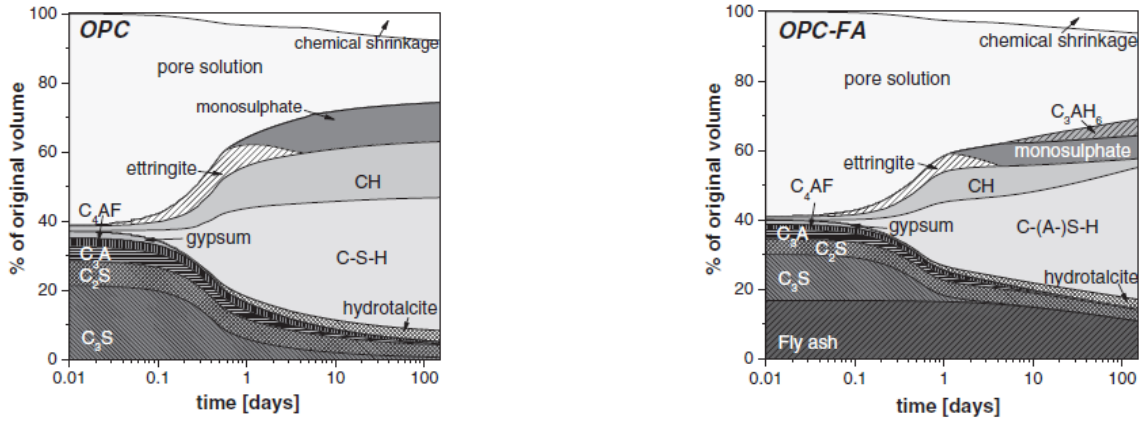

Figure 2.17. The volume of the different phases as function of time in hydrating cement pastes modelled by GEMS (w/cm=0.4) [35].

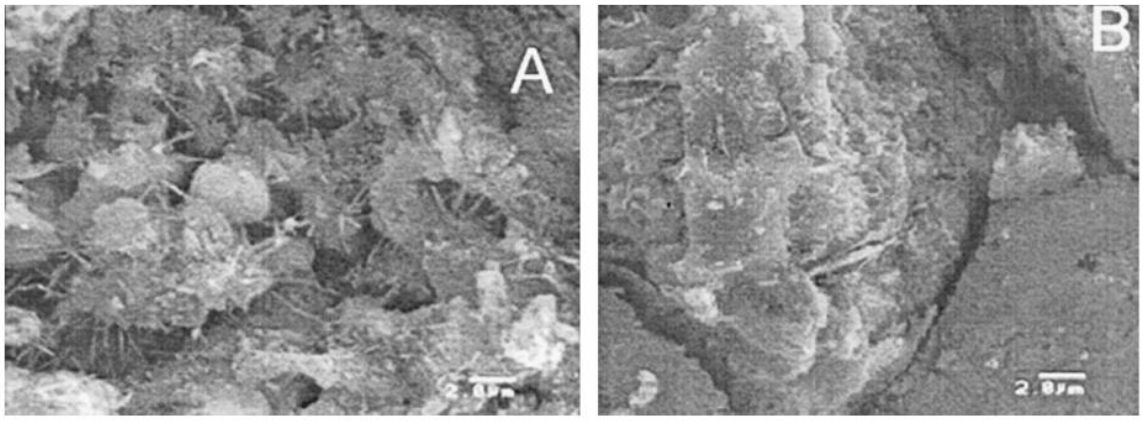

Figure 2.18. SEM micrographs of plain (A) and nano-silica modified cement paste (B) [21].

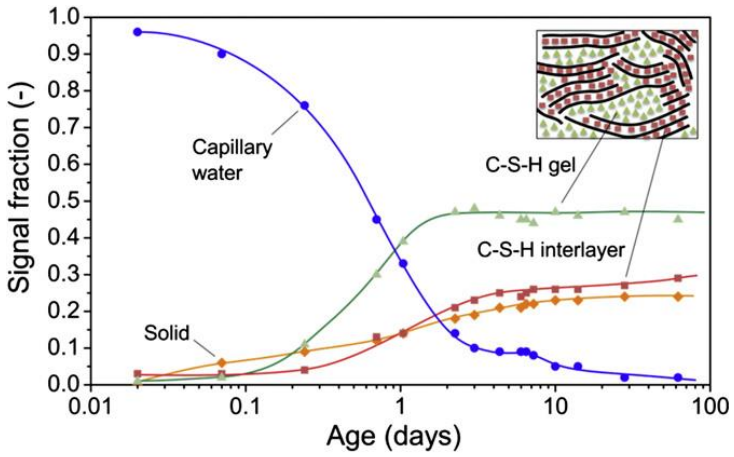

Figure 2.19. Evolution of states of water in white cement paste at w/c=0.4 [15].

CHAPTER 3. EFFECTS OF NANOMATERIALS ON THE HYDRATION KINETICS AND REHOLOGY OF PORTLAND CEMENT PASTES

Modified from a paper published in ASTM Advances in Civil Engineering Materials

Xin Wang[a], Kejin Wang[b], Jussara Tanesi[c], Ahmad Ardani[d]

[a]Dept. of Civil, Construction, and Environmental Engineering, Iowa State Univ., Ames, Iowa 50010. Tel: 515-294-2140. Email: wangxin@iastate.edu
[b]Dept. of Civil, Construction, and Environmental Engineering, Iowa State Univ., Ames, Iowa 50010. Tel: 515-294-2151. Email: kejinw@iastate.edu
[c]SES Group & Associates LLC, Turner Fairbank Highway Research Center/FHWA, 6300 Georgetown Pike, McLean VA 22101. Tel: 202-493-3485. Email: Jussara.Tanesi.CTR@dot.gov
[d]FHWA, Turner Fairbank Highway Research Center/FHWA, 6300 Georgetown Pike, McLean VA 22101. Tel: 202-493-3422. Email: ahmad.ardani@dot.gov

Abstract

In this paper, effects of nanomaterials on the hydration kinetics and rheology of ordinary portland cement pastes were investigated. Three nanomaterials, nano-limestone, nano-silica, and nano-clay (a highly purified magnesium aluminosilicate), were added to a cement paste at levels of 0.0, 0.5, 1.0, and 1.5% (by mass) of cement. Heat of the cement hydration of the pastes was measured using isothermal calorimetry. Rheological behavior of the pastes was characterized using a rotational rheometer. The rheology tests were performed at intervals of 10, 30, 60, 90, and 120 minutes after the cement was mixed with water. Set times of the pastes were measured according to ASTM C191. The experimental results indicate that the addition of nano-limestone and nano-silica accelerated cement early hydration, the maximum heat flow increased while the time to reach the heat flow peaks decreased. Initial and final set times were also reduced. These effects were enhanced with increased nano-addition level. The addition of nano-clay also significantly increased the intensity of the heat flow peaks, especially, the peak corresponding to the renewed reaction of the aluminate phase. Addition of these nanomaterials generally increased

yield stress and viscosity of the cement paste, especially after 60 min when cement hydration began to accelerate. Nano-clay greatly affected the rheological behavior of cement pastes. Significantly higher shear stresses were required to initiate the flow.

3.1 Introduction

In recent years, nanomaterials have been increasingly explored for their beneficial roles in the field of cement and concrete materials. Nanoparticles are defined as particles with lengths ranging from 1 to 100 nanometers in two or three dimensions [1]. The high surface area to volume ratio can provide nanoparticles with the potential for excellent chemical reactivity. Much of the work to date has been with nano-silica (nano-SiO_2) and nano-titanium oxide (nano-TiO_2) [2-4]. There has also been an increase in studies applying nano-limestone (nano-$CaCO_3$), nano-clay, nano-iron (nano-Fe_2O_3), nano-carbon, and nano-alumina (nano-Al_2O_3) particles [4-6].

The effects of nanomaterial on the performance of cement-based materials are reflected in the workability, the mechanical behavior, and durability properties of the resulting concrete, and are strongly influenced by the physical and chemical interactions involved and, consequently, the early hydration kinetics and rheological properties of cement pastes.

The primary focus of the research presented here is to study the effects of different nanomaterials on early hydration kinetics and rheological behavior of cement pastes. The kinetics of cement hydration has been measured using a variety of techniques [7]. Isothermal calorimetry has been widely applied for this purpose since it can conveniently and effectively measure the rate of cement hydration [7-9]. In this study, isothermal calorimetry tests and the rheology measurement were performed on cement paste right after mixing. Set times of the paste were also performed using the Vicat needle penetration test as a reference.

3.2 Background

Nanoparticles can accelerate early cement hydration by providing a multitude of additional sites for the precipitation and growth of new regions of calcium-silicate-hydration gel (C-S-H), the principal product of cement hydration [4, 7]. Lee and Kurtis [10] studied the influence of non-reactive nano-TiO_2 powder on early C_3S hydration through simulations and isothermal calorimetry measurements, and they reported that the extent of the acceleration was linked to an increase in available nucleation sites (i.e., increase in solid surface area) provided by the TiO_2 nanoparticles. Gurney et al. [11] have also shown that reductions in setting times are directly proportional to provided fine limestone surface area in systems with nano/fine limestone additions.

Moreover, most of the nanomaterials, such as nano-silica, nano-limestone and nano-clay examined in this study can affect cement hydration by chemically reacting in systems.

Thomas et al. [9] showed through isothermal calorimetry that the hydration of tricalcium silicate (C_3S) and portland cement can be accelerated by addition of colloidal nano-silica (2-10 mass %) and synthesized C-S-H particles (1-4 mass %). The model they used to describe these effects proposes an early pozzolanic reaction on the nano-silica surface to form C-S-H particles. These C-S-H particles spread in the capillary pore space between cement particles and serve as seeds for the formation of C-S-H hydration product (autocatalysis) away from the particle surfaces where they don't interfere with the dissolution of cement grain.

Conduction calorimetry results indicated that 10% nano-$CaCO_3$ replacement accelerated the hydration of C_3S and portand cement pastes [5, 12]. The formation of small fibrous C-S-H products around the nano-$CaCO_3$ particles was observed through scanning electron microscopy (SEM) [12]. Zajac et al. [13] suggested that a relatively small quantity of calcite reacted to form hemicarbonate

and monocarbonate in portland cements when the gypsum was depleted, indirectly leading to more ettringite.

Clay materials are increasingly used to modify thixotropy and improve shape stability in minimal compaction energy concrete [14]. ^{29}Si MAS NMR spectra demonstrated that the addition of micro- or nano-sized layer silicates to portland cements accelerated cement hydration [15, 16] by increasing the degrees of hydration for both alite and belite [16]. The activity of clays in pozzolanic reactions has also been demonstrated [17].

Cement pastes set during the acceleration period, during which hydration products that form on the surfaces of clinker particles intersect, leading to the formation of clusters that eventually join into a continuous elastic network [18].

In the period before setting, the fluid properties of cement pastes dominate. The rheology of cement-based materials is a quantitative property that describes the fluids' deformation and flow [42]. The rheological behavior of a fluid such as cement paste, mortar, or concrete is often characterized by two parameters: yield stress τ_0 and plastic viscosity μ, as defined by the Bingham equation

$$\tau = \tau_0 + u\gamma \qquad 3.1$$

where τ is the shear stress applied to the material (in Pa), τ_0 is the yield stress (in Pa), μ is the plastic viscosity (in Pa·s), and γ is the shear strain rate (also called the strain gradient) (in s^{-1}). Unlike in the Newtonian model, cement paste has a yield stress that reflects the minimum stress needed to initiate a flow. The plastic viscosity measures the resistance of cement paste against increase in speed of movement [19, 20].

Key parameters influencing the rheology of cement pastes include: particle size distribution, volume fraction of particles, colloidal forces (van der Waals forces, electrostatic forces, etc.), hydrodynamic effects, and hydration progress [21, 22].

Before the acceleration period of cement hydration, cement paste rheology is primarily controlled by attractive-particle interactions. When water content is kept constant, the addition of nanomaterials can adversely affect the flowability of cement pastes and increase the yield stress: (1) the high surface area of nanoparticles to be wet and their tendency to agglomerate may decrease the amount of free water; and (2) nanoparticles can fill the gaps between cement particles and increase the connectivity of the network structure [23-25]. On the other hand, the addition of nanoparticles in cement pastes can theoretically increase particle-packing density, decrease the void ratio of solid particles, and increase the amount of free water for lubrication [23, 26]. Thus, the plastic viscosity could increase or decrease depending on these competing effects. Research has shown that the addition of nano-silica in cement pastes usually increased water demand and the yield stress and viscosity [2]. On the other hand, no consensus has been reached with respect to the effect on paste fluidity of the addition of limestone [23, 27]. Small additions of clay have been shown to increase the floc size, flocculation strength, and shear-yield stress of cement pastes [25, 28].

During the cement hydration acceleration period, inter-particle force bonds are gradually replaced and augmented by “cement hydration product” bonds, until eventually a continuous elastic network was formed (cement paste's setting process) [29]. Rheological measurements have been used to monitor the microstructure formation and mechanical property development (i.e. setting) of cementitious materials [19, 30].

3.3 Materials and methods

3.3.1 Materials and mix proportions

A commercial Type I/II portland cement (PC) was used with the physical properties and chemical analysis given in Table 3.1. Nanomaterials, nano-silica (NS), nano-limestone (NL), and nano-clay (NC), were added to the cement paste (water-to-cement ratio of 0.5) at levels of 0.5, 1.0, and 1.5% (by mass) of cement. The properties of the nanomaterials are shown in Tables 3.1 (NC) and 3.2 (NL and NS). Nano-clay is a highly purified magnesium alumino silicate, chemically exfoliated from bulk attapulgite to remove high levels of water-demand impurities such as smectite, bentonite, and other swelling clays. Under shearing, nano-clay breaks down into needle-like structures about – 1.75 um in average length and 3 nm in average diameter [28, 31]. Figure 3.1 shows a block diagram of the experimental work.

3.3.2 Preparation of nano-suspension

Nanoparticles tend to agglomerate due to their strong interparticle attraction (i.e. van der Waals forces). As agglomerates, they behave in the same way as particles of similar size, so it is important to properly disperse them. High-intensity ultrasound has been widely used to disperse nanoparticles in a liquid. Ultrasonication generates intense shock waves by collapsing cavitation, leading to collisions among particles. The agglomerated particles are thus agitated and split apart by these collisions [32].

In the present study, the nanomaterials used were first dispersed in water to form nanoparticle suspensions. The suspensions were then used as “mixing water” for paste mixing. To form a nano-suspension, the nanomaterial was added to the mixing water (distilled water) and ultrasonicated (frequency: 20 kHz; generating power: 600W) for 9 min. To prevent the water from boiling, the

suspension was sonicated 3 times for 3 min each. After each 3-min continuous ultrasonication, the suspension was cooled to room temperature.

3.3.3 Preparation of cement pastes under high shear mixing

The cement pastes used for the rheological measurements, the Vicat set time measurement and the hydration kinetics measurements were prepared as a single batch in a high-shear mixer according to ASTM C1738 [33].

3.3.4 Isothermal calorimetry test

To measure the hydration kinetics, about 5 g of cement paste were tightly sealed inside a 15 ml glass ampoule immediately after mixing and then placed into a TAM Air 8-Channel isothermal calorimeter. All runs were conducted at 25 °C with a time resolution of 1 min. Samples were placed in the calorimeter about 10 min after initial contact of solids and water and, since another 30 min was required for the sample temperature to become completely equilibrated to that of the instrument, the very exothermic early rapid reaction was not captured. Isothermal calorimetry was conducted for about 24 hours and results were normalized to the water mass of each specimen. The average of two replicates for each mix is presented. The average absolute difference between replicate specimens of cement paste was previously measured to be 2.5 x 10^{-5} W/g (cement), for measurements conducted between 1 h and 7 d after mixing [34].

3.3.5 Rheology test

Rheological measurements were taken on a rotational rheometer using a parallel plate configuration. Serrated plates with 35 mm diameter were used. The testing regime was:

- Approximately 1.2 ml samples of paste were taken from the mixing bowl by disposable syringe and placed onto the lower plate of the rheometer;

- The two plates were driven to a preset gap of 0.4 mm selected based on previous experience [35];
- The samples were subjected to a pre-shear regime ranging from 0 to 50 s^{-1} over 160 s. Then a full cycle of increasing shear rate in 10 steps from 1 to 50 s^{-1} and back to 1 s^{-1} was carried out (Figure 2a). At each step, if a constant shear stress was not achieved within 20 s, the shear stress was calculated as the average of the last 5 values recorded. The slope of the line of shear stress versus shear rate of the downward ramp curve (last portion of the testing cycle) was used to calculate the apparent viscosity and the intercept was used to calculate yield stress (Figure 2b), according to the Bingham model [36]. It was found that the calculated values of the yield stress and plastic viscosity had a standard deviation of 5% [30];
- The temperature was held at 25 °C by circulating water through a metal jacket surrounding the outer cylinder;
- The rheology tests were performed at 10, 30, 60, 90, and 120 minutes after cement contacted water. Before each rheological measurement, pastes were remixed with a hand blender for 30 s and
- Between rheological measurements, the mixture was stored in a hermetically sealed flask.

3.3.6 Vicat set time tests

Initial and final set times for all the cement paste mixtures were measured according to ASTM C191 [37]. A needle weighing 300 g and diameter of 1 ± 0.05 mm was lowered into a specimen of fresh cement paste and the penetration depth is recorded. The Vicat initial time of setting is the time elapsed between the initial contact of cement and water and the time when the penetration is measured or calculated to be 25 mm. The Vicat final time of setting is the time elapsed between

initial contact of cement and water and the time when the needle does not leave a complete circular impression in the paste surface. In the ASTM C191 standard, the single laboratory precisions are listed as 12 min and 20 min for initial and final times of setting, respectively.

3.4 Results and discussions

3.4.1 Hydration kinetics

Figure 3.3 shows the isothermal calorimetry data for cement pastes with additions of various types and amounts of nanomaterials. Because of the previously-described test protocol, the first heat flow peak corresponding to the very exothermic initial dissolution of solids and the rapid formation of ettringite [7] in the first few minutes was not captured. For plain paste, the heat flow decreased thereafter to 1.4 mW/g, the first valley on the calorimetric curve, at the age of 51 min. This was followed by the acceleration period, involving acceleration of the silicate reactions and mass nucleation and precipitation of the hydration products, primarily C-S-H [7]. The paste set during this period (Figure 3.10) lasting up to a time of 301 min, at which point the calorimetric curve rose to a second peak (5.6 mW/g), followed by a reduction in heat flow until a second valley was reached at a time of 358 min. These reactions overlapped with the reactions between aluminate and calcium sulphate phases in cement. When the added calcium sulfate had all been consumed, the rate of aluminate phase reaction once again increased, establishing a third calorimetric curve peak (5.5 mW/g) at 382 min. The main aluminate hydration product at this time still appeared to be ettringite [7]. As can be seen, the amount of calcium sulphate in the cement was manipulated so that a renewed reaction of the aluminate phase took place after the hydration peak of the silicate phase, ensuring correct setting and hardening [7]. After the third peak, the heat flow declined and cement hydration entered the deceleration phase.

While essentially the same hydration reactions took place in each case, the addition of nanomaterials had an obvious hydration-accelerating effect, with the maximum heat flow increasing while the time to reach the silicate and aluminate reaction peaks decreased (Figures 3.4 and 3.5). Pastes with nano-clay displayed a different behavior in that the heat flow immediately after the second peak increased and was followed shortly thereafter by a large and relatively sharp third peak corresponding to the renewed reaction of the aluminate phase. As a consequence, in this case the second peak corresponding to the silicate hydration appeared as a shoulder peak and the second valley was not observed (Figure 3.3c). The time lag between the second and third peaks was also reduced (Figure 3.5c).

For pastes with nano-limestone and nano-silica additions, the hydration-accelerating effect increased with the level of addition. As the addition level increased, the heat flow at the silicate and aluminate peaks increased (Figures 3.4a and 3.4b) and the time to reach the peaks decreased (Figures 3.5a and 3.5b). The hydration-accelerating effect of nano-silica can be attributed to a nucleation seeding effect provided by C-S-H particles forming on the nano-silica surface [2, 9]. These C-S-H particles were formed from an early pozzolanic reaction of nano-silica with calcium ions released by the dissolving cement. As the addition level increased, the total nano-silica surface area increased, so more C-S-H particles could be formed to serve as seeds for nucleation and precipitation of C–S–H hydration products [2, 7]. The hydration-accelerating effect of nano-limestone can be attributed to: 1) the nucleation sites provided by the surface of the nano-limestone particles; and 2) the tendency for its dissociated ions to participate in exchange reactions with calcium silicate hydrate products [6]. Calcium carbonate can contribute $CO3^{2-}$ anions to the pore solution, and they can subsequently be incorporated within the C-S-H gel. OH^- anions released

from C-S-H to preserve charge neutrality would elevate the pH and hence the driving force for continuation of hydrate growth [6].

The silicate hydration-accelerating effect of nano-clay may originate from (1) the clay surface providing the nucleation sites for the hydrated phase growth [38, 39]; and (2) the ion absorbing capability of attapulgite particles resulting from their charged structure and high surface area. The decrease in Ca^{2+} ion concentration and consequently lower Ca/Si ratio due to Ca^{2+} ion capture by negatively-charged attapulgite particles may contribute to accelerated silicate hydration [16, 39].

The previously-described absence of the second valley, and the earlier and more intense third peak (Figure 3.3c) suggests that nano-clay more intensely accelerated the renewed reaction of the aluminate phase. This may be attributed to the adsorption of sulfate by nano-clay particles occurring by replacement of silanol (Si-OH) groups [40] and the Synergistic Calorific Effect (SCE) between the C_3A from the cement and the $Al_2O_3^{r-}$ present in nano-clay [41, 42].

It should be noted that the 0.5% nano-clay addition had a greater accelerative effect than the 1.0% nano-clay addition. That may be attributed to the needle-shaped nano-clay particles with charged surfaces. In higher concentrations, more particles attach to one other, leaving less available surface for forming nucleation sites for hydration products [43]. Nano-clay at 0.5% addition level seemed to represent the case providing most effective nano-particles in terms of acceleration of reaction compared to others. This can be attributed to their ability to accelerate hydration reactions of aluminate phase with high net heats of reaction.

3.4.2 Rheology results

Rheology measurements were taken from pastes rested 10 - 120 min after mixing. One sample was tested for each mix. The evolution of shear stress versus shear rate curves (down ramp) with hydration time of studied cement pastes is shown in Figure 3.6. The curves are recombined in

Figure 3.7 to show the effects of different nanomaterials on the rheological behavior of portland cement pastes. The effects of nanomaterials on the yield stress and viscosity calculated from the Bingham model are shown in Figure 3.8.

For plain paste (100% PC), the shear stress at any shear rate increased from one measurement to the next over a 60-min interval, but only to a small extent. Both yield stress and viscosity slightly increased during this testing period. There was a noticeable increase of shear stress at any shear rate and the calculated yield stress between 60 and 90 min, suggesting formation of an increased number of solid-solid contacts. This may be due to accelerated cement hydration starting after the end of induction period, i.e., the first valley on the isothermal calorimetry curve at 51 min (Figure 3.3). As hydration progressed, more hydration products formed and, since less free water was present, the number of solid-solid contacts increased [30], resulting in a sharp increase of shear stress between 90 and 120 min.

It should be noted that at 120 min the curve shear stress versus shear rate no longer followed the Bingham model and neither yield stress nor viscosity could be calculated. At higher shear rates ($> 35\ s^{-1}$), shear stress slightly increased as the shear rate increased. At lower shear rates ($< 35\ s^{-1}$), shear stress decreased as the shear rate increased. This transition in plain cement pastes (shear stress decreased as the shear rate increased) has also been observed by other researchers for low shear rate or at later ages (2 hours after mixing) [30]. Ancey and Coussot [44] interpreted this transition to be passing into a zone where the frictional forces prevail. The cement paste behaves at early age as a low-concentration suspension with lubrication provided by the free water. As hydration progresses, the number of points of contact between the particles increases and the free water available decreases, reducing the lubrication between particles provided by the water. As the cement paste is sheared at later ages, the higher shear rate is able to break direct contacts and the

medium forms a layer that provides lubrication [45]. As the shear rate is decreased, the contacts re-form, resulting in a high shear stress.

For pastes with nano-limestone addition, the viscosity and yield stress of cement pastes were not significantly changed during the early test times, up to 60 min. During this period, limestone can be treated as inert [6, 13] and effects on paste rheology are mainly due to particle size, i.e., competing effects between packing behavior and interparticle forces [23, 24, 26, 46]. During this period, there was no clear trend on the effect of nano-limestone on paste rheology, but the addition of 1.5% NL decreased viscosity without significantly changing yield stress. This behavior may be attributed to the decreased void ratio of solid particles and increased amount of free water for lubrication, implying that the solid particle packing effect is dominant.

After 60 min, the shear stress at any shear rate increased rapidly in proportion to the NL addition level; it is clear that hydration products were being formed and, the greater the addition of NL, the greater the effect on hydration, corroborating the results obtained by isothermal calorimetry. The distinct non-Bingham behavior observed in plain paste (i.e., at low shear rates, the shear stress decreased as the shear rate increased) was not observed here in pastes with NL. However, after 120 minutes, the shear stress versus shear rate curves of pastes with 1.0% and 1.5% NL fit poorly to the Bingham model, and the R^2 were 0.74 and 0.81, respectively. Similar to the implication of non-Bingham behavior of plain paste at 120 min, this may also suggest presence of a state in which colloidal forces between particles don't dominate. The shear stress versus shear rate curve is a result of an irregularly balance between the effects of hydration and the effects of colloidal forces in cement pastes.

Addition of nano-silica gradually increased viscosity in cement pastes. There was a significant increase in yield stress with increased nano-silica addition level as well as with hydration time.

Non-Bingham behavior was observed with NS but at an earlier time. After 60 min, the shear stress vs. shear rate relationship of paste with 1.5% NS had already cease to follow the Bingham model; shear stress decreased as the shear rate increased. This may be due to an early pozzolanic reaction in forming C-S-H particles on the surface of nano-silica, increasing solid-solid contacts and the connectivity of the network structure. At 90 min, the other NS mixtures showed an increase in yield stress and at 120 min none of them followed the Bingham model.

Pastes with NC behaved differently. As shown in Figure 3.9, significantly higher shear stresses had to be applied at the beginning of the pre-shear step to initiate shearing of the NC pastes. This may be attributed to the needle-shaped structure of nano-clay particle with charges on its surface: (1) the needle-like particles of the nano-clay interweave and bridge the solid particles, increasing the number of physical contact points and the connectivity of the network structure [25]; and (2) due to surface charge effects, clay minerals can form card-house type structures [25, 28]. Flocculation studies have shown that clays increase floc size and flocculation strength of cementitious materials and result in a more strongly-flocculated structure [25]. The incorporation of clay materials has been widely used in minimal-compaction energy concrete to improve shape stability [25, 26].

However, after shearing had been initiated, the shear stress required at any shear rate for the paste with 0.5% NC was close to or even slightly lower than that of plain paste during early test times (up to 60 minutes), as can also be observed in the down ramp of Figure 3.7c. On the other hand, for the paste with 1.0% NC, the shear stress required was significantly higher than that for plain paste. A possible explanation could be that, at a small dosage, i.e., 0.5% NC in this case, the high initial shear stress is mostly due to surface charge effects and an increase in the flocculation strength of the cement paste. Under shearing, nano-clay particles would be arranged into their

preferred direction and offset the structural connections between needles [28, 47]. As a consequence, shear stress at any shear rate was close to that of plain paste from the down ramp. When the NC addition level increased to 1.0%, the number of physical contact points between needle-like nano-clay particles and the cement grains increased, leading to a larger yield stress. After 60 min, when inter-particle force bonds are gradually replaced and augmented by "cement hydration product" bonds, the testing protocol and the shear rates applied were not sufficiently high to break the structure, and rheology tests cannot continue under the current testing protocol.

3.4.3 Vicat set time

The measured initial and final set times of the pastes studied are also shown in Figure 3.10. Both initial and final setting happened during the acceleration period; this involved acceleration of hydration reactions and mass precipitation of the hydration products, primarily C-S-H, confirming that the impingement, or intergrowth, of hydration products regions from different cement grains is responsible for setting of cement paste [48]. The addition of nanomaterials shortened the time to reach initial and final vicat set. For pastes with nano-limestone and nano-silica, the time to reach initial and final set decreased as the addition level increased. Paste with 0.5% nano-clay addition reduced initial and final set times more than paste with 1.0% nano-clay addition. The extent to which the set times are reduced correlates well with the ability of nanomaterials to accelerate silicate phase hydration.

3.5 Conclusions

Early hydration kinetics and rheology behavior of cement pastes with varying types and amounts of nanomaterials addition have been characterized. Specifically,

1) The addition of all the three nanomaterials studied had an obvious hydration-accelerating effect; the maximum heat flow increased while the time to reach silicate and aluminate reaction peaks decreased.
2) For pastes with nano-limestone and nano-silica addition, the hydration-accelerating effect increased with the addition level.
3) Addition of nano-clay accelerates the consumption of sodium sulphate and the reaction of the aluminate phase, resulting in an earlier and more intense aluminate hydration peak. A 0.5% nano-clay addition had a greater acceleration effect than did a 1.0% nano-clay addition.
4) Both initial and final setting happened during the acceleration period and the addition of nanomaterials reduced the initial and final set times. The extent to which the set times were reduced correlated well with the capability of nanomaterials to accelerate silicate phase hydration.
5) Before the acceleration period of hydration (60 min), the viscosity and yield stress of cement pastes with 0.5% and 1.0% nano-limestone addition changed little with time, but addition of 1.5% nano-limestone decreased viscosity without significantly changing yield stress during this period.
6) Addition of nano-silica gradually increased viscosity of cement pastes. There was a significant increase in yield stress with a nano-silica addition level as well as with increased hydration time.
7) The nano-clay studied had a considerable effect on the rheological behavior of cement pastes. Significantly higher shear stress was required to initiate the flow.
8) Non-Binghman (shear stress decreases as the shear rate increases) behavior was observed in many mixtures, especially those tested 120 min after mixing.

3.6 Acknowledgements

The authors would like to acknowledge the Oak Ridge Associated Universities (ORAU) - Tennessee Valley Authority (TVA) for sponsoring the present study (Grant No. 7-22976) and the Federal Highway Administration at TFHRC for help with testing.

3.7 References

[1] N. Lewinski, V. Colvin and R. Drezek, "Cytotoxicity of nanoparticles," *Small*, Vol. 4, 2008, pp. 26-49.

[2] L. Singh, S. Karade, S. Bhattacharyya, M. Yousuf and S. Ahalawat, "Beneficial role of nanosilica in cement based materials – A review," *Construction and Building Materials*, Vol. 47, 2013, pp. 1069–1077.

[3] S. Kawashima, P. Hou, D. J. Corr and S. P. Shah, "Modification of cement-based materials with nanoparticles," *Cement & Concrete Composites*, Vol. 36, 2013, pp. 8–15.

[4] F. Sancheza and K. Sobolevb, "Nanotechnology in concrete – A review," *Construction and Building Materials*, Vol. 24, 2010, pp. 2060–2071.

[5] T. Sato and J. J. Beaudoin, "Effect of nano-$CaCO_3$ on hydration of cement containing supplementary cementitious materials," *Advances in Cement Research*, Vol. 23, 2011, pp. 33-43.

[6] T. Oey, A. Kumar, J. W. Bullard, N. Neithalath and G. Sant, "The Filler Effect: The Influence of Filler Content and Surface Area on Cementitious Reaction Rates," *Journal of the American Ceramic Society*, Vol. 96, 2013, pp.1978-1990.

[7] J. W. Bullard, H. M. Jennings, R. A. Livingston, A. Nonat, G. W. Scherer, S. Schweitzer, K. L. Scrivener and J. J. Thomas, "Mechanisms of cement hydration," *Cement and Concrete Research*, Vol. 41, 2011, pp. 1208–1223.

[8] J. Tanesi, A. Ardani, R. Meininger and M. Nicolaescu, *Evaluation of High-Volume Fly Ash (HVFA) Mixtures (Paste and Mortar Components) Using a Dynamic Shear Rheometer (DSR) and Isothermal Calorimeter*, Report No. PB2012-112546, National Technical Information Service, Springfield, VA, 2012.

[9] J. J. Thomas, H. M. Jennings and J. J. Chen, "Influence of Nucleation Seeding on the Hydration Mechanisms of Tricalcium Silicate and Cement," *J. Phys. Chem. C* , Vol. 113, 2009, pp. 4327–4334.

[10] B. Y. Lee and K. E. Kurtis, "Influence of TiO_2 Nanoparticles on Early C_3S Hydration," *Journal of the American Ceramic Society*, Vol. 93, 2010, pp. 3399–3405.

[11] L. Gurney, D. Bentz, T. Sato and W. Weiss, "Reducing Set Retardation in High Volume Fly Ash Mixtures with the Use of Limestone: Improving Constructability for Sustainability," Transportation Research Record: Journal of the Transportation Research Board, No. 2290, 2012, pp. 139-146.

[12] T. Sato and F. Diallo, "Seeding Effect of Nano-CaCO3 on the Hydration of Tricalcium Silicate," Transportation Research Record: Journal of the Transportation Research Board, No. 2141, 2000, pp. 61-67.

[13] M. Zajac, A. Rossberg, G. L. Saout and B. Lothenbach, "Influence of limestone and anhydrite on the hydration of Portland cements," Cement and Concrete Composites, Vol. 46, 2014, pp. 99-108.

[14] B. Pekmezci, T. Voigt, K. Wang and S. Shah, "Low compaction energy concrete for improved slip-form casting of concrete pavements," ACI Materials Journal, Vol. 104, 2007, pp. 251-258.

[15] H. Krøyer, H. Lindgreen, H. Jakobsen and J. Skibsted, "Hydration of Portland cement in the presence of clay minerals studied by 29Si and 27Al MAS NMR spectroscopy," Advances in Cement Research, Vol. 15, 2003, pp. 103-112.

[16] V. Manic, I. Miljkovic and B. Djuric-Stanojevic, "The 1H T1 study of the influence of clay addition on Portland cement hydration," *Applied Magnetic Resonance*, Vol. 13, 1997, pp. 231–239.

[17] S. Schlorholtz and T. Demirel, "Quick lime-gypsum interactions in stabilized soil bases for concrete highways," *Cement and Concrete Research*, Vol. 14, 1984, pp. 529-532.

[18] G. W. Scherer, J. Zhang, J. A. Quintanilla and S. Torquato, "Hydration and percolation at the setting point," *Cement and Concrete Research*, Vol. 42, 2012, pp. 665–672.

[19] G. Sant, C. F. Ferraris and J. Weiss, "Rheological properties of cement pastes: A discussion of structure formation and mechanical property development," *Cement and Concrete Research*, Vol. 38, 2008, pp. 1286-1296.

[20] V. A. Hackley and C. F. Ferraris, "The Use of Nomenclature in Dispersion Science and Technology," *NIST Recommended Practice Guide*, SP 960-3, 2001.

[21] C. Rößler, A. Eberhardt, H. Kučerová and B. Möser, "Influence of hydration on the fluidity of normal Portland cement pastes," *Cement and Concrete Research*, Vol. 38, 2008, pp. 897–906.

[22] T. Powers, *The Properties of Fresh Concrete*, New York, Wiley, 1968.

[23] K. Vance, A. Kumar, G. Sant and N. Neithalath, "The rheological properties of ternary binders containing Portland cement, limestone, and metakaolin or fly ash," *Cement and Concrete Research*, Vol. 52, 2013, pp. 196-207.

[24] N. Diamantonis, I. Marinos, M. Katsiotis, A. Sakellariou, A. Papathanasiou, Kaloidas and M. Katsioti, "Investigations about the influence of fine additives on the viscosity of cement paste for self-compacting concrete," *Construction and Building Materials*, Vol. 24, 2010, pp. 1518-1522.

[25] R. D. Ferron, S. Shah, E. Fuente and C. Negro, "Aggregation and breakage kinetics of fresh cement paste," *Cement and Concrete Research*, Vol. 50, 2013, pp. 1-10.

[26] L. Li and A. Kwan, "Mortar design based on water film thickness," *Construction and Building Materials*, Vol. 25, 2011, pp. 2381-2390.

[27] N. Baldino, D. Gabriele, F. R. Lupi, L. Seta and R. Zinno, "Rheological behaviour of fresh cement pastes: Influence of synthetic zeolites, limestone and silica fume," *Cement and Concrete Research*, Vol. 63, 2014, pp. 38–45.

[28] N. A. Tregger, M. E. Pakula and S. P. Shah, "Influence of clays on the rheology of cement pastes," *Cement and Concrete Research*, Vol. 40, 2010, pp. 384-391.

[29] D. P. Bentz, C. F. Ferraris, M. A. Galler, A. S. Hansen and J. M. Guynn, "Influence of particle size distributions on yield stress and viscosity of cement–fly ash pastes," *Cement and Concrete Research*, Vol. 42, 2012, pp. 404–409.

[30] S. Amziane and C. Ferraris, "Cementitious paste setting using rheological and pressure measurements," *ACI Materials Journal*, Vol. 104, 2007, pp. 137-145.

[31] Active Minerals Company LLC, "What is Acti-Gel® 208 and how is it made?", 2007. [Online].

[32] K. Sato, J. Li, H. Kamiya and T. Ishigaki, "Ultrasonic Dispersion of TiO_2 Nanoparticles in Aqueous Suspension," *Journal of the American Ceramic Society*, Vol. 91, 2008, pp. 2481-2487.

[33] ASTM C1738-11: Standard Practice for High-Shear Mixing of Hydraulic Cement Paste, *Annual Book of ASTM Standards*, ASTM International, West Conshohocken, PA, 2011.

[34] D. P. Bentz and C. F. Ferraris, "Rheology and setting of high volume fly ash mixtures," *Cement & Concrete Composites*, Vol. 32, 2010, pp. 265–270.

[35] C. F. Ferraris, K. H. Obla and R. Hill, "Influence of Mineral Admixtures on the Rheology of Cement Paste and Concrete," *Cement and Concrete Research*, Vol. 31, 2001, pp. 245-255.

[36] ASTM C1749: Standard Guide for Measurement of the Rheological Properties of Hydraulic Cementitious Paste Using a Rotational Rheometer, *Annual Book of ASTM Standards*, ASTM International, West Conshohocken, PA, 2012.

[37] ASTM C191: Standard Test Methods for Time of Setting of Hydraulic Cement by Vicat Needle, *Annual Book of ASTM Standards*, ASTM International, West Conshohocken, PA, 2013.

[38] H. Taylor, "Reactions and reactivities of compounds in hydraulic cements," *Solid State Ionics*, Vol. 43, 1990, pp. 31-35.

[39] H. Lindgreen, M. Geiker, H. Krøyer, N. Springer and J. Skibsted, "Microstructure engineering of Portland cement pastes and mortars through addition of ultrafine layer silicates," *Cement and Concrete Composites*, Vol. 30, 2008, pp. 686–699.

[40] S. M. Rao and A. Sridharan, "Mechanism of Sulfate Adsorption by Kaolinite," *Clays and Clay Minerals*, Vol. 32, 1984, pp. 414-418.

[41] R. Talero and V. Rahhal, "Calorimetric comparison of portland cements containing silica fume and metakaolin," *Journal of Thermal Analysis and Calorimetry*, Vol. 96, 2009, pp. 383-393.

[42] R. Talero and V. Rahhal, "Influence of 'aluminic' pozzolans, quartz and gypsum additions on portland cement hydration," in *12th International Congress on the Chemistry of Cement*, Montreal, Canada, 2007.

[43] J. Xu, W. Wang and A. Wang, "Effects of solvent treatment and high-pressure homogenization process on dispersion properties of palygorskite," *Powder Technology*, Vol. 235, 2013, pp. 652–660.

[44] C. Ancey and P. Coussot, "Transition from frictional to viscous regime for granular suspensions," *Comptes Rendus de l'Academie des Sciences Series IIB Mechanics Physics Astronomy*, Vol. 327, 1999, pp. 515-522.

[45] P. Coussot and C. Ancey, "Rheophysical classification of concentrated suspensions and granular pastes," *Physical Review E*, Vol. 59, 1999, pp. 4445 – 4457.

[46] M. Jones, L. Zheng and M. Newlands, "Comparison of particle packing models for proportioning concrete constituents for minimum voids ratio," *Materials and Structures*, Vol. 35, 2002, pp. 301-309.

[47] N. Tregger, T. Voigt, K. Wang and S. Shah, "Improving the slip-form process via material manipulation," in *Advances in Construction Materials*, C. Grosse, Ed., New York, Springer Berlin Heidelberg, 2007, pp. 539-546.

[48] J. Stark, "Recent advances in the field of cement hydration and microstructure analysis," *Cement and Concrete Research*, Vol. 41, 2011, pp. 666-678.

Tables:

Table 3.1 Chemical and physical properties of cement and nano-clay.

Chemical composition	PC	nano-clay
	(mass %)	
SiO_2	20.2	49.57
Al_2O_3	4.7	9.44
Fe_2O_3	3.3	3.31
SO_3	3.3	-
CaO	62.9	1.88
MgO	2.7	8.81
Eq. Na_2O	0.54	1.02
TiO_2	-	0.42
LOI	1.1	<0.5
Physical Properties		
Specific gravity	3.15	2.62
Blaine fineness (m^2/g)	0.391	150

Table 3.2 Physical characteristics of nanomaterials.

Property	NL	NS
Color	White	White
Density (25 °C)	2.7 g/ml	2.2-2.6 g/ml
Content	$CaCO_3$ > 97.5%	SiO_2 > 99.5%
Particle size	15-40 nm	10-20 nm

Figures:

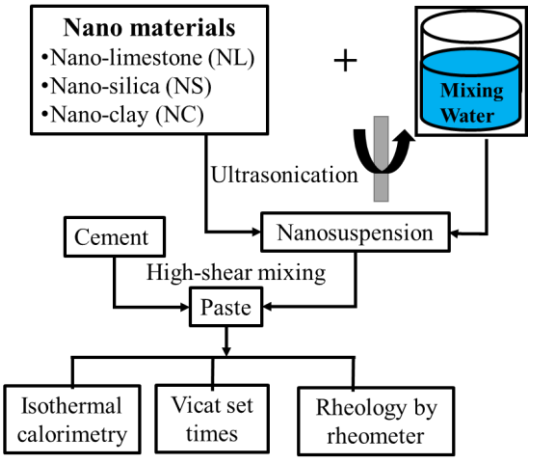

Figure 3.1. Block diagram of the experimental work.

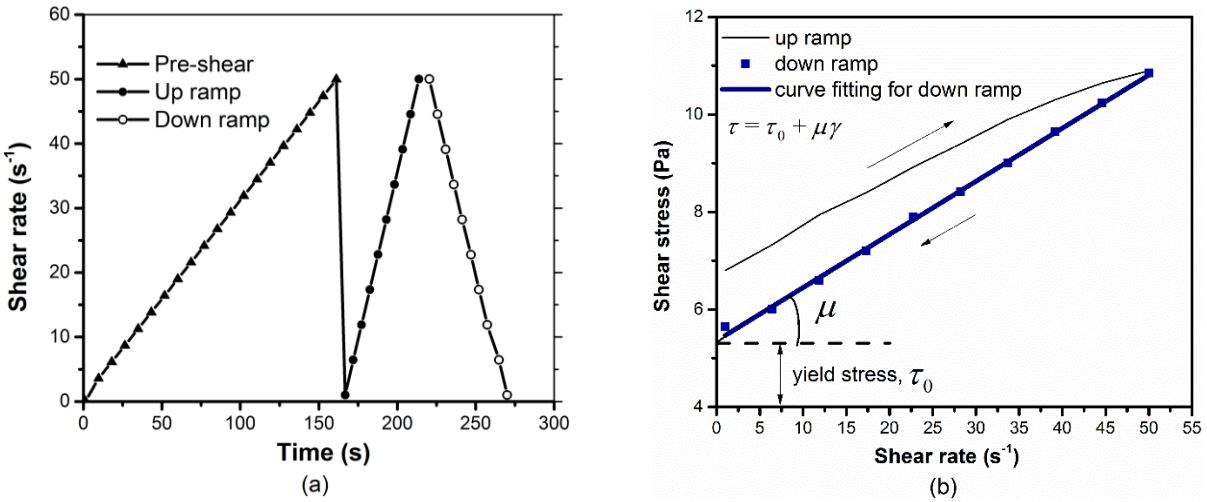

Figure 3.2. (a) Rheological test protocol, (b) Typical shear rate vs. shear stress curve.

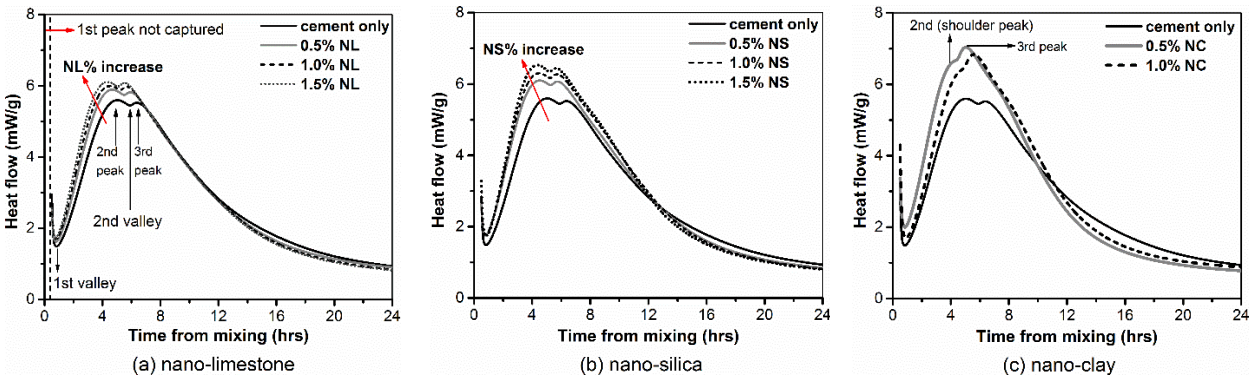

Figure 3.3. Effect of nanomaterials on the early hydration kinetics of Portland cement paste.

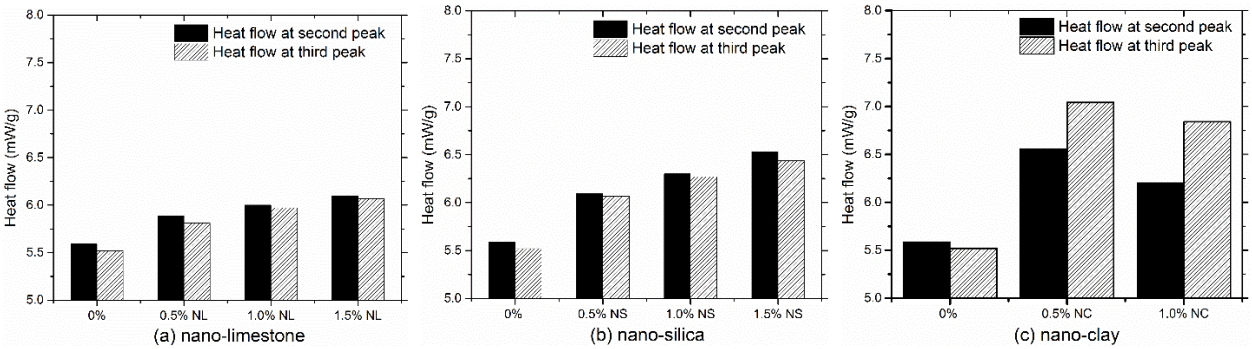

Figure 3.4. Effect of nanomaterials on the heat flow peak values of cement pastes.

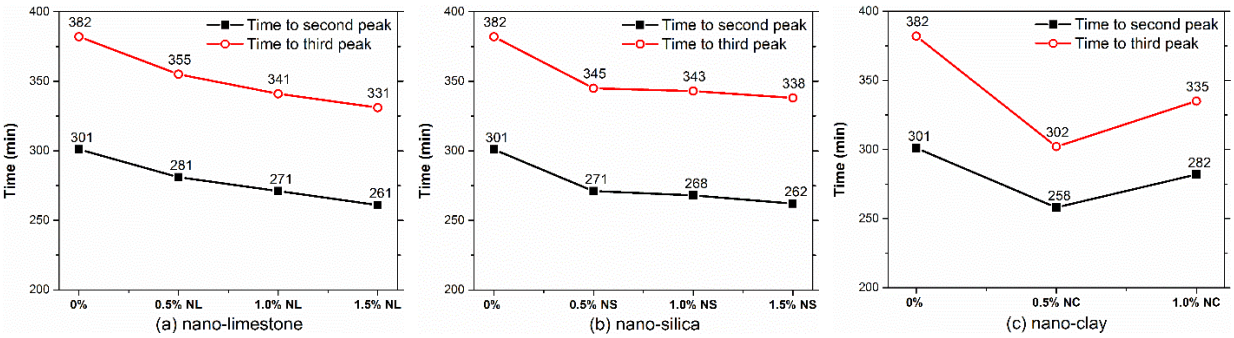

Figure 3.5. Effect of nanomaterials on the time to reach heat flow peaks of cement pastes.

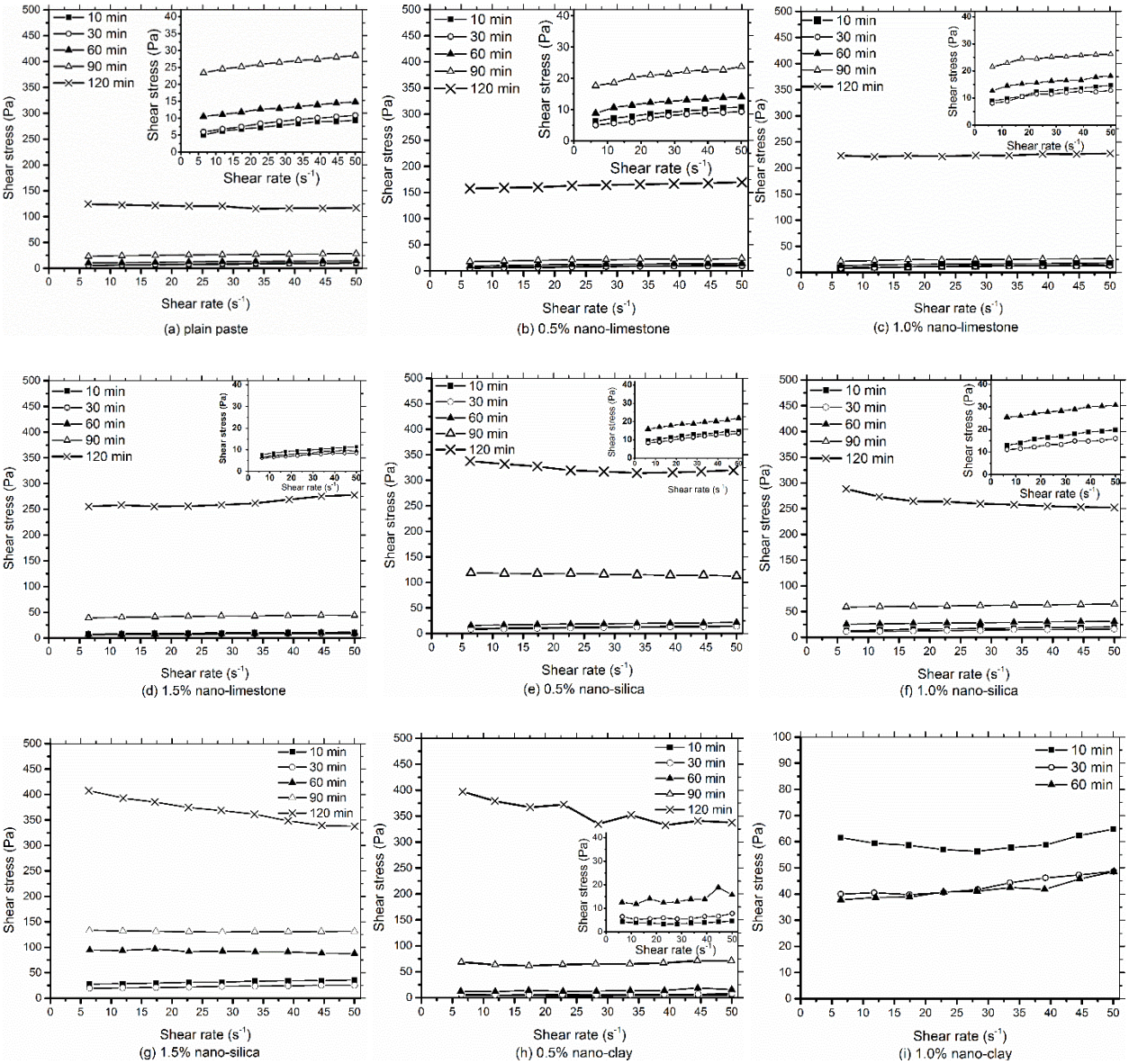

Figure 3.6. Evolution of shear stress versus shear rate curves (down ramp) with hydration time of studied cement pastes.

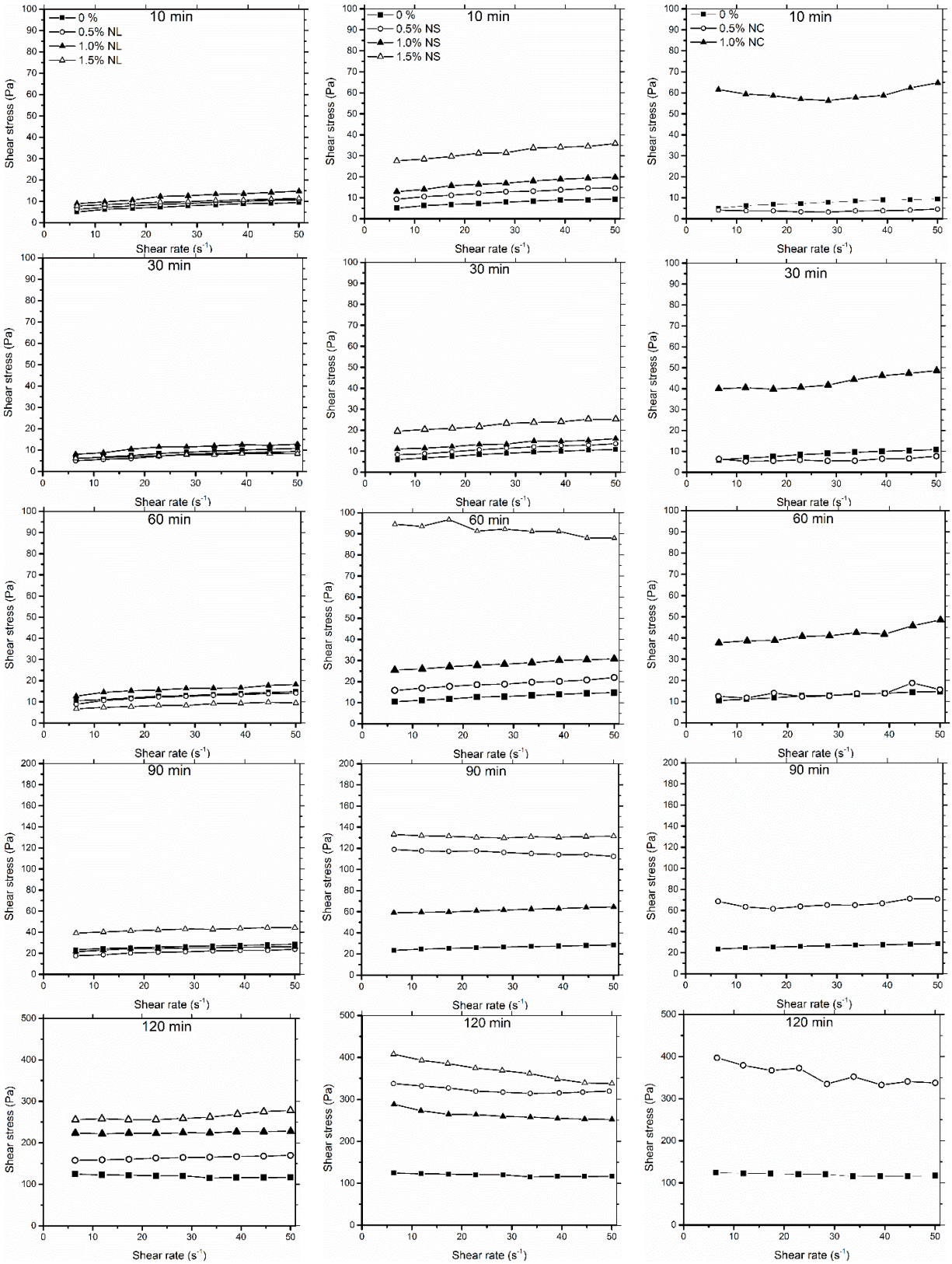

(a) nano-limestone (b) nano-silica (c) nano-clay

Figure 3.7. Effect of nanomaterials on the rheological behavior (down ramp curves) of cement paste.

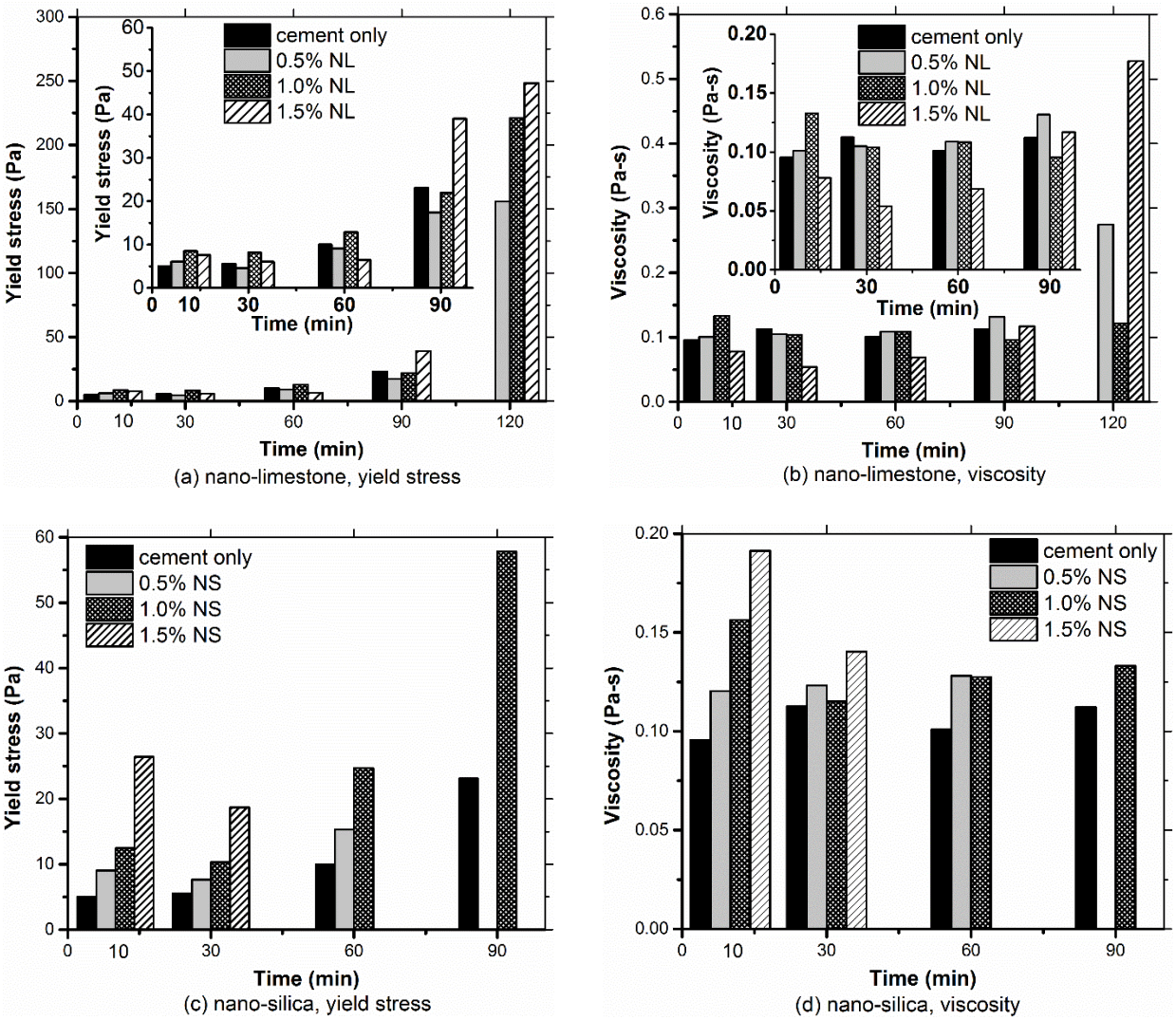

Figure 3.8. Effect of nanomaterials on the yield stress and viscosity of cement paste.

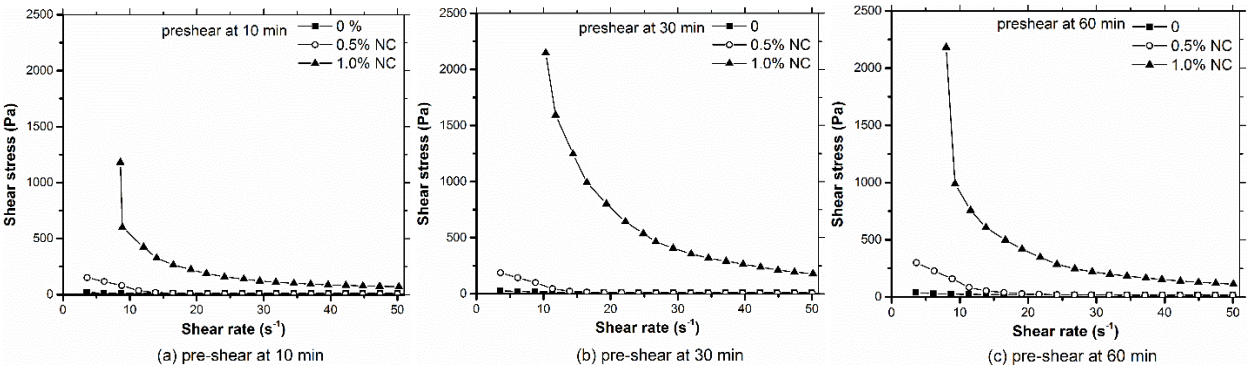

Figure 3.9. Shear stress versus shear rate curves of cement pastes with nano-clay during pre-shear.

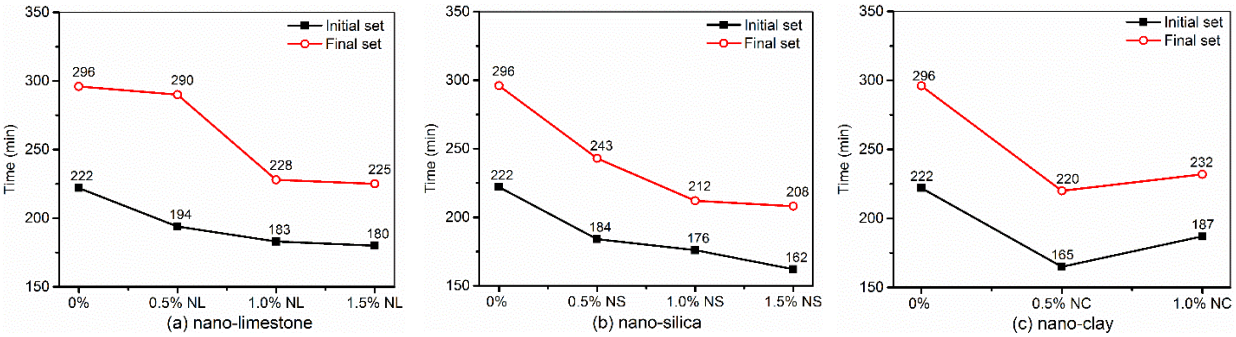

Figure 3.10. Effect of nanomaterials on the set times of cement pastes.

CHAPTER 4. HYDRATION AND COMPRESSIVE STRENGTH OF PORTAND CEMENT PASTES MODIFIED WITH NANOMATERIALS AND FLY ASH

Modified from a paper to be submitted to *Construction and Building Materials*

Xin Wang[a], Kejin Wang[b]

[a] Dept. of Civil, Construction, and Environmental Engineering, Iowa State Univ., Ames, Iowa 50010. Tel: 515-294-2140. Email: wangxin@iastate.edu
[b] Corresponding author, Dept. of Civil, Construction, and Environmental Engineering, Iowa State Univ., Ames, Iowa 50010. Tel: 515-294-2151. Email: kejinw@iastate.edu

Abstract

In this work, the effects of three nanomaterials, nano-limestone (NL), nano-silica (NS), and nano-clay (NC), on the hydration and compressive strengths of ordinary portland cement (OPC) with and without 30% fly ash (FA) replacement were investigated. Chemical shrinkage of the pastes were monitored as an indication of the hydration process. Thermogravimetric analysis (TGA) was used to determine the quantities of calcium hydroxide (CH) and chemically bound water. X-ray diffraction was conducted to identify new crystalline hydration products of the pastes. Regardless the types of the nanomaterials, 1% nanomaterial addition improved the compressive strength of both OPC and OPCFA pastes at all the ages studied (up to 28 days). It also noticeably increased the amount of chemically bound water in the early age pastes (before 7 days). Among three nanomaterials studied, NS appeared to be the most effective one in the cement hydration acceleration and strength improvement, possibly due to its smallest particle size and highest reactivity. A new hydration product, calcium hemicarboaluminate hydrate (Hc), was formed in the nanolimestone modified OPCFA paste (OPCFANL).

4.1 Introduction

Cement-based materials are the most widely used materials in construction worldwide. The basic material properties include workability, mechanical properties (mainly strength), and durability. All these properties are closely related to cement hydration and microstructure development. Hydrated cement is a multiscale material, having solids and pores ranging from nanosizes to microsizes. Among cement hydration products, approximately 50% (by volume) is calcium-silicate-hydrate (C-S-H) gel. In the past decade, growing research has been conducted using nanomaterials to modify cement-based materials [1-5]. Research has demonstrated that nanoparticles can alter microstructure of cement-based materials at a nanoscale level and consequently improve their bulk properties and performance. Well-dispersed nanoparticles (such as nano-limestone, nano-silica and nano-clay) can distinctly accelerate early cement hydration, modify rheology properties, reduce setting times and increase the early age compressive strength of the cement paste even at very small dosages (< 2%) [6-10].

There are two major mechanisms responsible for the nanomaterial modification on cement-based materials. First, these nanoparticles, spread in the capillary pore spaces between cement particles, provide additional nucleation sites for the precipitation and growth of new regions of C-S-H gel, thus prompting the more evenly distribution of hydration products [11]. Second, nanoparticles can function as nanofillers, filling the spaces between cement grains, refining and reducing capillary pores, and immobilizing the pore water [12]. In addition, nanoparticles can strengthen the interfacial bonding between cement paste and aggregate [13]. Beside the physical effects, the contribution of nanomaterials can also be attributed to their chemical characteristics. Thomas et al. proposed that when nano-silica was added to cement, an early pozzolanic reaction would occur on the nano-silica surface to form C-S-H particles, which in turn served as nucleation

seeds for the formation of C-S-H hydration product (autocatalysis) [11]. Oey et al. suggested that not only can limestone offer a lower energy barrier than tricalcium silicate (C_3S) for C-S-H nucleation, but it can also participate in ion-exchange during cement hydration, elevating the pH and hence the driving force for continuing hydrate growth [8, 14]. The excellent hydration accelerating efficacy of nanomaterials makes it a promising addition to eco-concrete mixes containing waste materials.

Fly ash (FA), a by-product from coal combustion, has been commonly used in concrete to partially replace ordinary portland cement (OPC) for its environmental (reduce carbon footprint) and engineering benefits (reduce heat of hydration, improve concrete workability and durability). However, the pozzolanic reaction of FA in cement-based systems only starts significantly after one or more weeks [15]. The delayed setting and retarded early-age strength development (up to 28 days) often limit the use of fly ash since 28-day strength is often specified in concrete industry. Nano-silica has been reported to improve early strength of concrete with fly ash as well as increase the pozzolanic reactivity of fly ash [16-19].

More recently, the chemical reactivity of limestone in a cement-based system and the synergy between fly ash and limestone have been explored [20-25]. Experimental investigation and thermodynamic modeling indicated that a relatively small quantity of calcite reacted with aluminate hydrates from cement hydration to form hemicarbonate and monocarbonate at the expense of monosulphate and thus indirectly stabilizing the ettringite [24]. Weerdt et al. showed that this effect was more pronounced for the fly ash blended cement due to the additional alumina provided by the fly ash reaction [20, 25]. It was suggested that the stabilization of the voluminous, water rich ettringite instead of the less voluminous monosulphate can result in an increase of the

total volume of hydration products, which potentially might result in a decrease in porosity and thus an increase in strength [24, 25].

Clay materials are increasingly used to modify thixotropy and improve shape stability in self-consolidating concrete [26-28]. As a source of nanoparticles, non-calcined nano-clay is less expansive, but has been found to enhance the early hydration of portland cement paste and improve the mechanical properties significantly [3, 6, 29]. As nanomaterials are often selected and used for specific purposes, the systematic study on the comparison of different nanomaterials is still limited.

The present work is to investigate the hydration kinetics of OPC-FA pastes modified by different nanomaterials and to examine how these hydration characteristics renovate compressive strength of these hardened cement pastes. In the study, three different nanomaterials (nanolimestone, nanosilica, and nanoclay) were used at small amounts (1%). Chemical shrinkage tests were performed to monitor the hydration process of the nanomaterial modified OPC-FA pastes. Thermogravimetric analysis (TGA) was used to determine the amount of cement hydration products, and X-ray diffraction (XRD) was used to identify the hydration products in the cement-fly ash-nanomaterial system.

4.2 Materials and methods

4.2.1 Materials and mix proportions

A Type I/II portland cement (PC), a Class F fly ash (FA), and three nanomaterials: nano-silica (NS), nano-limestone (NL), and nano-clay (NC) were used in this study; their important characteristics are summarized in Table 4.1. The major crystal phases detected by XRD in the studied fly ash included quartz, mullite, hematite, and magnetite. NC particles of highly purified magnesium alumino-silicates were supplied by Active Minerals [30]. They are chemically exfoliated from bulk attapulgite to remove high water demand impurities such as semectite,

bentonite and other swelling clays. Under shearing, NC particles break down into needle-like structures about 1.75 um in average length and 3 nm in average diameter [27].

Two series of cementitious mixes were studied, one with 30% fly ash replacement (denoted as OPCFA pastes) and one without fly ash replacement (denoted as OPC pastes). Each nanomaterial was used as an addition at the level of 1% by weight of cementitious materials. Distilled water was used for mixing, and the water-to-cementitious materials ratio was set to be 0.5 for all the mixes studied. The experimental matrix is given in Table 4.2.

4.2.2 Dispersion of nanoparticles

Nanoparticles tend to agglomerate due to their strong interparticle attraction (i.e. van der Waals forces). To achieve a homogeneous cement paste, the nano-material was first dispersed in the mixing water to form a nanoparticle suspension, and this nano-suspension was then used as the "virtual mixing water" for the mixing of cementitious materials as illustrated in Figure 4.1.

To de-agglomerate nanoparticles and form a well-dispersed nano-suspension, high intensity ultrasound was used in this study [31-33]. The ultrasonication was carried out in a beaker with a Sonicator® XL2020 (Qsonica, LLC., USA; frequency: 20 kHz; generating power: 600W). To prevent the water from heating, the beaker was kept in an ice bath, and the suspension was cooled to room temperature after each 3-min continuous ultrasonication (Figure 4.1).

Additionally, the loss of water and nanomaterial during ultrasonication were compensated: (1) the weight of the beaker was measured before and after the ultrasonication; (2) the particles adhered to the probe of the ultrasonic homogenizer were washed into the nano-suspension with a small amount of distilled water; (3) care was taken to ensure that the weight of the beaker are the same before and after ultrasonication.

4.2.3 Sample preparation and test methods

Cubic paste samples (50 x 50 x 50 mm) were prepared for compressive strength tests. Three samples were tested for each mix at each testing time (3, 7, and 28 days). After casting, the samples were left in the molds covered with wet towels and plastic sheets for 24 hours and then cured in saturated lime solution at 23 ± 2 °C after demolding.

The chemical shrinkage measurement was performed in accordance with ASTM C1608 Procedure A [34]. All paste mixes were mixed with de-aired water. A uniform water-to-cementitious material ratio of 0.5 was used to be consistent with the other measurements in this study. The height of the cement paste contained in each glass vial was kept constant at 7 mm (approximately 7 g of cement paste). Three specimens were run for each mix, with the average result being reported.

For thermogravimetric (TGA) and X-ray diffraction (XRD) analysis, paste samples were cast in 24 ml sealed cylindrical polystyrene vials, demolded after 24 h, and cured in saturated lime solution at 23 ± 2 °C. At 3, 7, and 28 days, crushed pieces were taken from the central part of the cylindrical samples and grounded into powders using mortar and pestle.

XRD data were collected using a Siemens D500 x-ray diffractometer employing $CuK\alpha_{1,2}$ radiation ($\lambda = 1.54$ Å) in a θ-2θ configuration. Prior to test, the hydration of the grounded powders was stopped via solvent exchange using isopropanol and vacuum [35]. When loaded into the sample holder, the powders were lightly pressed with a frosted glass side to minimize preferred orientation. The samples were scanned between 5 and 65 degrees.

TGA was performed in a Discovery TGA (TA Instruments, USA) on approximately 50 mg of each grounded sample. The weight change of each sample was monitored as a function of the temperature from 17 to 1000 °C under a nitrogen atmosphere.

Two important quantities were calculated from TGA: the amount of chemically bound water (H) and the weight loss corresponding to the decomposition of calcium hydroxide (CH). First, the amount of chemically bound water (H) was calculated as the mass loss recorded between 105 and 950 °C, exclusive of loss of ignition and weight loss due to decomposition of calcium carbonate:

$$\boldsymbol{H} = (\boldsymbol{m_{105}} - \boldsymbol{m_{950}}) - \boldsymbol{m_{950}} * (\boldsymbol{f_c} * \boldsymbol{LOI_c} + \boldsymbol{f_p} * \boldsymbol{LOI_p}) \; - \; \boldsymbol{m_{\mathrm{Ldc}}} \qquad 4.1$$

where m_{105} and m_{950} are respectively the sample weights measured at 105 °C and 950 °C, $f_{c,p}$ the mass fractions of PC and FA in binder, and $LOI_{c,p}$ the ignition losses of PC and FA. At last, m_{Ldc} represents weight loss due to decomposition of calcium carbonate which occurred between 550 and 800 °C.

On the other hand, weight loss due to the dehydration of calcium hydroxide (CH) was determined from the derivative curve (DTG) with a correction for the concurrent dehydration of other compounds, as outlined in [36, 37], and the start and ending of each temperature interval was determined for each sample.

Both CH and H contents were expressed as percentages of weight of the anhydrous ordinary portland cement present in the sample, with the assumption that the ignited sample at 950 °C contains all anhydrous cement in the case of the OPC mix and 70% cement and 30% fly ash for the OPCFA mix. The addition of nanomaterials was also accounted for in the calculation, with the assumption that 56% of the original nano-limestone, 100% of nano-silica, and 99.5% of nano-clay remained after ignition. For cement-fly ash pastes, the CH and H contents were also expressed as percentages of weight of the ignited sample.

4.3 Results

4.3.1 Early hydration during the first 24 h

During cement hydration the cement paste exerts chemical shrinkage as the volume of hydration products is smaller than the volume of the reactants. The amount of chemical shrinkage is believed directly proportional to degree of cement hydration [38]. A higher chemical shrinkage value mostly indicated that more hydration products are formed, or alternatively different hydrates are formed with even less volume relative to the reactants than the usual hydrates. The chemical shrinkage of the studied pastes up to 24 h after mixing has been plotted as cm3 per 100 g cement in Figures 4.2a and b. The reading 1 h after the paste was first mixed was used as the zero point in all calculations according to the standard (this allows time for the specimen to achieve temperature equilibrium within the water bath).

Figure 4.2a showed that the addition of nanomaterials increased chemical shrinkage of cement pastes after 4 h, suggesting that more hydration products were formed, which is in agreement with the heat of hydration results [6]. The OPCNL paste with nano-limestone displayed the highest chemical shrinkage. After one day of hydration, the chemical shrinkage of the OPCNS paste was close to that of the OPCNL paste. Comparing the chemical shrinkage curves of the reference cement (OPC) paste and cement-fly ash blended (OPCFA) paste, it is noted that replacing 30% of cement by fly ash did not change the chemical shrinkage per cement content much in the first 8 h, which is as expected. During the first hours of hydration, the fly ash particles are inert and only act as filler. It was reported that the replacement of cement by low calcium fly ash results in an increase and a delay of the maximum rate of hydration per cement content [25] as measured by isothermal calorimetry. After one day of hydration, chemical shrinkage per cement content in the OPCFA paste was considerably larger than that of the OPC paste. This enhanced cement hydration

is generally attributed to the filler effect. For the cement-fly ash pastes, nano-limestone addition noticeably increased chemical shrinkage (Figure 4.2b). Nano-silica and nano-clay addition did not change the chemical shrinkage much.

It is noted that in both cement pastes and cement-fly ash pastes, nano-limestone addition increased chemical shrinkage the most. Previously study on the heat of hydration of the four cement pastes showed that the paste with nano-silica released the most heat in the first hours. While hydration kinetics studied by heat of hydration (isothermal calorimetry) measures the rate of cement or C_3S consumption, chemical shrinkage reflects the formation of hydration products. This may indicate that nano-limestone particularly facilitate the nucleation of C-S-H.

4.3.2 Continuing hydration up to 28 days

4.3.2.1 Chemical shrinkage

The chemical shrinkage of the studied pastes as cm^3 per 100 g cementitious materials up to 28 days was plotted in Figure 4.3. For measurements after one day, a lower chemical shrinkage may otherwise be caused by the depercolation of the capillary porosity. For the cement pastes, nano-limestone and nano-silica addition increased the chemical shrinkage at almost all ages. The chemical shrinkage values in OPCNC paste and OPC paste were close.

The OPCFA paste had a higher chemical shrinkage per cement than the OPC paste from one day of hydration mostly caused by the filler effect of fly ash. On the other hand, the chemical shrinkage per cementitious materials (cement + fly ash) of the OPCFA paste was lower than that of the OPC paste, indicating that the filler effect didn't compensate for the reduction of the amount of hydration reactant. However, the chemical shrinkage curve of the OPCFA paste approached the OPC curve from 7 to 28 days (Figures 4.3a and b), and the total chemical shrinkage of the two pastes were about the same at the age of 28 days, i.e., the rate of hydration of the OPCFA paste

increased substantially during this period. This increased rate of hydration was attributed to the pozzolanic reaction of FA which causes a higher net volume decrease than cement hydration. The OPCFANL paste with nano-limestone showed higher chemical shrinkage values before 7 days, and lower chemical shrinkages at 28 days. Compared with the chemical shrinkage result of the OPCNL paste, not only the chemical shrinkage value of the OPCFA paste was reduced but also the rate of hydration decreased noticeably during the age of 7 to 28 days. A similar trend was observed for the paste with nano-clay (OPCFANC). It showed higher chemical shrinkage values up to 3 days and reduced chemical shrinkage values afterwards. A possible reason is that the hydrates formed had a strong pore filling ability, decreases in porosity and the connectivity of the capillary pores prevent water from permeating through the paste. Another possibility is that these two nanomaterials hindered the cement and fly ash hydration after 7 days. On the other hand, the OPCFANS paste with nano-silica addition showed higher chemical shrinkage than the OPCFA paste at 28 days. This will be discussed later.

4.3.2.2 Changes in the hydration products by XRD

X-ray diffraction patterns for the cement and cement-fly ash pastes are presented in Figures 4.4 and 4.5. Anhydrous phases (mainly belite and ferrite) are found in the samples. The main hydration products are portlandite, ettringite, and ill-crystallized C-S-H by the diffusive peak at 28-33˚.

The main difference regarding the hydration products formed in the studied pastes were found at low angles (8-13˚ 2θ), where the main peaks of the AFt (mostly, ettringite) and AFm (mainly hydroxy-AFm, hemicarbonate, monocarbonate and monosulfate) phases were found. As indicated in the literature, AFm phases have generally low crystallinity and variations in composition that lead to changes in position and intensity reflections in the XRD patterns [39].

After 3 days of hydration, ettringite (9.1˚ 2θ) were observed in all samples. In the absence of limestone, ettringite reacts with the remaining aluminates to form monosulfate (9.9˚ 2θ) after all gypsum was consumed. In the limestone containing pastes, monocarbonate (11.7˚ 2θ) and hemicarbonate (10.8˚ 2θ) were suggested to form instead of monosulfate. Small peaks representing hemicarbonate (Hc) could be observed in the OPCNL paste at 3 and 7 days. At 28 days, a broad peak located around 10.4˚ (between the peaks of monosulfate and hemicarbonate) was observed in the OPCNL paste, which might be associated with a carbonate and sulfate containing hydroxy-AFm.

In the cement-fly ash blended pastes, a hemicarbonate peak is clearly visible in the OPCFANL paste at 28 days (Figure 4.6). XRD results confirmed the formation of hemicarbonate in limestone-containing pastes and suggested that the reaction between limestone and aluminate phases was more pronounced in fly ash blended pastes at 28 days.

4.3.2.3 Analysis of TG and DTG curves

Thermogravimetric (TG) and differential thermogravimetric (DTG) curves of the samples after 3, 7, and 28 days of hydration are shown in Figures 4.7 and 4.8. In the cement pastes without fly ash replacement, the peak at about 80 ˚C in the DTG curves, partially due to the decomposition of ettringite, is larger in nano-limestone modified paste, showing that nano-limestone seems to stabilize ettringite. The nano-limestone modified pastes displayed a small bump at around 125 ˚C at 3 days, and this bump developed into a clear peak at 7 and 28 days, which might be associated with the decomposition of hemicarbonate AFm phase. Correspondingly, the other pastes displayed a peak at around 155 ˚C at 7 and 28 days which might be associated with the decomposition of monosulfate AFm phase. At 3 days, a vague bump at around 155 ˚C could be observed in the nano-silica and nano-clay modified pastes.

Similar observations can be made when 30% of portland cement was replaced by fly ash. It is noted that the peaks relating to the AFm phases (hemicarbonate and monosulfate) are not clear in the cement-fly ash pastes until 28 days.

4.3.2.4 Amount of chemically bound water and calcium hydroxide

The variations of calcium hydroxide (CH) and chemically bound water (H) contents with age for the studied pastes are shown in Figures 4.9 and 4.10, respectively. For cement-fly ash blended pastes, the CH and H contents are expressed as percentages both of weight of the ignited sample and weight of the anhydrous cement in the sample. Chemically bound water is split into two components: water held by calcium hydroxide (CH-water) and water held in other hydration products (H-water).

H% increased with the increase of curing age for all hydrated cement pastes. This is mainly due to the continuous hydration of cement grains leading to the formation of hydration products, which deposited in the available pore space. To examine the pozzolanic reactivity of fly ash and its effect on cement hydration, the CH and H contents of two pates, the ordinary portland cement paste (OPC) and the blend paste with 30% fly ash (OPCFA), are compared. That the amount of CH per cement was higher in OPCFA than in OPC at 3 days indicated that the presence of fly ash accelerated the early hydration of cement (Figure 4.9a and b). It was suggested that the presence of fly ash promoted the hydration of cement grains by the augmentation of available water and the heterogeneous nucleation of calcium hydroxide and calcium-silicate-hydrate on the fly ash surface [40]. On the other hand, the amount of total chemically bound water per gram of ignited sample was lower in OPCFA than in OPC at all tested ages (Figures 4.10a and c), indicating that the acceleration effect of fly ash did not compensate for the dilution effect (reduction in the amount of the most reactive component, cement). After certain period of hydration, the pozzolanic reaction

of fly ash with $Ca(OH)_2$ started, calcium hydroxide was consumed and C-S-H with a reduced Ca/Si was formed. The much larger increase in H-water/CH-water ratio (20.6%) from 7 to 28 days of the OPCFA paste comparing to the only 7.7% increase in H-water/CH-water ratio of the OPC paste indicated that fly ash reacted to consume calcium hydroxide and form C-S-H hydrates during this period (Figures 10a and b). However, the CH content in OPCFA still increased by 4.9% from 7 to 28 days suggesting that the calcium hydroxide consumed by fly ash was less than that produced by cement hydration during this period (Figure 4.9b).

When 1% nanomaterials were added to the portland cement (OPC) paste, increases in both the chemically bound water and calcium hydroxide contents were observed at 3 days (Figures 4.9a and 4.10a). This mostly may be attributed to the heterogeneous nucleation accelerating effect of nanoparticles. The OPCNS paste modified with nano-silica displayed the highest CH% and H% at this time. This may suggest that at this time, rate of Ca $(OH)_2$ liberation enhanced by the addition of nano-silica was much higher than the rate of consumption by pozzolanic reaction with nano-silica.

At 7 and 28 days, nano-limestone and nano-silica increased the amount of total chemically bound water, probably resulting from their continuous nucleation accelerating effects. H-water content increased while water from calcium hydroxide tended to decrease (Figures 4.9a and 4.10a). This may due to (1) depression in the hydration reaction of C_2S and C_3S, and acceleration in the hydration of aluminate phases, and (2) the consumption of calcium hydroxide and the formation of new hydration product. In the paste with limestone, previous research had suggested that calcium hydroxide can intervene in systems containing calcium carbonate and tricalcium aluminate to form a calcium hemicarboaluminate hydroxide ($C_3A{\cdot}0.5\ CaCO_3{\cdot}0.5\ Ca(OH)_2{\cdot}11.5\ H_2O$) [21, 22, 41]. This may be the case for the OPCNL paste with nano-limestone at 7 days. The

existence of hemicarboaluminate at 7 days in the OPCNL paste was confirmed in the TGA curves. In the nano-silica modified OPCNS paste, it is suggested that nano-silica reacted with calcium hydroxide to form C-S-H hydration product. The reactivity of nano-silica was confirmed by the considerably increment in the H-water content. Nano-clay addition also increased chemically bound water content and decreased calcium hydroxide content at 7 days. One possible explanation is that this nano-clay also displayed pozzolanic reactivity. The chemically bound water content in the OPCNC paste at 28 days was close to that of the OPC paste.

In the fly ash blended pastes, similar observations were made when 1% nanomaterial was added (Figures 4.9b and 4.10b), but more pronounced. It is noted that the pozzolanic reaction in the OPCFANS paste was more pronounced at early ages. At 3 days, nano-silica was the least effective in increasing the calcium hydroxide content, while it was the most effective in increasing the chemically bound water content. This implied that the early age pozzolanic reaction in the OPCFANS paste was significantly activated at early ages. Besides, the reduction in the CH-water caused by nano-limestone addition at 28 days was more significant in the presence of fly ash, probably due to the additional alumina provided by the late fly ash reaction.

4.3.3 Compressive strength

The compressive strengths of ordinary portland cement and cement-fly ash blended pastes with and without nanomaterial at 3, 7, and 28 days are presented in Figures 4.11a and b. Each compressive strength value was the average of three samples. The replacement of 30% of cement with fly ash led to a decrease in compressive strength at all tested ages, especially at 3 days. It can be seen that regardless their types, addition of 1% nanomaterial increased the compressive strength of portland cement and cement-fly ash pastes at all tested ages. The increase appeared more substantial at the age of 7 days, especially for cement-fly ash pastes. This is consistent with some

previous research, which had found that nano-silica clearly improved the early-age strength (before 7 days) of OPCFA systems, but the strength gain diminished at later ages (after 28 days) [19]. It can also be observed that among three types of nanomaterials studied, addition of 1% nano-silica improved the strength of both cement pastes and cement-fly ash pastes the most at almost all ages.

4.3.4 Effects of cement hydration characteristics on paste strength

Cement hydration contributes to concrete strength in two major ways: (a) providing cementing property to bond particles together and (b) filling spaces between particles in the system. The cementing property is mainly resulting from C-S-H gel. The TGA test results from the present study have shown that the addition of 1% nanomaterials, regardless their types, increased H-water or C-S-H content for both cement and cement-fly ash pastes at all ages (Figure 4.10), thus enhancing the strength of the pastes with nanomaterials (Figure 4.11). As discussed previously, the increased H-water or C-S-H content is largely attributed to the nucleation effect of the nanoparticles.

It can be observed in Figures 4.10a and b that at the age of 28 days, the amount of H-water and the total chemically bounded water in the pastes with nano-silica (OPCNS and OPCFANS) were lower than those in the pastes with nano-limestone (OPCNL and OPCFANL). However, the strength of the pastes with nano-silica is higher than the pastes with nano-limestone. This may be attributed to the smaller size of nano-silica particles (10-20 nm), compared with 15-40 nm for nano-limestone particles. The nano-silica particles have a stronger hydration accelerating ability and pozzolanic reactivity which result in more C-S-H hydration products. This effect is even more pronounced in the presence of fly ash. On the other hand, nano-limestone is confirmed to react in cement pastes as early as 3 days and to result in a larger volume of the hydration products then the reference paste. Perhaps more important is the possible relationship of this structure to

permeability and transport properties, suggesting more research. In the presence of fly ash, the additional aluminates brought into the system by fly ash due to its pozzolanic reaction at 28 days amplify the reaction of nano-limestone.

4.4 Conclusions

The effect of three nanomaterials, nano-limestone (NL), nano-silica (NS), and nano-clay (NC) on the hydration and strength development of ordinary portland cement pastes and cement-fly ash blended cement pastes were investigated. The following conclusions can be drawn:

1. Regardless the types of nanomaterials, 1% nanomaterial addition improve the compressive strength of both cement and cement-fly ash pastes at all ages studied (up to 28 days). Among three nanomaterials studied, NS appeared to be the most effective one in the strength development, possibly due to its smallest particle size and highest reactivity.

2. Chemical shrinkage and thermogravimetric analysis (TGA) results indicated that FA replacement for cement accelerated cement hydration while having a dilution effect. From 7 to 28 days, fly ash started to react and consume calcium hydroxide. When 1% nanomaterials were added to the cement or cement-fly ash paste, the amounts of both CH-water and H-water increased, indicating that the nanomaterials accelerated cement hydration. This acceleration effect resulting from nanomaterial additions was more profound for the OPCFA pastes.

3. For the cement pastes, nanomaterial addition generally increased chemical shrinkage values, which confirmed the hydration acceleration effects of nanomaterials. However, for the cement-fly ash paste, only nano-silica addition increased chemical shrinkage of the paste at all ages tested. At 28 days, the nano-limestone and nano-clay additions actually reduced chemical shrinkage value of the pastes. This implied that in these pastes, the permeation of water was inhibited.

4. TGA and XRD results confirmed that nano-limestone reacted in the hydrated pastes to form new hydration products which consumed calcium hydroxide. In the presence of fly ash, the reaction between nano-limestone and the aluminate phases was amplified at 28 days, probably due to the additional alumina provided by the late fly ash reaction.

4.5 Acknowledgements

The authors would like to acknowledge the Oak Ridge Associated Universities (ORAU) - Tennessee Valley Authority (TVA), USA, for sponsoring the present study (Grant No. 7-22976).

4.6 References

[1] B. Birgisson, A. K. Mukhopadhyay, G. Geary, M. Khan, and K. Sobolev, "Nanotechnology in Concrete Materials-A synopsis," Transportation Research Circle E-C170, 2012.

[2] F. Pacheco-Torgal, and S. Jalali, "Nanotechnology: Advantages and drawbacks in the field of construction and building materials," Construction and Building Materials, vol. 25, pp. 582-590, 2011.

[3] M. L. Nehdi, "Clay in cement-based materials: Critical overview of state-of-the-art," Construction and Building Materials, vol. 51, pp. 372–382, 2014.

[4] F. Sanchez, and K. Sobolev, "Nanotechnology in concrete – A review," Construction and Building Materials, vol. 24, pp. 2060–2071, 2010.

[5] K. Sobolev, "Nanotechnology and Nanoengineering of Construction Materials," presented at the 5th International Symposium on Nanotechnology in Construction, Chicago, 2015.

[6] X. Wang, K. Wang, J. Tanesi, and A. Ardani, "Effects of nanomaterials on the hydration kinetics and rheology of portland cement pastes," Advances in Civil Engineering Materials, vol. 3, pp. 142-159, 2014.

[7] X. Wang, K. Wang, J. Li, N. Garg, and S. P. Shah, "Properties of self-consolidating concrete containing high volume supplementary cementitious materials and nano-limestone," Journal of Sustainable Cement-Based Materials, vol. 3, pp. 245-255, 2014.

[8] X. Liu, L. Chen, A. Liu, and X. Wang, "Effect of nano-CaCO3 on properties of cement paste," Energy Procedia, vol. 16, pp. 991-996, 2012.

[9] L. P. Singh, S. R. Karade, S. K. Bhattacharyya, M. M. Yousuf, and S. Ahalawat, "Beneficial role of nanosilica in cement based materials – A review," Construction and Building Materials, vol. 47, pp. 1069–1077, 2013.

[10] A. Hakamy, F. U. A. Shaikh, and I. M. Low, "Characteristics of nanoclay and calcined nanoclay-cement nanocomposites," Composites Part B, vol. 78, pp. 174-184, 2015.

[11] J. J. Thomas, H. M. Jennings, and J. J. Chen, "Influence of nucleation seeding on the hydration mechanisms of tricalcium silicate and cement," The Journal of Physical Chemistry C, vol. 113, pp. 4327-4334, 2009.

[12] X. He and X. Shi, "Chloride permeability and microstructure of Portland cement mortars incorporating nanomaterials," Transportation Research Record: Journal of the Transportation Research Board, vol. 2070, pp. 13-21, 2008.

[13] Z. Li, H. Wang, S. He, Y. Lu, and M. Wang, "Investigations on the preparation and mechanical properties of the nano-alumina reinforced cement composite," Materials Letters, vol. 60, pp. 356–359, 2006.

[14] T. Oey, A. Kumar, N. Neithalath, J. W. Bullard, and G. Sant, "The filler effect: the influence of filler content and surface area on cementitious reaction rates " Journal of the American Ceramic Society, vol. 96, pp. 1978–1990, 2013.

[15] F. T. Shunsuke Haneharaa, Makoto Kobayakawa, KwangRyul Hwang, "Effects of water/powder ratio, mixing ratio of fly ash, and curing temperature on pozzolanic reaction of fly ash in cement paste," Cement and Concrete Research vol. 31, pp. 31-39, 2001.

[16] M.-H. Zhang and J. Islam, "Use of nano-silica to reduce setting time and increase early strength of concretes with high volumes of fly ash or slag," Construction and Building Materials, vol. 29, pp. 573-580, 2012.

[17] G. Li, "Properties of high-volume fly ash concrete incorporating nano-SiO2," Cement and Concrete Research, vol. 34, pp. 1043-1049, 2004.

[18] A. M. Said and M. S. Zeidan, "Enhancing the reactivity of normal and fly ash concrete using colloidal nano-silica," ACI Special Publication, vol. 267, pp. 75–86, 2009.

[19] P. Hou, K. Wang, J. Qian, S. Kawashima, D. Kong, and S. P. Shah, "Effects of colloidal nanoSiO2 on fly ash hydration," Cement and Concrete Composites, vol. 34, pp. 1095–1103, 2012.

[20] K. D. Weerdt, K. O. Kjellsen, E. Sellevold, and H. Justnes, "Synergy between fly ash and limestone powder in ternary cements," Cement and Concrete Composites, vol. 33, pp. 30-38, 2011.

[21] B. Lothenbach, G. L. Saout, E. Gallucci, and K. Scrivener, "Influence of limestone on the hydration of Portland cements," Cement and Concrete Research, vol. 38, pp. 848–860, 2008.

[22] G. Kakali, S. Tsivilis, E. Aggeli, and M. Bati, "Hydration products of C3A, C3S and Portland cement in the presence of CaCO3," Cement and Concrete Research, vol. 30, pp. 1073-1077, 2000.

[23] A. Ipavec, R. Gabrovšek, T. Vuk, V. Kaučič, J. Maček, and A. Meden, "Carboaluminate phases formation during the hydration of calcite-containing Portland cement," Journal of the American Ceramic Society, vol. 94, pp. 1238–1242, 2011.

[24] M. Zajac, A. Rossberg, G. L. Saout, and B. Lothenbach, "Influence of limestone and anhydrite on the hydration of Portland cements," Cement and Concrete Composites, vol. 46, pp. 99-108, 2014.

[25] K. D. Weerdt, M. B. Haha, G. L. Saout, K. O. Kjellsen, H. Justnes, and B. Lothenbach, "Hydration mechanisms of ternary Portland cements containing limestone powder and fly ash," Cement and Concrete Research, vol. 41, pp. 279-291, 2011.

[26] B. Y. Pekmezci, T. Voigt, K. Wang, and S. P. Shah, "Low compaction energy concrete for improved slip-form casting of concrete pavements," ACI Materials Journal vol. 104, pp. 251-258, 2007.

[27] N. A. Tregger, M. E. Pakula, and S. P. Shah, "Influence of clays on the rheology of cement pastes," Cement and Concrete Research vol. 40, pp. 384-391, 2010.

[28] L. Ruiz-Ripoll, S. P. Shah, B. E. Barragan, and J. Turmo, "Effect of mix design on fresh self-consolidating concrete and inferences on formwork pressure," Journal of Materials in Civil Engineering, vol. 27, pp. 1-7, 2015.

[29] H. Lindgreen, M. Geiker, H. Krøyer, N. Springer, and J. Skibsted, "Microstructure engineering of Portland cement pastes and mortars through addition of ultrafine layer silicates," Cement and Concrete Composites, vol. 30, pp. 686-699, 2008.

[30] "What is Acti-Gel® 208 and how is it made?," Active Minerals Company LLC, 2007.

[31] S. J. Doktycz and K. S. Suslick, "Interparticle collisions driven by ultrasound," Science, vol. 247, pp. 1067-1069, 1990.

[32] K. Higashitani, K. Yoshida, N. Tanise, and H. Murata, "Dispersion of coagulated colloids by ultrasonication," Colloids and Surfaces A: Physicochemical and Engineering Aspects, vol. 81, pp. 167-175, 1993.

[33] K. Sato, J. G. Li, H. Kamiya, and T. Ishigaki, "Ultrasonic dispersion of TiO2 nanoparticles in aqueous suspension," Journal of the American Ceramic Society, vol. 91, pp. 2481-2487, 2008.

[34] ASTM C1608: Standard Test Method for Chemical Shrinkage of Hydraulic Cement Paste," Annual Book of ASTM Standards, ASTM International, West Conshohocken, PA, 2012.

[35] J. Zhang and G. W. Scherer, "Comparison of methods for arresting hydration of cement," Cement and Concrete Research, vol. 41, pp. 1024-1036, 2011.

[36] B. K. Marsh and R. L. Day, "Pozzolanic and cementitious reactions of fly ash in blended cement pastes," Cement and Concrete Research, vol. 18, pp. 301-310, 1988.

[37] B. K. Marsh, "Relationships between engineering properties and microstructural characteristics of hardened cement paste containing pulverised-fuel ash as a partial cement replacement," Doctor of Philosophy, The Hatfield Polytechnic, 1984.

[38] L. J. Parrott, M. Geiker, W. A. Gutteridge, and D. Killoh, "Monitoring Portland cement hydration: Comparison of methods," Cement and Concrete Research, vol. 20, pp. 919-926, 1990.

[39] T. Matschei, B. Lothenbach, and F. P. Glasser, "The AFm phase in Portland cement," Cement and Concrete Research vol. 37 pp. 118-130, 2007.

[40] Q. Zeng and K. Li, "Reaction and microstructure of cement–fly-ash system," Materials and Structures, vol. 48, pp. 1703-1716, 2015.

[41] V. L. Bonavetti, V. F. Rahhal, and E. F. Irassar, "Studies on the carboaluminate formation in limestone filler-blended cements," Cement and Concrete Research, vol. 31, pp. 853–859, 2001.

Tables:

Table 4.1 Chemical composition (wt. %) and physical characteristics of materials used in this study.

Chemical composition	PC	FA	NC	NL	NS
			(wt.%)		
SiO_2	20.20	46.00	49.57		
Al_2O_3	4.70	17.80	9.44		
Fe_2O_3	3.30	18.20	3.31		
SO_3	3.30	2.59	-		
CaO	62.90	8.40	1.88		
MgO	2.70	0.95	8.81		
Na_2O	-	0.59	0.59	$CaCO_3$ > 97.5%	SiO_2 > 99.5%
K_2O	-	2.16	0.66		amorphous
Eq. Na_2O	0.54	2.01	-		
P_2O_5	-	0.11	-		
TiO_2	-	0.93	0.42		
SrO	-	0.03	-		
BaO	-	0.05	-		
LOI	1.10	1.49	<0.50		
Physical Properties					
Specific gravity	3.15	2.51	2.62	2.70	2.30
Specific surface area	391 (Blaine, m^2/kg)	310	150 (BET, m^2/g)	-	-
Particle size (BET, nm)	-	-	-	15-40	10-20

Table 4.2 Mix proportions for the studied cementitious pastes in wt. %

Mix ID	PC	FA	NL	NS	NC
OPC	100	-	-	-	-
OPCNL	100	-	1	-	-
OPCNS	100	-	-	1	
OPCNC	100	-	-	-	1
OPCFA	70	30	-	-	-
OPCFANL	70	30	1	-	-
OPCFANS	70	30	-	1	
OPCFANC	70	30	-	-	1

Figures:

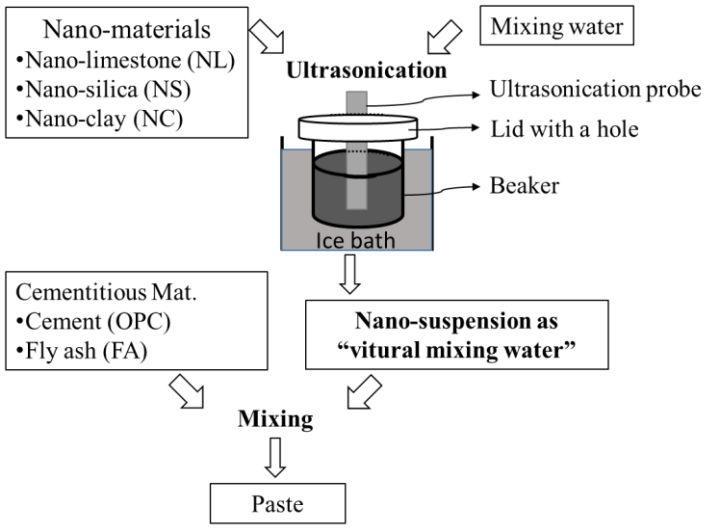

Figure 4.1. Diagram illustration of the mixing process.

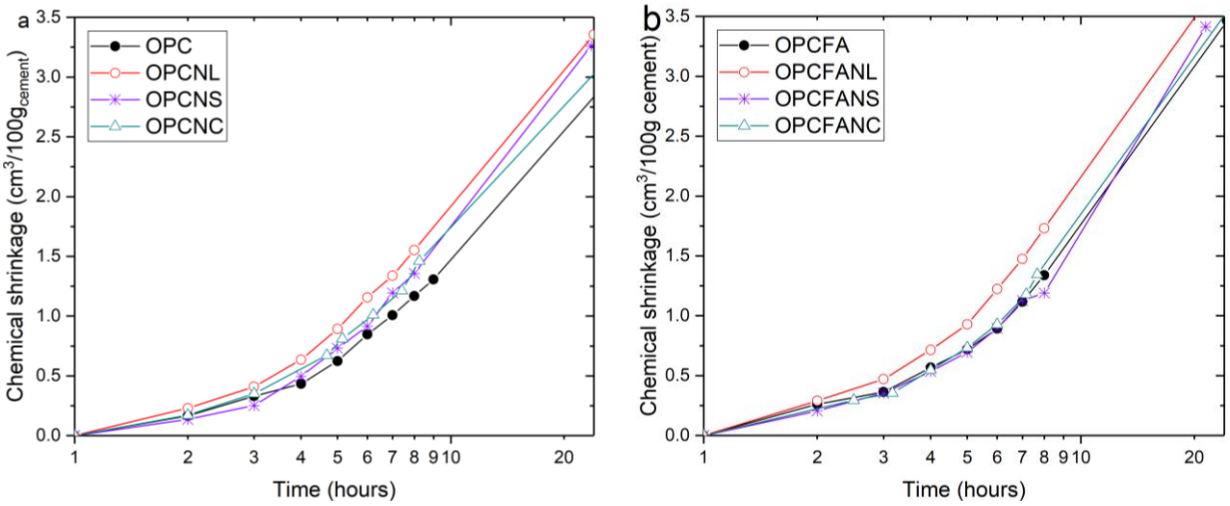

Figure 4.2. Chemical shrinkage relative to the cement content during the first 24 h for (a) cement pastes and (b) cement-fly ash pastes.

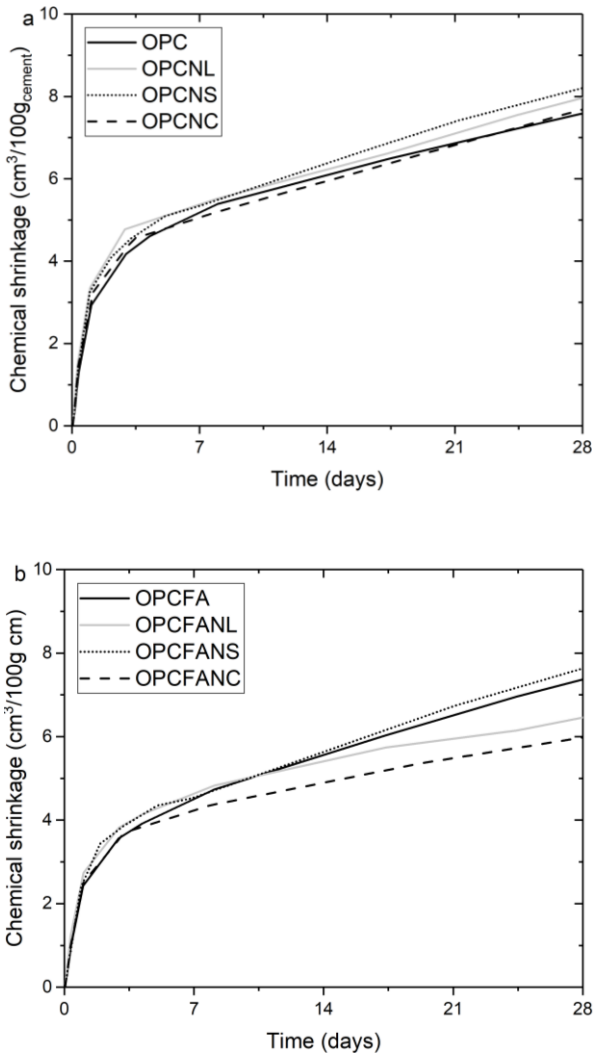

Figure 4.3. Chemical shrinkage relative to the cementitious materials content up to 28 days for (a) cement pastes and (b) cement-fly ash pastes.

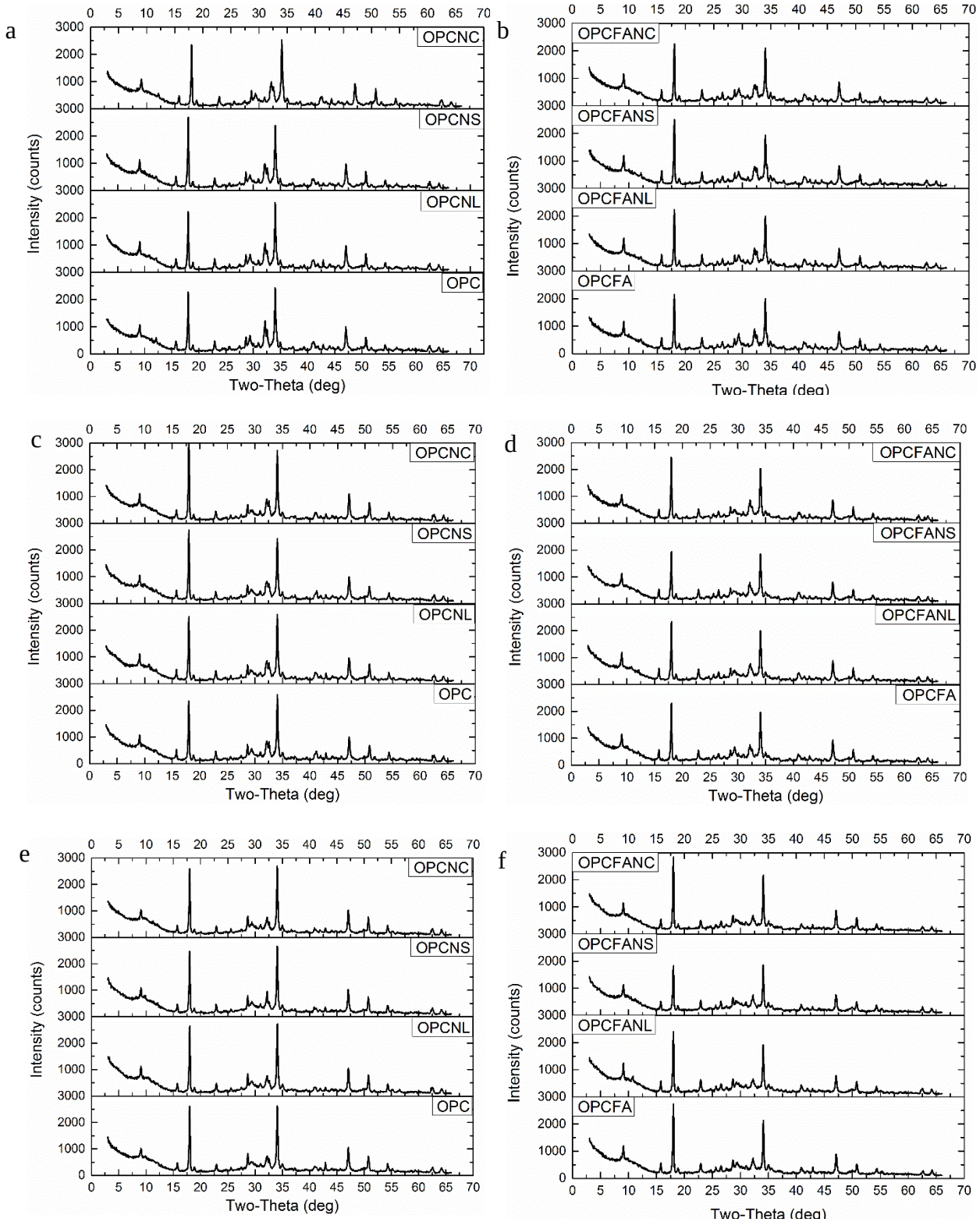

Figure 4.4. X-ray diffraction patterns for (a) cement pastes at 3 days, (b) cement-fly ash pastes at 3 days, (c) cement pastes at 7 days, (d) cement-fly ash pastes at 7 days, (e) cement pastes at 28 days, (f) cement-fly ash pastes at 28 days.

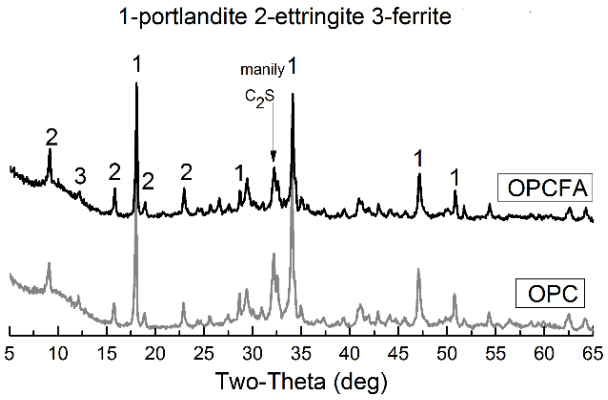

Figure 4.5. Diffraction patterns with peak assignments for the ordinary portland cement paste (OPC) and the cement-fly ash blended paste (OPCFA) at 3 days.

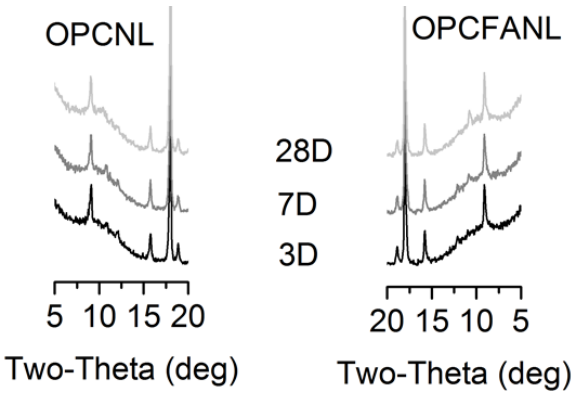

Figure 4.6. X-ray diffraction patterns for the cement paste with nano-limestone (OPCNL) and cement-fly ash paste with nano-limestone (OPCFANL) at 28 days.

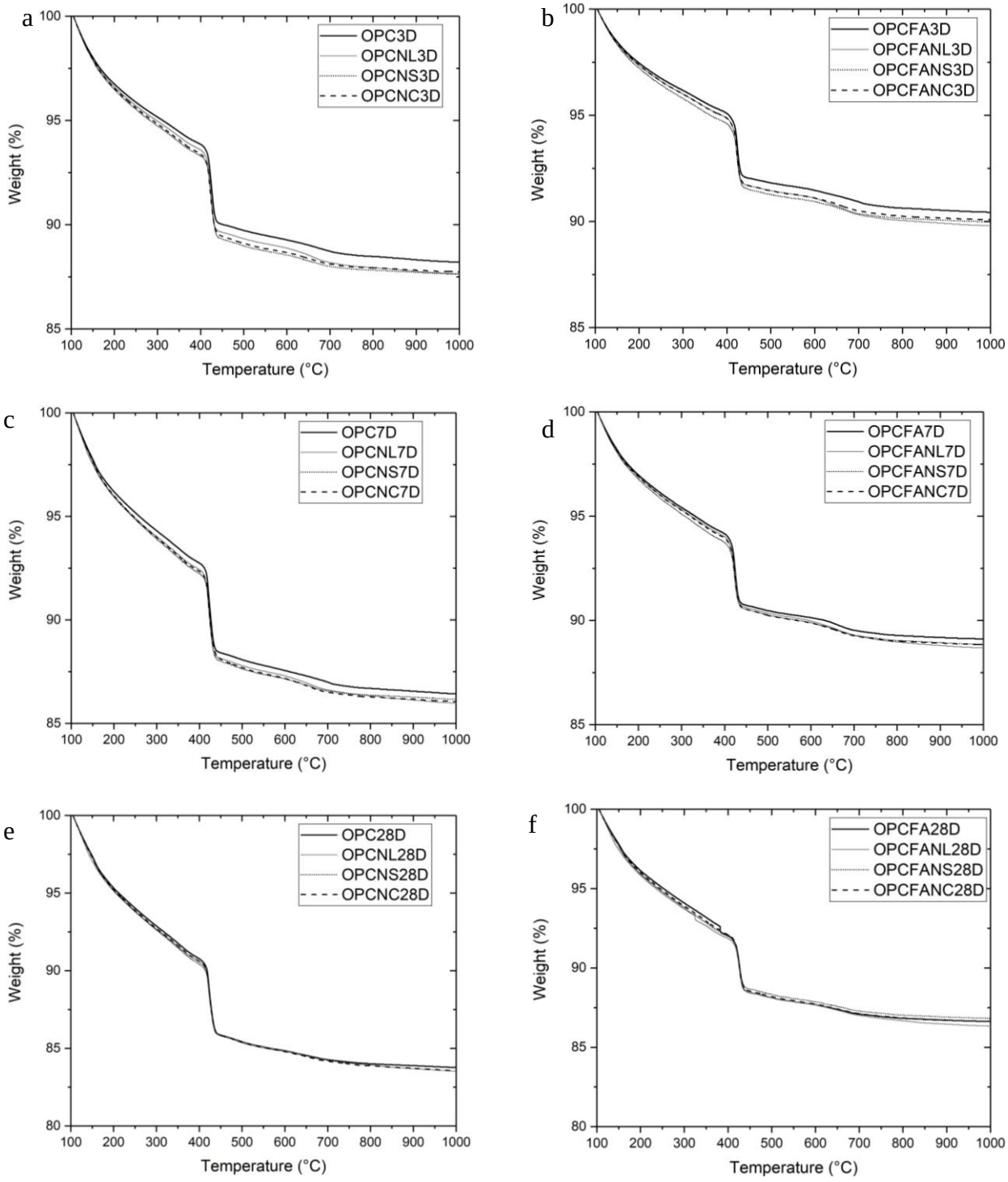

Figure 4.7. The thermogravimetric (TG) curves for cement and cement-fly ash blended cement pastes with and without nanomaterials.

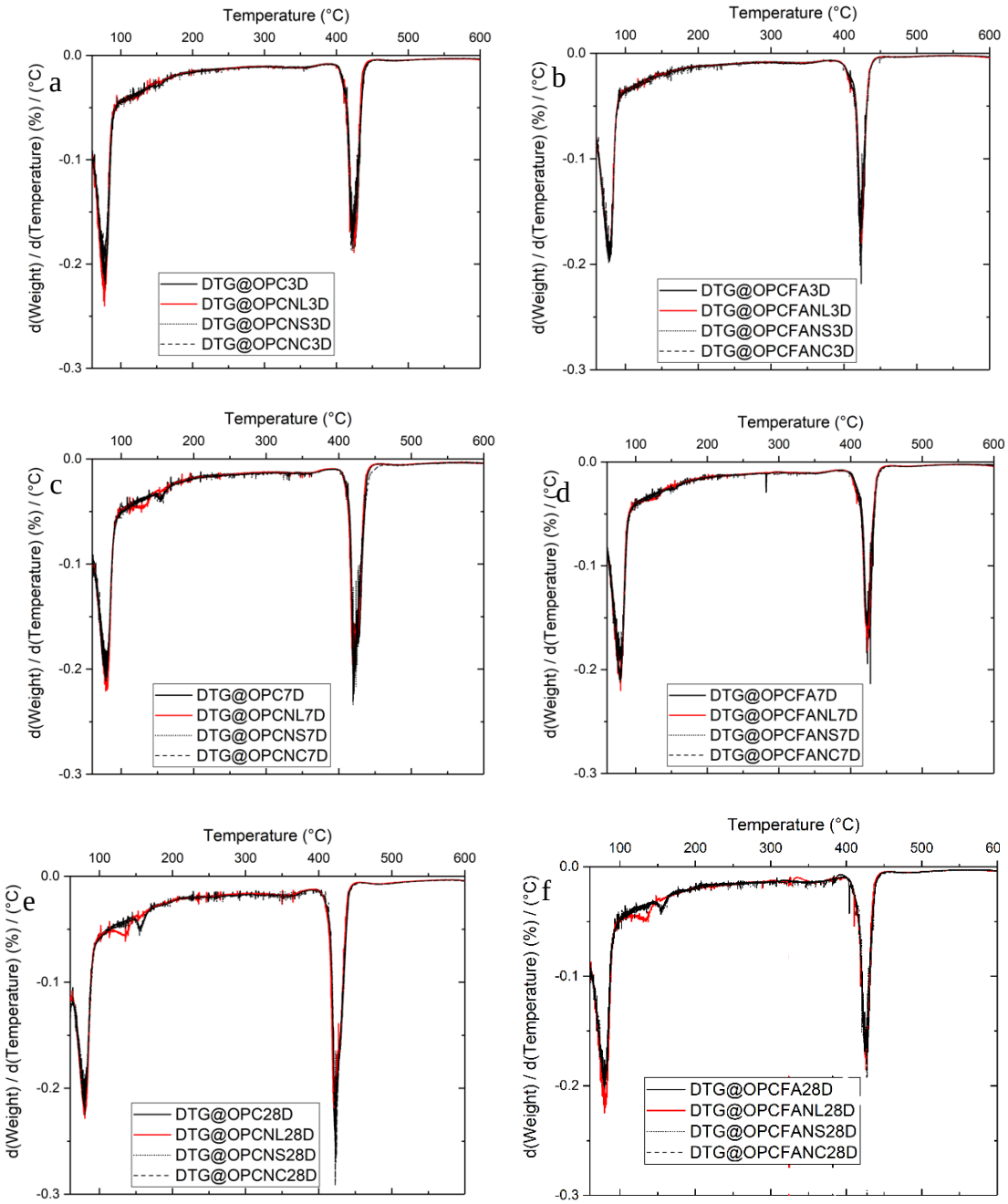

Figure 4.8. The differential thermogravimetric (DTG) curves for cement and cement-fly ash blended cement pastes with and without nanomaterials.

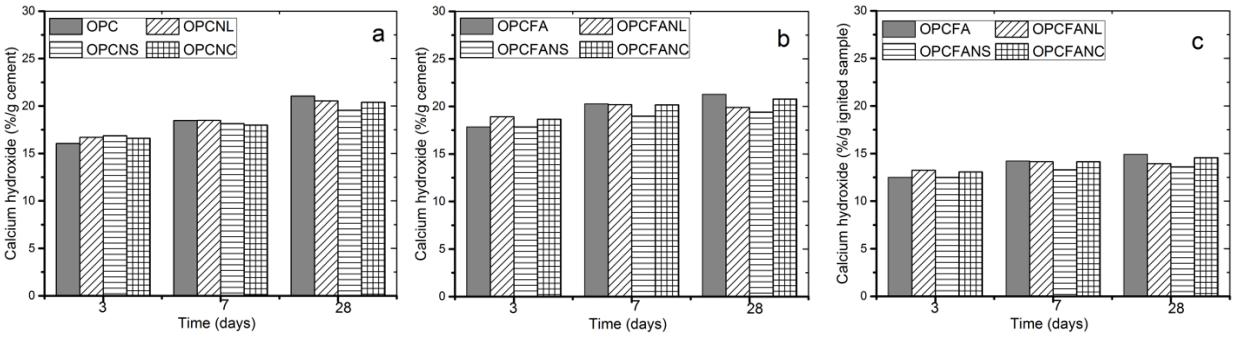

Figure 4.9. The calcium hydroxide (CH) contents for (a) nanomaterial modified ordinary portland cement pastes and (b) and (c) nanomaterial modified cement-fly ash blended cement pastes after 3, 7, and 28 days of curing.

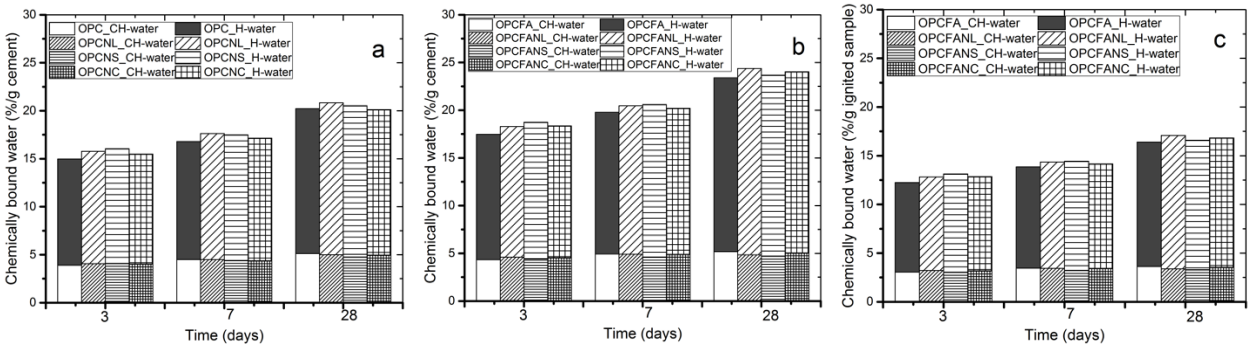

Figure 4.10. The chemically bound water (H) contents for (a) nanomaterial modified ordinary portland cement pastes and (b) and (c) nanomaterial modified cement-fly ash blended cement pastes after 3, 7, and 28 days of curing. Chemically bound water was split into two components: water held by calcium hydroxide (CH-water) and water held in other hydration products (H-water).

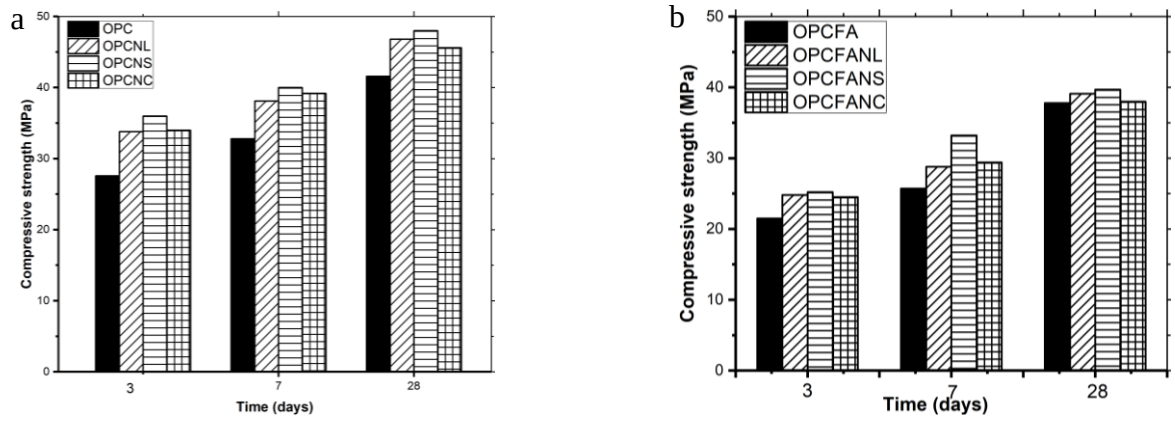

Figure 4.11. The compressive strength after 3, 7, and 28 days of curing for (a) ordinary portland cement pastes, and (b) fly ash blended cement pastes.

CHAPTER 5. EFFECTS OF NANOMATERIALS ON THE DRYING SHRINKAGE AND PORE STRUCTURE OF CEMENT PASTES

Modified from a paper to be submitted to *Cement and Concrete Research*

Xin Wang[a], Kejin Wang[b]

[a] Dept. of Civil, Construction, and Environmental Engineering, Iowa State Univ., Ames, Iowa 50010. Tel: 515-294-2140. Email: wangxin@iastate.edu
[b] Corresponding author, Dept. of Civil, Construction, and Environmental Engineering, Iowa State Univ., Ames, Iowa 50010. Tel: 515-294-2151. Email: kejinw@iastate.edu

Abstract

In this work, the effects of nano-limestone (NL) and nano-silica (NL) on the pore structure and drying shrinkage of portland cement pastes with and without 30% fly ash (FA) replacement were investigated. Cement pastes were prepared with a water-to-cementitious material ratio (w/cm) of 0.5, and nanomaterials were incorporated into these pastes as an addition at the level of 1% (by wt. of cementitious materials). After 7 and 28 days of curing, stepwise drying-shrinkage tests were performed on thin disc paste samples (with a diameter of 25 mm and thickness of 0.80 mm). The disc samples were dried from the saturated surface dry condition (100% RH) to 33% RH and then re-saturated to 100% RH. Pore structures of the samples were examined using nitrogen adsorption tests. The effects of pore size and volume on the total, reversible, and irreversible drying shrinkage of the pastes were then analyzed. The results indicate that additions of the nanomaterials increased the specific surface area and the amount of gel pores (2-10 nm) in the early age (7 days) cement pastes. At 28 days, addition of nano-silica continued to increase the specific surface area and the amount of gel pores, especially in the fly ash blended paste. However, addition of nano-limestone reduced the specific surface area and the total amount of pores (2-100 nm) at 28 days, especially in the portland cement paste. An additional signature pore peak located around 18 nm was observed

in the nano-silica modified and 28-days fly ash blended pastes. Additions of nano-silica generally increased the total shrinkage of cement pastes. However, addition of nano-limestone sometimes reduced drying shrinkage, especially for the later age cement pastes. The shrinkage in each relative humidity range was found to be dependent on the volume of pores evaporate in the corresponding RH range and the resistance of the paste to deformation, especially at 7 days. Nanomaterial additions and extended curing increased reversible drying shrinkage, which suggests that the volume of gel (2-10 nm) pores appeared more closely related to reversible shrinkages. The 7-day OPCFA pastes were more prone to irreversible drying shrinkage, especially with the addition of nanomaterials.

5.1 Introduction

Nanoparticles are increasingly used in cement-based materials for the improvements of concrete workability, mechanical properties, and durability. Research has indicated that well dispersed nanoparticles can act as nucleation sites for crystallization of cement hydrates, thus accelerating cement hydration, and they can serve as a filler to fill the pores between cement grains, thereby refining pore structure and immobilizing free pore water [1]. However, as more hydration products form and more pores are refined, smaller radii of water menisci will form between solid particles when concrete is subjected to drying. This in turn creates high capillary pressure, causes concrete to shrink, and sometimes leads to crack [2]. There is a great concern for shrinkage of concrete containing nanoparticles.

Drying shrinkage is a volume reduction resulting primarily from loss of water in the concrete that is exposed to a low environmental humidity, and it is one of the most common causes of concrete cracking. Water in concrete can be classified in different ways. Based on its mobility, water can be categorized as (a) bulk water, which is often free to move, (b) surface water, which

is adsorbed on the surface of pores, and (c) interlayer water, which is chemically bonded between the layers of calcium-silicate-hydrate (C-S-H) gel, the major hydration product of a cement paste [3]. Based on the sizes of the pores that it stays, water can be sorted as (a) capillary water, in pores with sizes ranging approximately from 10 nm to 10 um, (b) gel water, in pores with sizes ranging approximately from 0.5 nm to 10 nm, and (c) interlayer water, in the C-S-H gel spaces mostly less than 0.5 nm [4].

A hydrated cement paste consists of mostly capillary pores, namely the unfilled spaces between cement grains. Large capillary pores (>50 nm) are mainly filled with bulk water when concrete is under a saturated condition, where the portion of surface water is small. When saturated concrete is subjected to drying (relative humidity (RH) <100%), bulk water can easily and freely evaporate without producing menisci and causing cement paste to shrink. As pore sizes decrease, surface water becomes a significant portion of the total water in pores. In the pores are partially water-filled, adhesion of water to the walls of the pores is larger than the cohesion of water molecules, thus producing an upward force on the edges of the water and generating a concave meniscus (the interface between water and air). When such water evaporates, tension builds up in the remaining water. This induces a capillary tension and exerts a compression on the walls of the pores, thus bringing about concrete volume change. Based on the Kelvin's and Laplace's laws, the capillary tensile stress increases as the pore size decreases [5]. When water in medium capillary pores (10 nm - 50 nm) evaporates (usually under a high RH, around 85%), moderately strong menisci produces, and shrinkage of the cement paste becomes significant. When water in small gel pores (2.5 nm -10 nm) vaporizes (under a RH close to 50%), strong menisci produces under a strong capillary tension, and shrinkage of the cement paste becomes much more significant. The shrinkage resulting from the evaporation of water in pores $\geqslant$2.5nm may be reversible upon

resorption of moisture [3]. However, research also suggested that capillary pressures could not exist below about 40% RH because the liquid/vapor menisci would become unstable below such a low RH. Therefore, the water adsorbed on the surfaces of micro-gel pores (0.5 nm-2.5 nm) is generally non-evaporable due to the intermolecular interactions. When it is removed by a strong drying force (RH=11-35%), surface energy of the C-S-H gel solid increases. To minimize the surface energy, a compression will be exerted to the surrounding C-S-H gel solid and causes the C-S-H gel to shrink. Finally, the chemically bonded water in the C-S-H interlayer spaces (<0.5 nm) can only be removed by a thermal treatment (under RH<11%). Shrinkage resulting from water removal in the pores 2.5 nm is often considered as irreversible [4].

Although the concept of the effect of concrete pore size on concrete shrinkage is well accepted, quantitative models relating bulk concrete shrinkage with pore sizes are rarely reported. According to Thomas and Jennings [6], it is an often-argued and seldom-resolved issue. It is not clear if only bulk water, adsorbed water, or other water would be evaporated under a given RH and whether or not the evaporation of adsorbed water is truly reversible. Furthermore, as use of nanoparticles in concrete materials is still in its infancy, limited work has been conducted on the shrinkage behavior of nanoparticle-modified concrete. In the present study, the effects of nano-limestone and nano-silica on the drying shrinkage and pore structure of cement pastes containing fly ash are studied. The reversible and irreversible drying shrinkage behaviors of the cement pastes are analyzed, and their relationships with cement paste pore structure are explored.

5.2 Materials and methods

5.2.1 Materials and mix proportions

The cementitious materials used in the present study were Type I/II ordinary portland cement (OPC) and Class F fly ash (FA). Two nanomaterials, nano-silica (NS) and nano-limestone (NL),

were also incorporated into the cementitious system. The chemical and physical properties of the cementitious and nanoparticle materials are summarized in Table 5.1.

In the cement pastes studied, fly ash was used as an OPC replacement, while nanoparticle materials were used as an addition at the level of 1% by weight of cementitious materials. Distilled water was used for mixing, and the water-to-cementitious materials ratio (w/cm) was 0.5. Table 5.2 presents the proportions of the paste mixes evaluated.

5.2.2 Mixing procedures

Nanoparticles tend to agglomerate due to their strong interparticle attraction (i.e. van der Waals forces). To de-agglomerate nanoparticles and achieve a well-dispersed nanomaterial suspension, high intensity ultrasonication was used in this study [7-9]. As illustrated in Figure 5.1, to achieve a homogeneous cement paste, the nanomaterial was first dispersed in mixing water to form a nano-suspension using ultrasonication, and this nano-suspenstion was then used as "virtual mixing water" for the mixing of cementitious materials according to ASTM C1738, Standard Practice for High-Shear Mixing of Hydraulic Cement Pastes.

The ultrasonication was carried out in a beaker with a Sonicator® XL2020 (Qsonica, LLC., USA; frequency: 20 kHz; generating power: 600W). To prevent the water from heating, the beaker was kept in an ice bath, and the suspension was cooled to room temperature after each 3-min continuous ultrasonication (Figure 5.1). Additionally, the losses of water and nanomaterial during ultrasonication were compensated through three steps: (1) the weight of the beaker was measured before and after the ultrasonication; (2) the particles adhered to the probe of the ultrasonic homogenizer were washed into the nano-suspension with a small amount of distilled water; and (3) care was taken to ensure that the weight of the beaker are the same before and after each ultrasonication.

5.2.3 Sample preparation

Cylinder samples (25 mm in diameter and 50 mm in height) were first cast in polystyrene vials sealed in airtight containers, and submerged in a 24 °C water bath. After 24 hours, the samples were demolded and cured at room temperature (24 ± 3 °C) in an airtight container filled with lime-saturated water. After cured for 7 and 28 days, samples were removed from the limewater and the middle parts of the samples were used for pore structure analysis and drying shrinkage tests.

5.2.4 Pore structure analysis

Nitrogen adsorption was chosen to study the pore structure in this study because it depicts the range of pores that are well related to drying shrinkage of the cement pastes. To perform nitrogen adsorption tests, samples were first ground to particle sizes in the range of 600 (No.30 sieve) to 1180 um (No.16 sieve) and then dried using a D-drying apparatus that consisted of a vacuum desiccator and was connected to a trap held at the temperature of dry ice (–79 °C) according to the method of Copeland and Hayes [10]. Samples were dried as they reached the equilibration to the vapor pressure of water at the temperature of dry ice (5 X 10^{-4} torr). Two tests were run for a given type of samples. As illustrated in Figure 5.2, the D-drying was performed using a desiccator evacuated by a vacuum pump with a water vapor pressure of 5×10^{-4} Torr and stored in a dry ice-alcohol bath at a temperature of -79 °C. To prevent samples from carbonation, the desiccator was opened in a ‘‘Nitrogen glove box” when samples were removed from the desiccator. Samples were tested immediately after D-drying so that the measurements would not be affected by the storage time and conditions [11].

After the D-drying, the paste samples (approximately 0.8-1.0 g in weight [12]) were then analyzed for pore size distributions using a nitrogen surface area analyzer (Micromeritics ASAP 2020). The device measures the amount of liquid nitrogen adsorbed by the tested material across

a wide range of relative pressures (p/p^0) with time at a constant temperature. Conversely, it also measures the amount of liquid nitrogen desorbed when gas removed as pressure is reduced. The hysteresis between the adsorption and desorption isotherms can then be obtained.

To start the test, the samples were first degassed at 313K for at least 6 hours under a vacuum of $5*10^{-2}$ torr. The aim of degas is to eliminate most of the species physisorbed onto the sample (e.g. water vapor and CO_2 in the air, etc.) and to make the surface clean for gas adsorption [13]. During the test, an incremental pressure was applied to the tested material and then removed to zero. The corresponding amount of nitrogen absorbed and desorbed was recorded. Porosities and pore size distribution of the tested samples were calculated by the Barret, Joyner and Hallenda (BJH) method from both the adsorption and desorption isotherm. Surface areas were calculated by the Brunauer, Emmett and Teller (BET) method over a relative pressure range of 0.05–0.25 on the adsorption isotherm.

5.2.5. Stepwise drying-shrinkage test

In conventional drying shrinkage tests, relative large specimens are often used. Drying shrinkage strains of these specimens are often obtained under strong hydric gradients. As a result, shrinkage is not truly one-dimensional length change, and a moisture gradient across a specimen may occur and result in subsequent differential shrinkage, which may subsequently cause surface cracking and alter the bulk shrinkage response. To minimize this effect, very thin samples are used in this study. The equilibrium drying experiments were conducted according to the method proposed by Roper and Jennings [14, 15], wherein weight loss and shrinkage were measured simultaneously.

To perform the test, thin (0.80 mm) discs were sliced from the 25 mm x 50 mm cylinder samples using a water-lubricated diamond wire. Four discs were tested for each paste mix. Three lines were drawn across the diameter of each sample for shrinkage measurements (Figure 5.3).

Initially, saturated discs were measured for their weights and diameters and then placed in sealed desiccators (Figure 5.3). Drying shrinkage of the samples occurred when the samples were placed into different desiccator with different RH. As shown in Table 5.3, the RH of desiccators changed from 100% to 84%, 54%, and 33% when different type of salt solutions were placed in the desiccators. All desiccators were filled with nitrogen gas to prevent carbonation, and the temperature was maintained at 22 ± 3 °C. At regular time intervals, the tested paste discs were weighed, and their diameters were measured using a micrometer. Only when the sample diameter and weight measurements are stabilized in one desiccator with a given RH, the sample discs will be moved to the desiccators containing the next-level RH. It is assumed that very little hydration continues during the drying period as the rate of water loss is fast, effectively halting further hydration [16, 17]. Irreversible drying shrinkage was then determined by re-saturating the specimens step-by-step and the last step was placing specimens in limewater. The drying regime used is demonstrated in Figure 5.4, where the total shrinkage under drying as well as reversible and irreversible shrinkage after rewetting are also illustrated.

5.3 Results and discussions

5.3.1 Pore structure analysis

5.3.1.1 Adsorption-desorption isotherms

The adsorption-desorption isotherms of the studied pastes are presented in Figure 5.5. All studied pastes give Type II isotherms, which exhibit Type H3 hysteresis. This isotherm shape can be designated as a Type IIb isotherm [12]. Such an isotherm shape indicates that the material

contains both mesopores (pores of widths between 2 nm and 50 nm as per IUPAC classification), which is responsible for the hysteresis loop and macropores (pores with widths exceeding about 50 nm), which results in the absence of the plateau at high relative pressures like mesoporous Type IV isotherms and the steep loops near saturation pressure (0.98-1.00 p/p^0).

One distinctive feature of the H3 hysteresis is the "forced closure" of the hysteresis loop which is due to a sudden drop in the quantity adsorbed along the desorption branch in the p/p^0 range (0.41-0.48). This characteristic step down, originating from the existence of "ink-bottle" pores (wide pores with narrow entrance), was often discussed within the framework of the tensile strength effect (TSE) hypothesis [17]. During desorption, the "ink-bottle" pores can only empty via narrow necks and accordingly will empty at lower pressures. The TSE hypothesis states that a liquid (capillary) can exist in the pores only if the capillary tension under the meniscus (which is given by the Kelvin Laplace equation) does not exceed the tensile strength of the liquid, which is often thought to be exhausted at no less than 45% of the saturation pressure, if not much higher. When the critical pressure (p/p^0) is reached, the meniscus collapses and the pores are immediately emptied.

In the event of the tensile strength effect, pore structure analysis obtained from the desorption branch of the isotherm can greatly underestimate the average pore radius, and the adsorption isotherm can give a better approximation of the pore structure. Therefore, pore structure data obtained from the adsorption branch was used in this study to discuss the effects of nanomaterials on the pore structure. On the other hand, pore structure data obtained from desorption isotherm was used to relate the pore structure to the drying shrinkage behavior of cement pastes, since drying itself is a desorption process during which "ink-bottle" pores empty through the neck.

5.3.1.2 BET Specific surface area

Surface areas are calculated by the Brunauer, Emmett and Teller (BET) method over a relative pressure range of 0.05–0.25 on the adsorption isotherm. The results are presented in Figure 5.6. For all measurements, the determined C-values fall with the range of 70-100 and the linearity coefficient R^2 were larger than 0.9999.

It should be noted that the main hydration products (>100 m^2/g) have very much greater specific surface areas than unhydrated cement (<1 m^2/g). Consequently, almost immediately after hydration begins, the surface contributed by the unhydrated cement becomes negligible. As shown in Figure 5.6, at the age of 28 days, the specific surface area of all pastes increased when compared with that of the corresponding pastes at 7 days. These increases were attributed to the continued cement hydration. More C-S-H were formed with "intrinsic" gel porosity, and the other hydration products (mainly portlandite, ettringite and AFm phases) also have greater specific surface areas than cement grains.

Comparing the specific surface areas of OPC and OPCFA pastes without nanomaterial additions in Figure 5.6, it is noted that at the age of 7 days, the specific surface are of the OPCFA paste was only slightly lower than that of the OPC paste. While the total amount of hydration product of the OPCFA paste is noticeably lower than that of the OPC paste at this time, the amount of calcium silicate hydrate (C-S-H) accessible to nitrogen is close in these two pastes. This may suggest that a larger portion of low density calcium silicate hydrate (LD C-S-H) was formed in the OPCFA paste, probably due to the relatively more space available for the hydration products to form in. On the other hand, at the age of 28 days, the specific surface are of the OPCFA paste was noticeably lower than that of the OPC paste, which is in accordance with the lower amount of

hydration products in the OPCFA paste. At this time, the main hydration product in the OPCFA paste is C-S(A)-H.

Figure 5.6 shows that nanomaterial additions increased the specific surface area of both portland cement pastes and cement-fly ash pastes at the age of 7 days. This might result from the combination of the hydration acceleration effect and high specific surface area of the nanomaterials (in the same order of the hydration products), the latter of which reflects the filling effects of nanomaterials. Both portland cement pastes and cement-fly ash pastes with nano-silica addition displayed the highest specific surface area, which is in agreement with some previous studies [18] and the fact that nano-silica has a smaller particle size range (10-20 nm, Table 5.1) and high pozzolanic reactivity. Moreover, in the nano-silica modified pastes, C-S-H with a lower Ca/Si was formed which may possess a higher specific surface area.

Similar to what was observed on the pastes cured for 7 days, NS addition increased the specific surface area of both OPC and OPCFA pastes with no nanomaterial at 28 days. However, when compared with the paste with no nanomaterial, NL decreased the specific surface area of pastes at 28 days, especially the OPC paste. This implies that the addition of nano-limestone to an OPC paste might impair cement hydration at a later age (28 days). Another possible explanation is that a higher portion of high density calcium silicate hydrate (HD C-S-H) was formed in the OPCNL paste at 28 days.

5.3.1.3 BJH cumulative pore volume and pore size distribution

Pore structure data were calculated by the Barret, Joyner and Hallenda (BJH) method from both the adsorption and the desorption isotherm. The pore diameter ranges from 2 nm to 100 nm, and the amount of those pores are primarily related to the degree of cement hydration. This porosity is

broken down into various pore size components as shown in Figures 5.7 and 5.8. Differential pore size distributions of the studied pastes are shown in Figures 5.9 and 5.10.

As shown in Figures 5.7a and b, at the age of 28 days, the total pore volume and the pore volume in each individual size ranges of all pastes increased when compared with that of the corresponding pastes at 7 days. The only exception is the OPC paste without nanoparticles, i.e., the amount of pores in the range of 50-100 nm decreased from 7 to 28 days in the OPC paste. Figure 9a showed a significant peak between 50–60 nm in the 7-day OPC paste. This peak was not shown in the 28-day OPC paste.

It can also be observed from Figures 5.7a and b that for the pastes without nanomaterials, the total pore volume of the OPC paste was larger than that of the OPCFA paste at both 7 and 28 days. At 7 days, the OPC paste had a comparable pore volume in the range of 2-10 nm, a smaller pore volume in the range of 10-50 nm, and a larger pore volume in the range of 50-100 nm, comparing to the OPCFA paste. Differently, at 28 days, the OPC paste had larger pore volumes in all size ranges, comparing to the OPCFA paste.

The addition of nanomaterials generally increased the total pore volume of both OPC and OPCFA pastes at the age of 7 days. For the pastes made with OPC and cured for 7 days (Figure 5.7a), addition of 1% of nanomaterials noticeably increased the amount of pores in the range of 2-10 nm (gel pores) and 10-50 nm. This suggests that addition of these nanomaterials increased cement hydration, or C-S-H gel formation. It is noted that the volume of pores in the range of 50-100 nm reduced (Figure 5.7a) and the significant peak between 50–60 nm (Figure 9a) in the 7-day OPC paste disappeared when 1% nanomaterials were added to the paste. This strongly evidenced that nanomaterial addition had modified/refined the paste pore structures. Similar to what was observed on the 7-day OPC pastes, addition of nano-limestone and nano-silica clearly increased

the amount of gel pores (2-10 nm) for the pastes made with 70%OPC-30%FA and cured for 7 days (Figure 5.7a), suggesting the formation of more C-S-H gel products. However, nano-silica increased the volume of pores in all size ranges while nano-limestone did not change the volume of pores in the range of 10-100 nm much for the 7-days OPCFA paste.

For the OPC pastes cured for 28 days (Figure 5.7b), addition of nano-limestone reduced the amount of pores in all size ranges, consequently, the total pore volume of the paste with nano-limestone was lower than that of the OPC paste with no nanomaterial. This is in accordance with the BET specific surface area results and suggest that the addition of nano-limestone to an OPC paste might impair cement hydration at a later age (28 days). Differently, addition of nano-silica reduced the amount of pores with a size larger than 30 nm but increased the amount of pores in the range of 4-10 nm and 10-30 nm. Consequently, the total pore volume of the OPC paste with 1% nano-silica was the same to that of the OPC paste with no nanomaterial at 28 days. It should be noted that the 28-days OPC paste with nano-silica addition had a distinctive adsorption-desorption isotherm (Figure 5d), the hysteresis loop is larger and the drop in the desorption isotherm is sharper. This indicates that nano-silica increased the amount of "ink-bottle" pores in the 28-day OPC paste. Wider pores only empty via narrow necks and accordingly will empty at lower pressures. As shown in Figure 5.8b, nano-silica significantly increased the amount of pores in the range of 2-4 nm and 4-10 nm while significantly decreased the amount of pores in the range of 10-30 nm, 30-50 nm, and 50-100 nm.

For the OPCFA pastes made with 70%OPC-30%FA and cured for 28 days (Figure 5.7b), the addition of nano-limestone slightly reduced the total pore volume when compared with the paste having no nanomaterial. Different to what was observed in the corresponding 28-day OPC pastes, the volume of gel pores in the range of 2-4 nm and 4-10 nm were nearly the same for OPCFA

pastes with and without nano-limestone addition. Again, this suggests that nano-limestone addition did not help hydration of the 70%OPC-30%FA paste at the age of 28 days. On the other hand, addition of nano-silica significantly increased the volume of pores in all size ranges for the 28-days OPC paste, similar to that occurred in the 7-day pastes. These indicate that the combination of nano-silica and fly ash effectively modified/refined the paste pore structure.

It can be seen from the differential pore size distribution curves (Figures 5.9a and b) that for the pastes studied, there was a signature peak in the pore size range of 3-4 nm (nano-sized gel pores). For the 7-day OPC paste, a significant peak was observed in the pore size range of 50-60 nm (relatively large capillary pores), and addition of nano-limestone and nano-silica eliminated this peak. For the 7-day 70%OPC-30%FA paste, a significant peak around 100 nm (large capillary pores) was observed, and addition of nano-limestone and nano-silica eliminated this peak. These strongly evidenced that nanomaterial addition had modified/refined the paste pore structures. It can also be noticed in Figures 5.9a, b, c, and d that prolonged curing had the same effect. Curing can facilitate cement hydration and the hydration products filled the large capillary pores.

Interestingly, Figures 5.9a, b, c, and d also suggests another signature peak around 18 nm (small capillary pores) in the nanomaterial modified pastes, especially in the nano-silica modified pastes at both 7 and 28 days. This signature peak was also clearly seen in the 28-day OPCFA paste. One possible explanation was that this peak was related to the packing of low Ca/Si C-S-H.

5.3.2 Drying shrinkage

5.3.2.1 Shrinkage behavior

Figures 5.11 and 5.12 illustrate the shrinkage behavior of the pastes studied at 7 and 28 days, respectively. During drying, there was a continuous increase in shrinkage and as RH decreased.

During re-wetting, shrinkage continued to recover as RH increased. However, a considerable portion of the shrinkage was irreversible.

It is generally acknowledged that no water leaves the interlayer spaces during drying until approximately RH<25% is achieved [18]. Therefore, length change due to loss of interlayer water was not considered in this study since the lowest RH achieved is 33%. Capillary pressure and surface energy theories were applied to interpret the drying shrinkage behavior of the studied pastes. Portland cement paste is considered to be viscoelastic material, therefore this volume change have both elastic and viscous, i.e. creep, components. The mechanisms for the irreversible shrinkage are not clear yet, and plastic microstructural deformations and viscous effects (creep) were considered to interpret the irreversible drying shrinkage in this study.

Generally, extended curing (from 7 to 28 days) increased the total drying shrinkage (drying to 33% RH) of both the OPC and OPCFA pastes without nanomaterial additions. 30% FA replacement did not change the total drying shrinkage of the OPC paste without nanomaterial additions cured for 7 days, but noticeably reduced the total drying shrinkage of the OPC paste without nanomaterial additions cured for 28 days.

For OPC pastes cured for 7 days (Figure 5.11a), nanomaterial additions increased drying shrinkage during the drying process. The paste with nano-silica addition displayed the largest equilibrium shrinkage at each relative humidity level, especially at the RH of 33%. Specifically, the addition of nano-silica noticeably increased shrinkage in the RH range of 100-85% and 54-33%, but slightly decreased shrinkage in the RH range of 85-54%. The addition of nano-limestone slightly increased shrinkage in the RH range of 100-85%, slightly decreased shrinkage in the RH range of 85-54%, and noticeably increased shrinkage in the RH range of 54-33%. The capillary pores (>10nm) are responsible for the shrinkage that occurs above 85%RH. As stated by the

Laplace equation, the absolute value of the negative capillary pressure increases with decreasing capillary radius. Therefore, the higher shrinkage in the nano-limestone and nano-silica added pastes in the RH range of 100-85% might be attributed to the refined capillary pore structures as shown in Figure 9a. When the pastes were dried from 85% to 54% RH, large gel pores (4-10 nm) began to empty, and capillary stresses should still dominate. Less volume of large gel pores were emptied in the OPCNL paste with nano-limestone addition than in the OPC paste without nanomaterial as shown in Figure 5.8a, in accordance with the slightly lower shrinkage in the RH range of 85-54% in the OPCNL paste. Differently, in the OPCNS paste with nano-silica addition, more volume of large gel pores were emptied than in the OPC paste without nanomaterial addition, but slightly less shrinkage occurred in the RH range of 85-54%. This may be attributed to the increased resistance to deformation of the OPCNS paste. The drying process may cause microstructural changes to the cement paste and increase its resistance to deformation. Lastly, when the pastes were dried from 54% to 33% RH, capillary pressures still dominate above 45% RH. Below 45% RH, capillary pressures could not exist because the liquid/vapor menisci would become unstable and surface energy effects should dominate. The higher shrinkage values in the nano-limestone and nano-silica added pastes in the RH range of 54-33% than in the OPC paste without nanomaterial addition may be attributed to the higher amount of small gel pores in the size range of 2-4 nm. When the pastes were rewetted, Figure 5.11a shows that the amount of shrinkage of the paste with nano-silica recovered, especially when the paste was re-immersed in lime water, leaving the value of its irreversible shrinkage slightly lower than that of OPC paste and the same as that of OPCNL paste.

For OPCFA pastes cured for 7 days, nanomaterial additions increased the total drying shrinkage and drying shrinkage in all relative humidity ranges during the drying process. The OPCFANL

paste with nano-limestone addition displayed the largest equilibrium shrinkage during the drying process, mostly due to the shrinkage occurred in the RH range of 100-85%. The higher shrinkage in the nano-limestone and nano-silica added pastes in the RH range of 100-85% might also be attributed to the refined capillary pore structures as shown in Figure 9c. The higher shrinkage of the nano-limestone added paste than that of the nano-silica added paste in this RH range may indicate the stronger resistance of the OPCFANS paste to deformation. Different from what was observed in the 7-day OPC pastes, it is noted that nano-limestone and nano-silica addition both increased the shrinkage in the RH range of 85-54%. As shown in Figure 5.8a, slightly more volume of large gel pores were emptied in the OPCFANL paste with nano-limestone addition than in the OPCFA paste without nanomaterial, in accordance with the higher shrinkage in the RH range of 85-54% in the OPCFANL paste. Similar, significantly more gel pores were emptied in the OPCFANS paste with nano-silica addition than in the OPC paste without nanomaterial, in accordance with the higher shrinkage in the RH range of 85-54% in the OPCFANS paste. During rewetting, most part of the total shrinkage was not recovered until the pastes were re-immersed in lime water.

For the OPC pastes cured for 28 days, the paste with nano-silica addition had noticeably higher drying shrinkage than the paste with no nanomaterials, in accordance with its more volume of gel pores and refined pore structure (Figures 5.8b and 5.10b). On the other hand, the paste with nano-limestone addition had noticeably lower drying shrinkage than the paste with no nanomaterials, in accordance with its less volume of pores in all size ranges (Figure 5.8b). Besides, the paste with nano-limestone addition displayed the lowest irreversible drying shrinkage. For the OPCFA pastes cured for 28 days, nano-silica addition noticeably increased the paste shrinkage in the RH range of 100-84% and 54-33%. It is noted that the increase in the volume of pores in the size range of 4-

10 nm did not cause a higher shrinkage in the RH range of 85-54% in the 28-day OPCNS, when compared to the 28-days OPC paste. This suggest that drying in this RH range may particularly cause the aging of the paste and consequently increase the resistance to deformation of the paste. The addition of nano-limestone decreased the paste shrinkage in the RH range of 100-84% and increased the paste shrinkage in the RH range of 54-33%. Both nano-limestone and nano-silica addition decreased irreversible drying shrinkage.

5.3.2.2 Reversible and irreversible shrinkage

Figure 5.13 provides the total, reversible and irreversible shrinkage values of all cementitious pastes studied. As indicated in Figure 5.4, the total shrinkage is the maximum shrinkage value when a tested sample reached at the RH of 33%. The reversible shrinkage is the linear shrinkage recovery and the irreversible shrinkage is the unrecovered shrinkage of the tested sample when it was subjected to rewetting and re-saturating to a RH of 100% (saturated surface dry). In the discussion, the total drying shrinkage is considered to be composed of three components: reversible shrinkage, reversible creep, and irreversible creep.

It can be observed from Figures 5.13a and b that for the OPC paste without nanomaterial additions, the total shrinkage of the 28-day paste increased by 28% when compared with that of the corresponding paste cured for 7 days. The increase in the total shrinkage was due to the increase in the reversible shrinkage. Interestingly, prolonged curing slightly reduced irreversible drying shrinkage. It is noted that the reversible shrinkage of the 28-day OPC paste are much higher than their irreversible shrinkage. The same observations could be made for the OPCFA paste without nanomaterial additions. These indicate that the shrinkage of the 28-day pastes come largely from the reversible creep component, consequently, the formation of C-S-H increase the reversible creep.

It can also be observed that at 7 days (Figure 5.13a), addition of nano-limestone and nano-silica increased the total shrinkage of the OPC paste, especially increased reversible shrinkage at 7 days. NL and NS additions slightly reduced irreversible shrinkage. The reversible shrinkage values of this group pastes are slightly higher than the irreversible shrinkage values. For the OPCFA pastes at 7 days (Figure 5.13c), the shrinkage values of the OPCFA paste with no nanomaterials are similar to those of OPC paste with no nanomaterials. Addition of nanomaterials increased the total shrinkage of the OPCFA paste, especially increased irreversible shrinkage at 7 days. Therefore, different from what is observed from Figure 5.13a, the irreversible shrinkage values of the OPCFA pastes with nanomaterial additions are higher than the irreversible shrinkage values of the corresponding OPC pastes. The reversible shrinkage values of this group pastes are lower than the irreversible shrinkage values. These infers that the C-S-H formed in the early age (7 days) in the OPC and OPCFA pastes were different. While the formation of C-S-H in the 7-day OPC paste increased the reversible shrinkage, the formation of C-S-H in the 7-day OPCFA paste increased the irreversible shrinkage. The C-S-H formed in the 7-day OPCFA paste possess larger potential for microstructural deformation. This is in accordance with the obtained BET specific surface area result in the previous section. i.e., the addition of nano-limestone and nano-silica increased the amount of low-density C-S-H.

At the age of 28 days (Figure 5.13b), the addition of nano-limestone decreased the total drying shrinkage and irreversible drying shrinkage of the OPC paste, and increased the reversible drying shrinkage of the OPC paste. As can be seen from Figure 5.7b, the addition of nano-limestone reduced the pore volume in all size ranges. Differently, the addition of nano-silica increased the total, irreversible, and reversible drying shrinkage of the OPC paste.

As can be seen from Figure 5.13d, the addition of nano-limestone and nano-silica decreased irreversible drying shrinkage and increased reversible drying shrinkage. The OPCFANL paste with nano-limestone addition had a similar total drying shrinkage as compared to the OPCFA paste without nanomaterial addition. Differently, the OPCFANS paste with nano-silica addition had a large total shrinkage than the OPCFA paste without nanomaterial and the OPCFANL paste with nano-limestone addition.

5.3.2.3 Drying shrinkage and pore size relationships

The microstructural parameters, including calcium hydroxide content, chemically bound water content, and pore structure, and drying shrinkage data of studied pastes collected from this study and a previous study [19] were summarized in Table 5.4.

The shrinkage in each relative humidity range was found to be dependent on the volume of pores evaporate in the corresponding RH range and the resistance of the paste to deformation, especially at 7 days. Nano-silica more effectively increase the resistance of the paste to deformation. Drying in the RH range of 85-54% may particularly cause the aging of the paste and consequently increase the resistance to deformation of the paste.

Linear regression analysis indicates that the volume of 2-4 nm and 4-10 nm pores appeared more closely related to reversible shrinkages.

5.4 Conclusions

Two nanomaterials (NS and NL) were incorporated into portland cement paste with and without 30% fly ash replacement as 1% (by weight) addition. Pore structure and shrinkage behavior of these pastes under drying and re-saturating at the ages of 7 and 28 days were investigated. The following conclusions can be drawn:

(1) Additions of the nanomaterials increased the specific surface area and the amount of gel pores (2-10 nm) in the early age (7 days) cement pastes. The results indicate that nanomaterial additions effectively accelerated early age cement hydration.

(2) At 28 days, addition of nano-silica continued to increase the specific surface area and the amount of gel pores, especially in the fly ash blended paste. However, addition of nano-limestone reduced the specific surface area and the total amount of pores (2-100 nm) at 28 days, especially in the Portland cement paste.

(3) Two major volumes of pores were observed in the differential pore size distribution curves of pastes without nanoparticles at the age of 7 days: one was in the pore size range of 3-4 nm (nano-sized gel pores) and the other in the pore size range of 50-60 nm (relatively large capillary pores). The peaks in the pore size range of 50-60 nm all disappeared as 1% nanomaterial was added to these pastes, regardless the nanomaterial type and paste composition. This clearly evidenced that nanomaterial additions refined pore structures of the early age pastes.

(4) An additional signature pore peak located around 18 nm was observed in the nano-silica modified and 28-days fly ash blended pastes. This peak may be related to the packing of low Ca/Si C-S-H.

(5) Extended curing (from 7 to 28 days) increased the total drying shrinkage of both the OPC and OPCFA pastes without nanomaterial additions. 30% FA replacement slightly reduced drying shrinkage of the OPC paste without nanomaterial additions cured for 7 days, and noticeably reduced the drying shrinkage of the OPC paste without nanomaterial additions cured for 28 days.

(6) Additions of nano-silica generally increased the total shrinkage of cement pastes. However, addition of nano-limestone sometimes reduced drying shrinkage, especially for the later age cement pastes.

(7) For OPC pastes, reversible shrinkage was the major portion of the total shrinkage, especially for the pastes at 28 days. For OPCFA pastes, reversible and irreversible shrinkage was close for the paste with no nanomaterials at 7 days, and nanomaterials addition increased irreversible shrinkage of the paste. Extended curing from 7 to 28 days significantly increased reversible shrinkage of the pastes.

(8) Nanomaterial additions and extended curing increased reversible drying shrinkage, which suggests that the volume of gel (2-10 nm) pores appeared more closely related to reversible shrinkages.

It should be noted that the present study focused on the investigation into the effects of pore size distribution on shrinkage of cementitious pastes. In fact, many other microstructural and chemical changes also contribute to irreversible shrinkage of a cement paste, which shall be studied further.

5.5 Acknowledgement

The authors would like to acknowledge the Oak Ridge Associated Universities (ORAU) - Tennessee Valley Authority (TVA), USA, for sponsoring the present study (Grant No. 7-22976).

5.6 References

[1] F. Sanchez and K. Sobolev, "Nanotechnology in concrete – A review," Construction and Building Materials, vol. 24, pp. 2060-2071, 2010.

[2] F. H. Wittmann, "On the action of capillary pressure in fresh concrete," Cement and Concrete Research, vol. 6, pp. 49-56, 1976.

[3] P. K. Mehta and P. J. M. Monteiro, Concrete: Microstructure, Properties, and Materials: McGraw-Hill Education, 2014.

[4] J. J. Thomas and H. M. Jennings. (2017, Aug. 19). The Pore System and Classification of Pores. Available: http://iti.northwestern.edu/cement/monograph/Monograph7_2.html

[5] P. Lura, O. M. Jensen, and K. v. Breugel, "Autogenous shrinkage in high-performance cement paste: An evaluation of basic mechanism," Cement and Concrete Research, vol. 33, pp. 223-232, 2003.

[6] J. J. Thomas and H. M. Jennings, "Changes in the size of pores during shrinkage (or expansion) of cement paste and concrete," Cement and Concrete Research, vol. 33, pp. 1897-1900, 2003.

[7] S. J. Doktycz and K. S. Suslick, "Interparticle Collisions Driven by Ultrasound," Science, vol. 247, pp. 1067-1069, 1990.

[8] K. Higashitani, K. Yoshida, N. Tanise, and H. Murata, "Dispersion of coagulated colloids by ultrasonication," Colloids and Surfaces A: Physicochemical and Engineering Aspects, vol. 81, pp. 167-175, 1993.

[9] K. Sato, J. G. Li, H. Kamiya, and T. Ishigaki, "Ultrasonic Dispersion of TiO2 Nanoparticles in Aqueous Suspension," Journal of the American Ceramic Society, vol. 91, pp. 2481-2487, 2008.

[10] L. E. Copeland and J. C. Hayes, "Determination of non-evaporable water in Portland cement pastes," ASTM Bull., vol. 194, pp. 70-74, 1953.

[11] J. J. Thomas, J. H. Seieh, and H. M. Jennings, "Effect of carbonation on the nitrogen BET surface area of hardened Portland cement paste," Advanced Cement Based Materials, vol. 3, pp. 76-80, 1996.

[12] J. Rouquerol, F. Rouquerol, P. Llewellyn, G. Maurin, and K. S. W. Sing, Adsorption by Powders and Porous Solids (Second edition): Academic press, 2014.

[13] F. G. R. Gimblett, K. S. W. Sing, and Z. M. A. (Grande-Bretagne), "Influence of pre-treatment on the microstructure of calcium silicate hydrate gels," in 7th International Congress on the Chemistry of Cement, Paris, 1980, pp. 225-231.

[14] H. M. Jennings, J. J. Thomas, J. S. Gevrenov, G. Constantinides, and F.-J. Ulm, "A multi-technique investigation of the nanoporosity of cement paste," Cement and Concrete Research, vol. 37, pp. 329-336, 2007.

[15] H. Roper, "Dimensional Change and Water Sorption Studies of Cement Paste," presented at the Symposium on Structure of Portland Cement Paste and Concrete, Washington, D.C., 1966.

[16] J. J. Thomas, A. J. Allen, and H. M. Jennings, "Structural Changes to the Calcium–Silicate–Hydrate Gel Phase of Hydrated Cement with Age, Drying, and Resaturation," Journal of American Ceramic Society, vol. 91, pp. 3362–3369, 2008.

[17] Z. P. Bazˇant and M. Z. Bazant, "Theory of sorption hysteresis in nanoporou ssolids: PartI Snap-through instabilities," Journal of the Mechanics and Physics of Solids, vol. 60, pp. 1644–1659, 2012.

[18] X. Wang, K. Wang, J. Tanesi, and A. Ardani, "Effects of nanomaterials on the hydration kinetics and rheology of portland cement pastes," Advances in Civil Engineering Materials, vol. 3, pp. 142-159, 2014.

[19] M. B. Pinson, E. Masoero, P. A. Bonnaud, H. Manzano, Q. Ji, S. Yip, et al., "Hysteresis from Multiscale Porosity: Modeling Water Sorption and Shrinkage in Cement Paste," Phys. Rev. Applied, vol. 3, pp. 1-17, 2015.

Tables:

Table 5.1Chemical and physical properties of materials used in this study.

Chemical composition	PC	FA	NL	NS
	(wt.%)			
SiO_2	20.20	46.00		
Al_2O_3	4.70	17.80		
Fe_2O_3	3.30	18.20		
SO_3	3.30	2.59		
CaO	62.90	8.40		
MgO	2.70	0.95		
Na_2O	-	0.59	$CaCO_3$ > 97.5%	SiO_2 > 99.5%
K_2O	-	2.16		amorphous
Eq. Na_2O	0.54	2.01		
P_2O_5	-	0.11		
TiO_2	-	0.93		
SrO	-	0.03		
BaO	-	0.05		
LOI	1.10	1.49		
Physical Properties				
Specific gravity	3.15	2.51	2.70	2.30
Specific surface area (Blain, m^2/g)	0.390	0.310	-	-
Particle size (nm)	-	-	15-40	10-20

Table 5.2 Mix proportions for cement pastes studied (wt. %).

Mix ID	OPC	FA	NL	NS
OPC	100	-	-	-
OPCNL	100	-	1	-
OPCNS	100	-	-	1
OPCFA	70	30	-	-
OPCFANL	70	30	1	-
OPCFANS	70	30	-	1

Table 5.3 Saturated salt solutions used for controlling RH.

Chemical	RH@20°C	RH@25°C
$MgCl_2$	33.07±0.18	32.78±0.16
$Mg(NO_3)_2$	55.87±0.27	54.38±0.23
KCl	85.11±0.29	84.34±0.26

Table 5.4 Microstructural parameters and drying shrinkage of studied pastes

Age	days	7	7	7	28	28	28	7	7	7	28	28	28
CH	%	18.467	18.485	18.149	21.057	20.552	19.562	14.213	14.150	13.298	14.911	13.949	13.600
H	%	16.793	17.623	17.497	20.227	20.841	20.523	13.858	14.344	14.435	16.428	17.117	16.536
Specific surface area	m^2/g	50.578	53.428	55.510	68.060	60.218	70.906	49.280	52.780	57.005	62.032	60.320	68.828
Total drying shrinkage	%	0.301	0.323	0.349	0.387	0.353	0.415	0.298	0.350	0.334	0.344	0.346	0.389
100-85% drying shrinkage	%	0.147	0.155	0.166	0.175	0.142	0.182	0.156	0.195	0.178	0.160	0.142	0.180
85-54% drying shrinkage	%	0.108	0.103	0.101	0.144	0.125	0.156	0.094	0.107	0.102	0.130	0.131	0.127
54-33% drying shrinkage	%	0.046	0.065	0.082	0.069	0.086	0.078	0.047	0.049	0.054	0.054	0.068	0.047
Irreversible drying shrinkage	%	0.155	0.146	0.147	0.149	0.095	0.155	0.155	0.202	0.184	0.135	0.116	0.122
Reversible drying shrinkage	%	0.146	0.177	0.202	0.238	0.258	0.260	0.142	0.148	0.150	0.209	0.230	0.267
Total pore volume	m^3/g	0.120	0.122	0.128	0.152	0.140	0.149	0.114	0.119	0.132	0.147	0.142	0.167
2-4 nm pore volume	m^3/g	0.030	0.032	0.033	0.039	0.036	0.046	0.031	0.034	0.035	0.035	0.037	0.042
4-10 nm pore volume	m^3/g	0.030	0.028	0.032	0.034	0.031	0.044	0.027	0.028	0.033	0.031	0.032	0.035
10-30 nm pore volume	m^3/g	0.035	0.035	0.037	0.043	0.039	0.036	0.030	0.033	0.037	0.043	0.039	0.047
30-50 nm pore volume	m^3/g	0.013	0.014	0.013	0.018	0.017	0.012	0.012	0.013	0.014	0.019	0.018	0.023
50-100 nm pore volume	m^3/g	0.012	0.013	0.013	0.018	0.017	0.011	0.013	0.012	0.013	0.018	0.017	0.020

Figures:

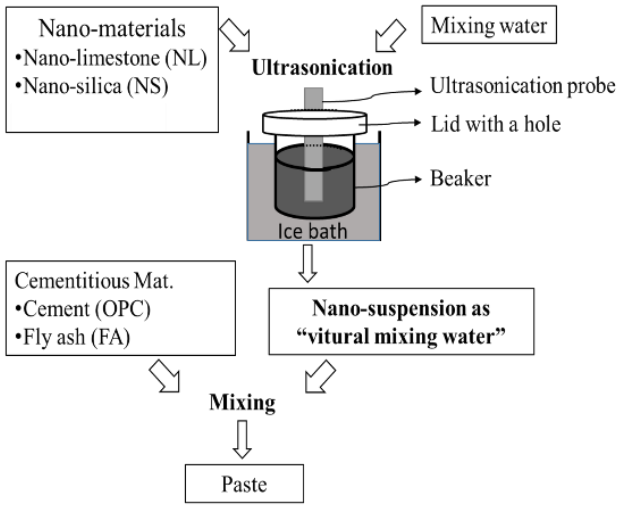

Figure 5.1. Diagram illustration of the mixing process.

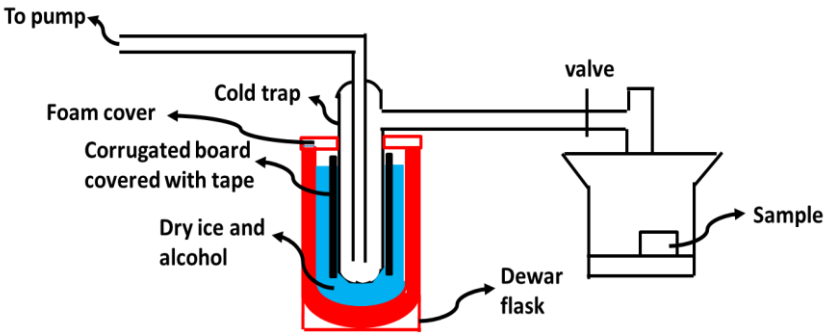

Figure 5.2. Schematic representation of D-drying set-up (after [15]).

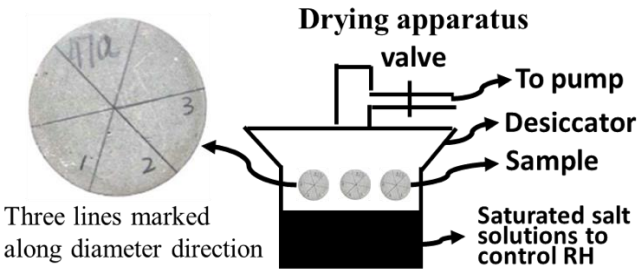

Figure 5.3. Schematic representative of drying apparatus.

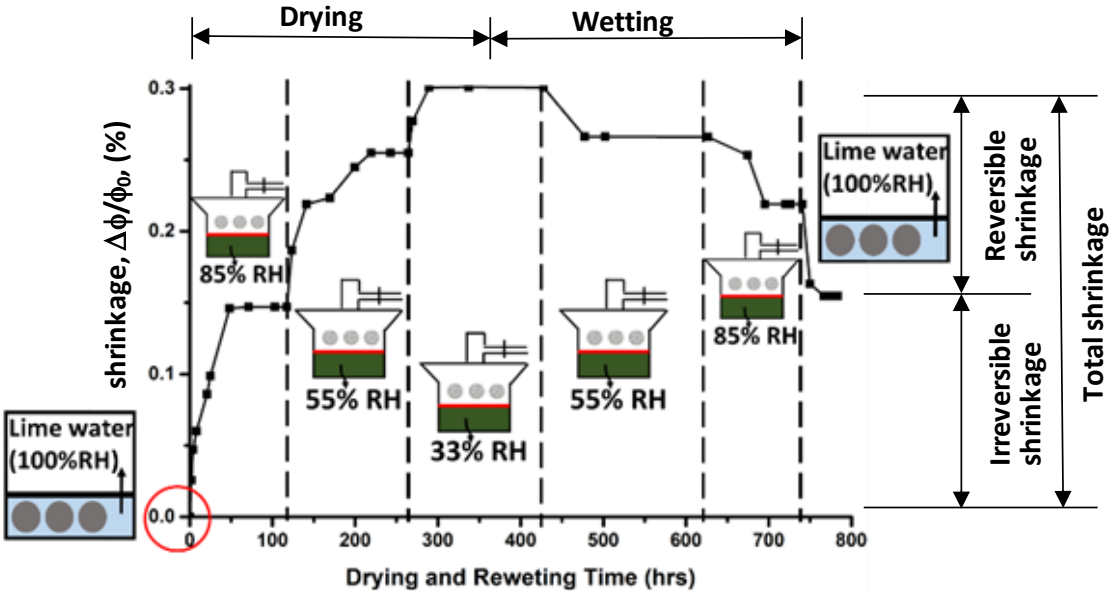

Figure 5.4. Drying shrinkage test regime.

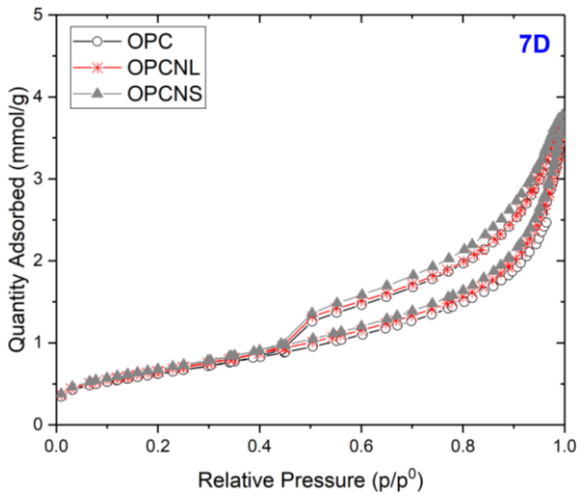

(a) OPC pastes at 7 days

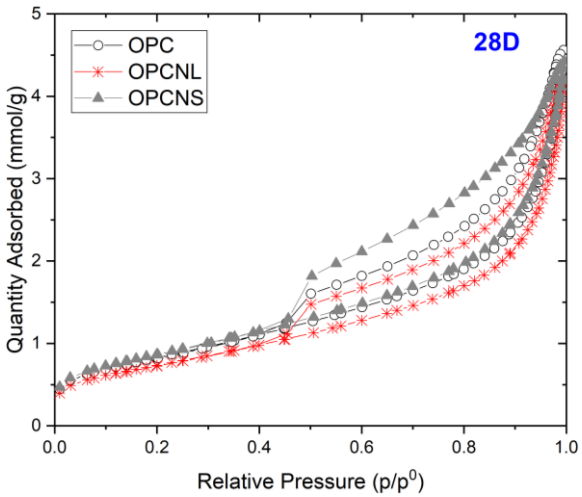

(b) OPC pastes at 28-days

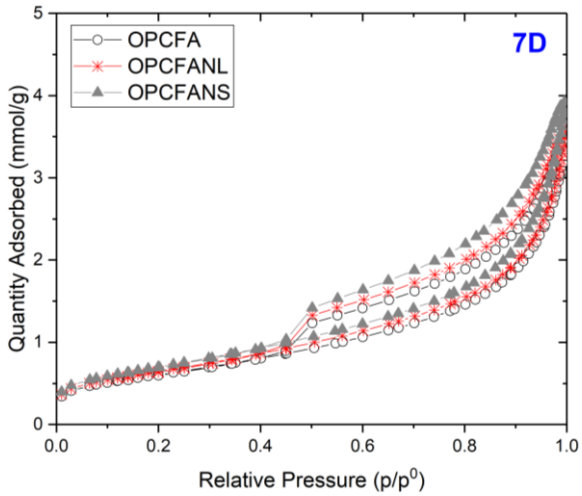

(c) OPCFA pastes at 7 days

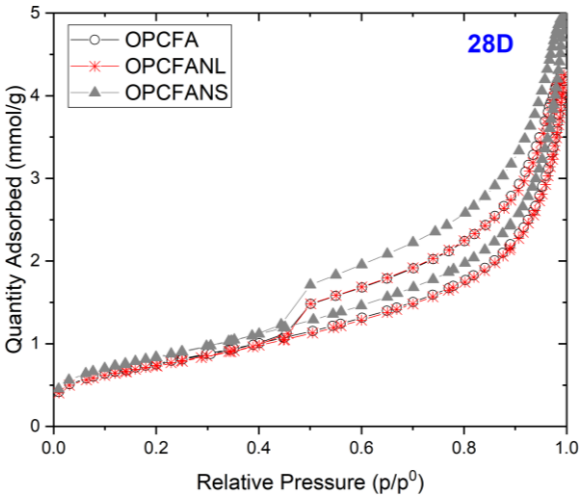

(d) OPCFA pastes at 28-days

Figure 5.5 The adsorption-desorption isotherm of the studied pastes (N2, 77K).

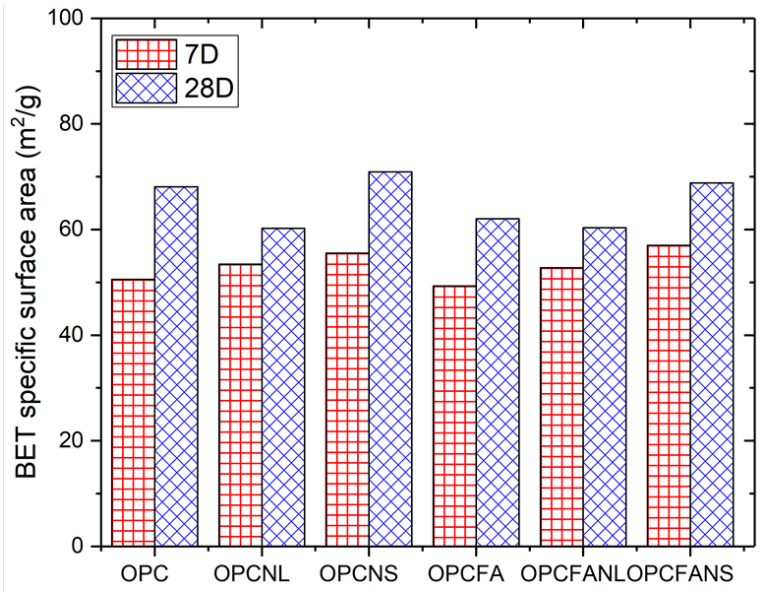

Figure 5.6 The BET specific surface area.

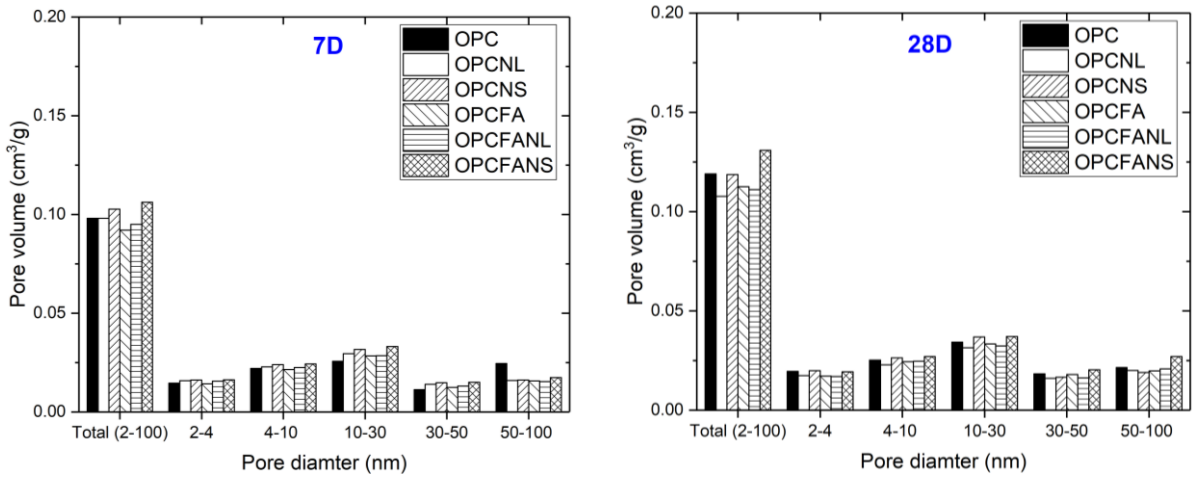

(a) 7 days (b) 28 days

Figure 5.7. Pore volume distribution in the studied pastes at 7 and 28 days (Adsorption).

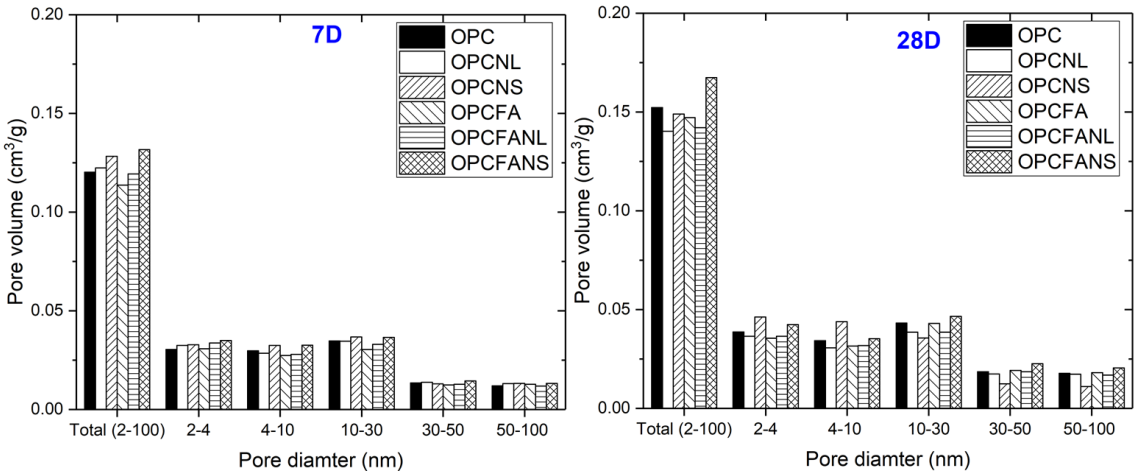

(a) 7 days (b) 28 days

Figure 5.8. Pore volume distribution in the studied pastes at 7 and 28 days (Desorption).

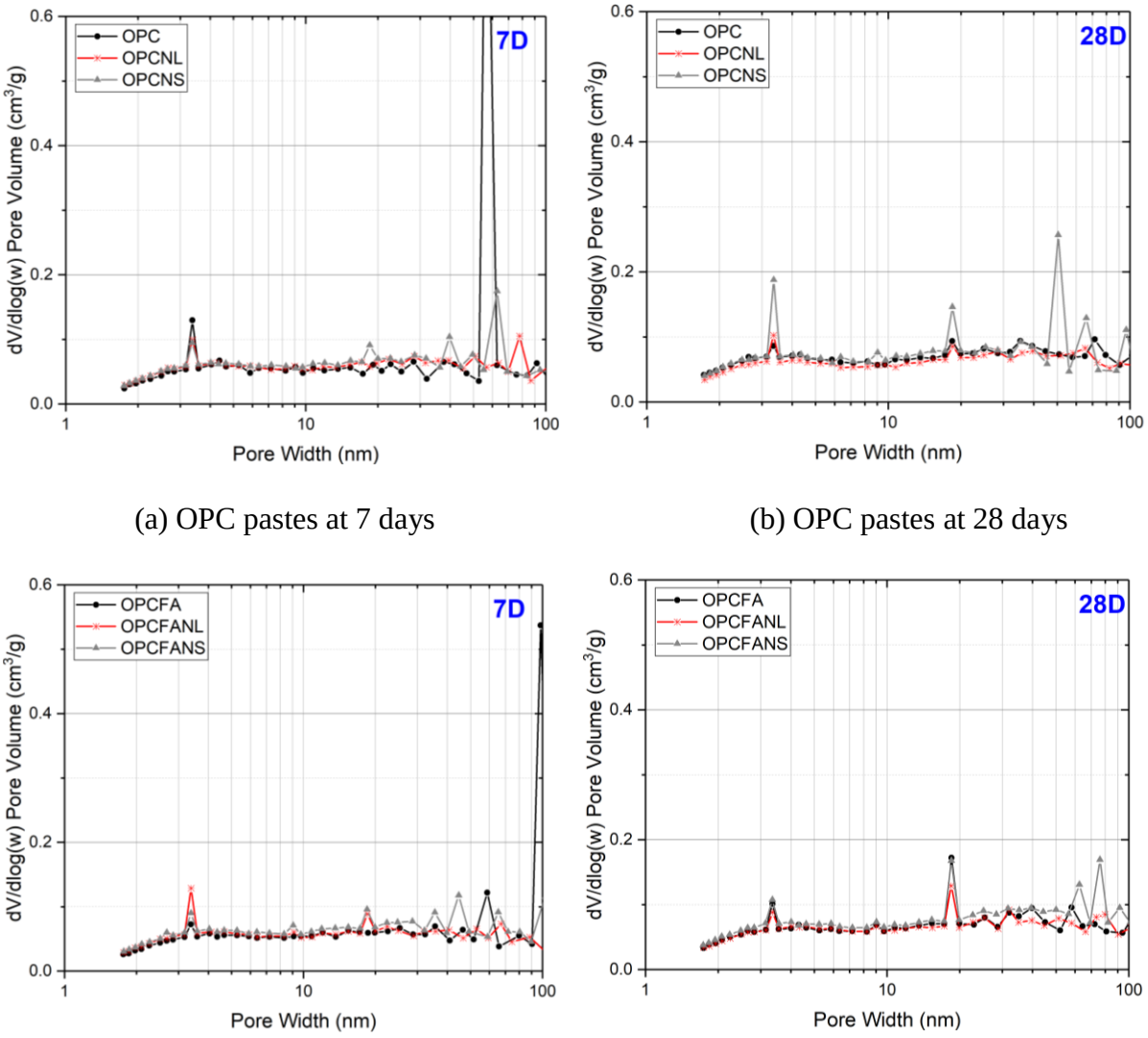

(a) OPC pastes at 7 days

(b) OPC pastes at 28 days

(c) OPCFA pastes at 7 days

(d) OPCFA pastes at 28 days

Figure 5.9. BJH differential pore size distribution (Adsorption).

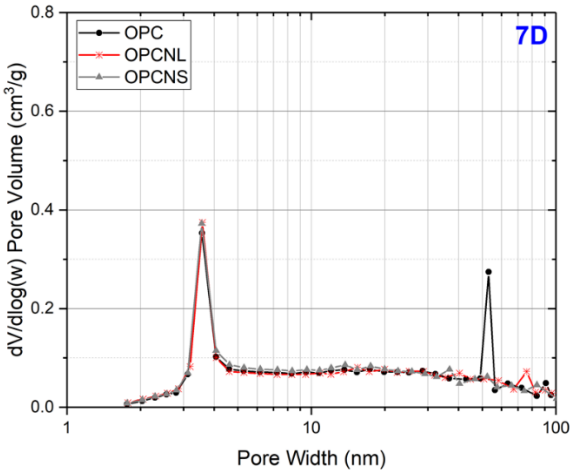

(a) OPC pastes at 7 days

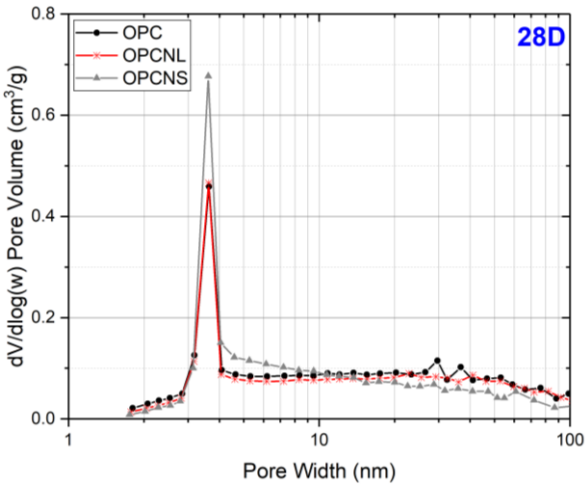

(b) OPC pastes at 28 days

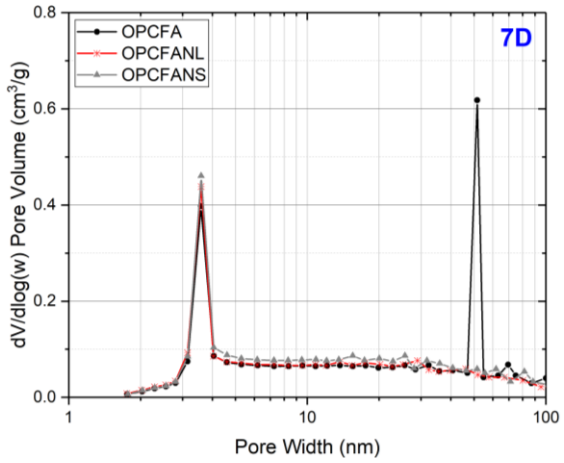

(c) OPCFA pastes at 7 days

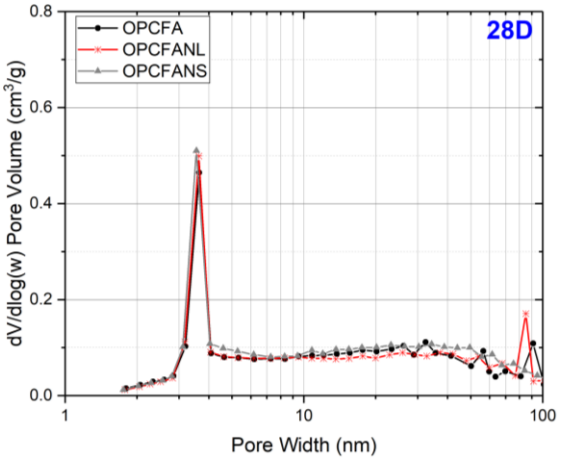

(d) OPCFA pastes at 28 days

Figure 5.10. BJH differential pore size distribution (Desorption).

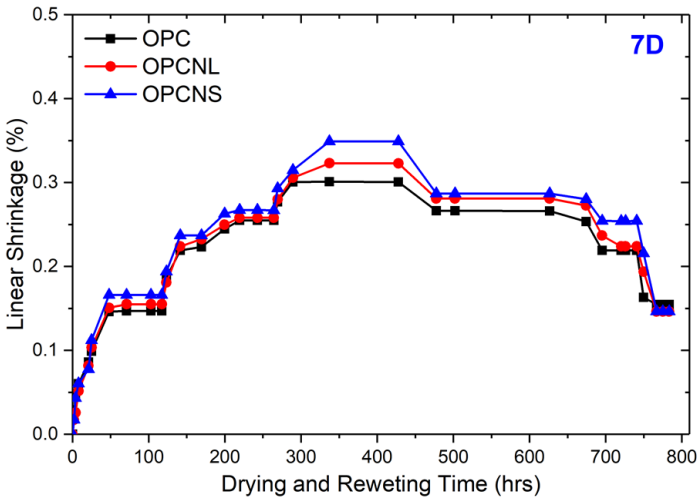

(a) OPC pastes

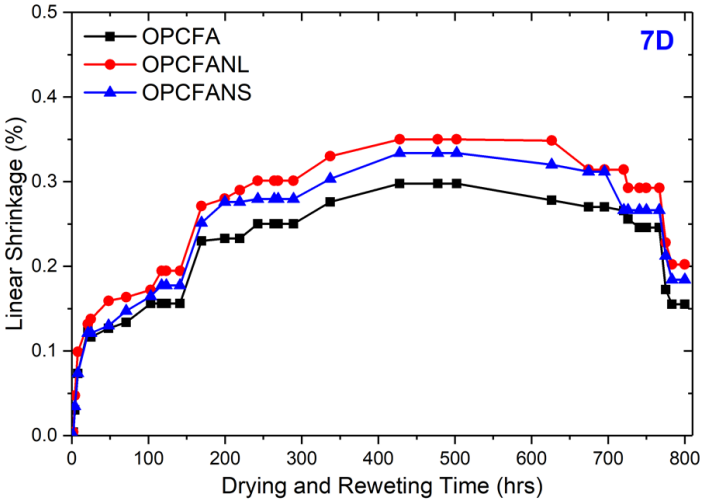

(b) OPCFA pastes

Figure 5.11. Shrinkage behavior of pastes at 7 days.

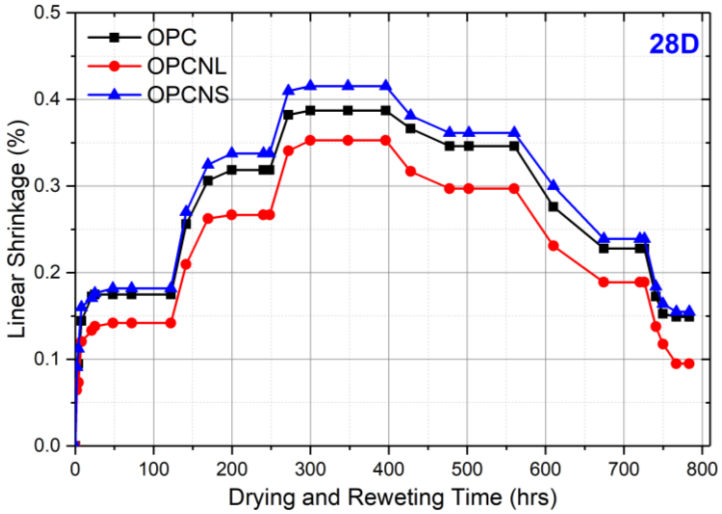

(a) OPC pastes

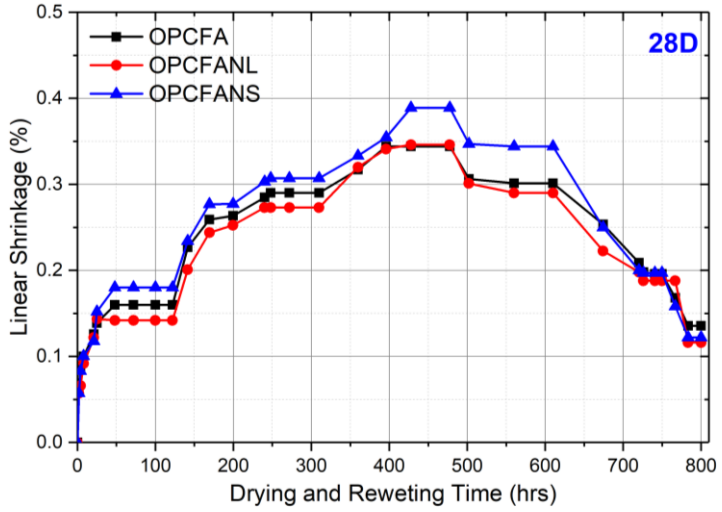

(b) OPCFA pastes

Figure 5.12. Shrinkage behavior of pastes at 28 days.

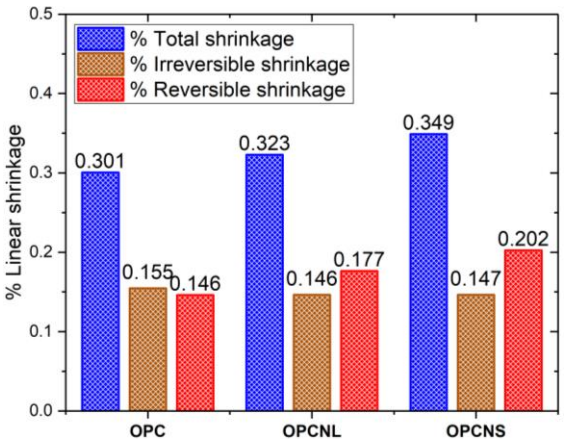

(a) OPC pastes at 7 days

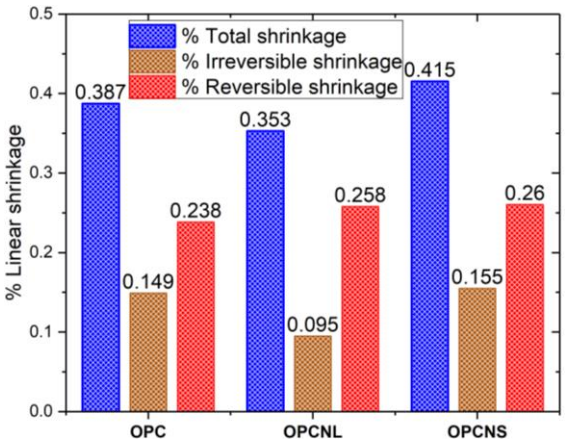

(b) OPC pastes at 28 days

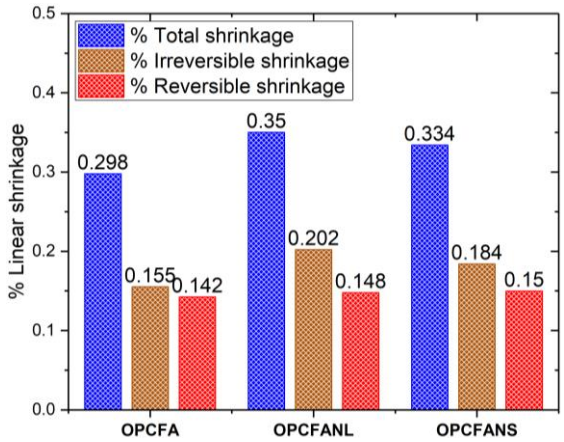

(c) OPCFA pastes at 7 days

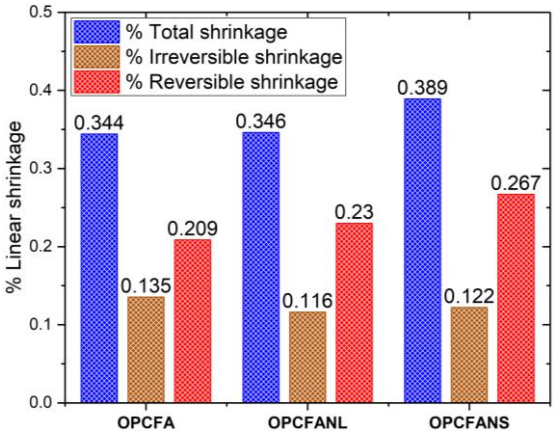

(d) OPCFA pastes at 28 days

Figure 5.13. Total, reversible, and irreversible shrinkage of cementitious pastes studied

CHAPTER 6. PROPERTIES OF SELF-CONSOLIDATING CONCRETE CONTAINING HIGH VOLUME SUPPLEMENTARY CEMENTITIOUS MATERIALS AND NANO-LIMESTONE

Modified from a paper published in *Journal of Sustainable Cement-based Materials*

Xin Wang[1], Kejin Wang[2], Jinxin Li[3], Nishant Garg[4], Surendra P. Shah[5]

[1]Graduate Research Assistant, Dept. of Civil, Construction, and Environmental Engineering, Iowa State Univ., Ames, Iowa, 50010, USA. Tel: 515-509-0902. Email: wangxin@iastate.edu
[2]Corresponding author, Professor, Dept. of Civil, Construction, and Environmental Engineering, Iowa State Univ., Ames, Iowa, 50010, USA. Tel: 515-294-2151. Email: kejinw@iastate.edu
[3]Graduate Research Assistant, Dept. of Civil, Construction, and Environmental Engineering, Iowa State Univ., Ames, Iowa, 50010, USA. Tel: 515-509-3558. Email: jinxin23@iastate.edu
[4]Graduate Research Assistant, Dept. of Chemistry and Interdisciplinary Nanoscience Center, Aarhus University, Denmark, Tel: +45 8159 5424, Email: ngarg@chem.au.dk
[5]Professor (emeritus), Dept. of Civil and Environmental Engineering, Northwestern University, Illinois, USA, Tel: 847-491-7878, Email: s-shah@northwestern.edu

Abstract

This paper reports on a study of conventional self-consolidating concrete (SCC) incorporating 40% Class F fly ash (FA) replacement for cement, and semi-flowable self-consolidating concrete (SFSCC) incorporating 40% FA and 15% metakaolin (MK) replacement for cement, both with and without addition of 1% nano-limestone (nanoLS). Properties of fresh concrete mixtures, such as air content, slump flow, and J-ring flow, were tested. Properties of hardened concretes, including compressive strength, rapid chloride permeability, freezing-thawing resistance, and free drying shrinkage, were also examined. The results indicated that a SCC mixture with 40% FA replacement displayed good workability and adequate compressive strength (33 MPa) at 28 days. In addition to enhancing strength (especially at early ages) and durability, MK also improved the shape-holding ability of SFSCC. Addition of nanoLS further increased concrete strength and freezing-thawing resistance and reduced concrete permeability.

6.1 Introduction

Both research and practice have demonstrated that use of fly ash (FA) as a supplementary cementitious material (SCM) in concrete not only reduces cost and makes a more environmental friendly construction material but also enhances the key properties of the concrete. Because of its small, smooth, and spherical shape as well as its pozzolanic property, FA can improve fluidity of fresh concrete mixtures for easier and faster placement. FA replacement in concrete reduces the heat of cement hydration and the rate of free shrinkage, minimizing the concrete thermal and shrinkage cracking. The slowly hydrated FA particles and the pozzolanic reaction products can refine concrete pore structure and reduce permeability, leading to FA concrete with increased long-term strength and durability. In many advanced concrete technologies, such as self-consolidating concrete (SCC) in which concrete flows like a liquid and requires no external vibration for consolidation, FA has played a vital role in manipulating concrete rheology.

Recent research on semi-flowable self-consolidating concrete (SFSCC) for slip-form paving applications has demonstrated that if properly designed, concrete containing up to 40% FA can perform equally well or even better than conventional concrete [1, 2]. SFSCC shall be not only be self-consolidating but should also be able to hold its shape immediately after being extruded from a slip-form paver [3]. A newly-developed SCC, semi-flowable self-consolidating concrete, could be achieved by adopting and modifying the mix proportions of conventional SCC to achieve good balance between flowability and shape stability [3]. Clay materials are increasingly being used in concrete to modify its thixotropy and improve its shape stability [4, 5]. Metakaolin (MK) is manufactured from kaolinite, one of the most abundant natural clay minerals, by calcination at moderate temperatures (650-900 °C). This thermal treatment results in dehydroxylation of the aluminate octahedral in the layered structure, forming an amorphous or semi-amorphous material

with high surface area and high chemical reactivity [6, 7]. Although it requires a higher quantity of water for given flowability, MK increases viscosity, yield stress, and thixotrophy of concrete mixes, improving concrete shape-holding ability and finishing ability [8, 9]. Studies have also demonstrated that MK is a very effective pozzolan and results in enhanced early strength, refined pore structure, and improved durability performance [9-11].

Nanomaterials, such as nano-silica (nanoSiO_2) and nano-limestone (nanoLS), have also been increasingly used in FA concrete. Research studies indicate that, if well dispersed, nanomaterials can accelerate early cement hydration, further refine micro-pores in concrete, and modify the internal structure of C-S-H gel, thereby significantly reducing concrete permeability and improving concrete mechanical properties and durability (chemical attack, ASR expansion, freezing-thawing resistance, etc.) [12-17]. Several mechanisms have been proposed for these effects, including (a) seeding effect – suggesting that nanoparticles can provide a multitude of additional sites for nucleation of cement hydration products and growth of new regions of calcium-silicate-hydration gel (C-S-H), the principal product of cement hydration, (b) filler effect – signifying that nanoparticles can function as nanofillers and change pore structure of cement-based systems, and (c) additional hydration effect – denoting that nanoparticles can react with cementitious materials (i. e., nano-limestone with AFm and AFt phases), giving rise to an increase in total volume of hydration products [18-21].

While the production of SCC commonly involves use of FA only, use of MK and nanoLS together with FA in SCC represents a relatively new approach. The basic concept underlying this study is that, when used together, the deficiencies of each material will be compensated for by advantages of one or more of the others, and in-common advantages of these three materials will be further enhanced, thus developing a new nano-material, modified high volume SCMs concrete

with tailored fresh and hardened properties. In the present study, mix proportions of conventional SCC and SFSCC were developed using a large volume of FA together with MK and a small quantity (1% by wt. of cementitious materials) of nanoLS. The resulting fresh and hardened properties (compressive strength, rapid chloride permeability, freezing-thawing resistance and free-drying shrinkage) of these concrete mixtures have been evaluated.

6.2 Materials and test methods

6.2.1 Materials and mix proportions

The cementitious materials studied include: a commercial Type I/II portland cement (PC), a class F fly ash (FA) with a lime content of 8.40%, and a high-reactivity metakaolin (MK) whose physical and chemical properties are presented in Table 6.1. FA had the lowest specific surface area of 310 m^2/kg, the cement had a surface specific area of 391 m^2/kg, and the specific area of the MK was 13,000 m^2/kg. A white nano-sized (15-40 nm) limestone powder ($CaCO_3$% > 97.5) was added. Local natural sand and crushed limestone of 25mm maximum size were used as the fine and coarse aggregates, respectively. These aggregates had specific gravities of 2.68 and 2.64, respectively, and water adsorptions of 0.71% and 1.6%, respectively. The coarse aggregate was separated into different-sized fractions and recombined into a specific grading as shown in Figure 6.1, which also shows the grading of the fine aggregate. A polycarboxylate-based high-range water reducer (HRWR) and a synthetic resin-type air-entraining agent (AEA) were used in all concrete mixtures.

Three mixtures were prepared, including one SCC mixture containing 40% FA replacement for cement and two other SFSCC mixtures containing 40% FA and 15% MK replacement for cement, one with and one without a 1% nanoLS addition (Table 6.2). The total amount of cementitious materials (PC+FA+MK) and water-to-cementitious ratio were kept constant at 535 kg/m^3 and 0.36,

respectively. The amounts of HRWR were varied to obtain the desired slump flow as will be described in the next subsection. An air entraining agent was used; the target air content was 7 ± 1 %.

6.2.2 Samples and test methods

When the mixing procedure in accordance with ASTM C192 [22] was completed, tests were conducted on the fresh concrete. The ability of SCC mixture to flow was evaluated using the inverted slump flow test (Procedure B, ASTM C1611) and the J-ring test [23, 24]. The ability of SFSCC mixtures to flow was evaluated using the modified slump test [3], and the slump and spread of an unrodded slump test were measured; the slump cone was filled with concrete without rodding, similar to Procedure A, ASTM C1611 [23]. The shapes of the SFSCC mixtures were inspected at the end of the slump tests to assess the shape-holding ability of the mixtures. The target slump flow for the SCC mix was 710 ± 50 mm, the designed slump for the SFSCC mix was 203 ± 25 mm, and the designed slump spread for SFSCC was 305 ± 25 mm, in accordance with the SFSCC mix design criteria [3]. It was found that, to have proper shape-holding ability, the shape of the SFSCC after removing the cone from the unrodded slump test should be a symmetric conical shape with the slump and spread values mentioned above. These values indicate a uniform distribution of mixture through the preservation of symmetric shape and the ability to maintain shape of its sides after extrusion from the slipform because it maintains a slump and sufficient flowability based on its spread. Entrained air content was determined for each mix. Segregation was also visually checked during the slump test.

Cylindrical and prismatic samples were cast in accordance with ASTM C192 but without either compaction or vibration. Specimens were covered by plastic sheets and wet towels to avoid moisture loss during the first 24 hours, and then removed from molds and cured in a moist chamber

maintained at a relative humidity greater than 95% and at a temperature of 23 ± 2 ºC until the time of testing. The compressive strength of each concrete mix was determined using three 100 × 200 mm cylinders in accordance with ASTM C 39 [25] at the ages of 7 and 28 days.

The drying shrinkage for each mixture was measured using three 75 mm × 75 mm × 285 mm prisms in accordance with ASTM C157 [26]. In this test, immediately after samples were removed from the molds at the age of 24 hours, they were placed in saturated lime water for 30 min. They were then removed from the lime water and initial comparator and weight readings were taken. Following this, the specimens were stored in the moist chamber until they reached an age of 28 days. At the end of the 28-day curing period, the specimens were stored for testing in a drying room maintaining a relative humidity of 50 ± 4 % and a temperature of 23 ± 2 ºC.

At 28 days, a rapid-chloride permeability test (RCPT) of each mix was carried out on two 50 mm-thick samples cut from 100 mm diameter concrete cylinders in accordance with ASTM C1202 [27]. Also at 28 days, the resistance of each mixture to repeated cycles of freezing and thawing was determined using four 75 mm × 102 mm × 405 mm prisms in accordance with ASTM C 666 (procedure A) [28]. The deterioration of samples over time was evaluated by measuring change in weight and relative dynamic modulus (RDM) of elasticity. The measurements were carried out every 30 cycles and terminated either after 300 cycles or when the relative dynamic modulus of elasticity reached a value of 60% of the initial modulus.

6.3 Results and discussion

6.3.1 Fresh concrete properties

Table 6.3 lists the results of tests performed on the fresh concrete and Figure 6.2 shows the three mixes used in the slump test. Flowability and passing ability of the SCC were evaluated based on the results of slump flow and J-ring flow tests. The flowability of SFSCC was evaluated

from both slump and slump spread measurements. No visible segregation was observed for any of these three mixes, and the SCC mix achieved a slump flow of 692 mm. The difference between slump flow and J-ring flow for the SCC mix was less than 25.4 mm, suggesting no visible blocking. Two SFSCC mixtures, one with and one without nanoLS, had a slump of 203 mm - 216 mm, a slump spread of 305 mm, and a regular cone shape, meeting the SFSCC mix design criteria [3]. As mentioned above, dosages of HRWR were varied to obtain the desired slump flow. Addition of 1% nanoLS increased the requirement of SFSCC for HRWR by 9%.

6.3.2 Hardened concrete properties

6.3.2.1 Compressive strength

The results of the 7- and 28- day compressive strength tests of the SCC and SFSCC mixtures are shown in Figure 6.3; each value is the average from the results for three cylinders. The SCC mixture with 40% FA replacement for cement showed a compressive strength of 19.4 MPa at 7 days and 33 MPa at 28 days, a significant increase (by 68.3%) during this interval that may be attributed to the slow pozzolanic reaction of low-calcium FA [29, 30] and the pozzolanic reaction between FA and calcium hydroxide (CH) after 7 days [31].

With an additional 15% MK replacement for cement, the SFSCC mixture showed an improved compressive strength of 24.2 MPa at 7 days, a 24.1% increase from that of the SCC mixture. There are three possible mechanisms contributing to this improvement: (1) filler effect. The small MK particles support more efficient paste packing, and improvement in particle packing at the aggregate/paste interface can result in a thinner transition zone with a denser, more homogeneous microstructure; (2) the acceleration of early hydration (mainly during the first day) of PC. The small (sub-micron to several microns) particles of MK can act as heterogeneous nucleation sites at which calcium silicate hydrate (C-S-H) could precipitate; (3) the pozzolanic reaction of MK

with CH. MK has been demonstrated to significantly reduce the CH content of plain paste/mortar/concrete at an age as low as 3 days [6, 32, 33]. Previous research has shown that cement pastes and concrete (self-consolidating concrete included) containing 5% to 20% MK displayed higher compressive strengths than the control samples at all tested ages, from 3 to 90 days, although the degree to which strength was enhanced declined beyond 14 days [10, 33-37]. At an age of 28 days, the compressive strength of SFSCC mixture increased to 36.2 MPa (a 47.1% increase from that at 7 days).

As it can be seen, the difference in compressive strength between SCC and SFSCC mixes decreased with time, i.e., the SCC mix developed strength faster in the interval from 7 to 28 days compared to the SFSCC mix. There are two possible reasons for this behavior. First, the MK is most effective with respect to strength improvement at very early ages, while the degree to which strength is enhanced by MK declines at an age greater than about 14 days [6, 32, 38]. Second, the lower cement content in SFSCC mix might result in lower CH content available for pozzolanic reaction, so the FA in the SFSCC might react to a lesser degree than that in the SCC mix.

The addition of 1% nanoLS to the SFSCC mix increased the compressive strength by 9.7% at 7 days and 5.0% at 28 days. This enhancement in compressive strength by nanoLS was also more pronounced before 7 days because the nanoLS particles contributed mainly through accelerating early cement hydration by providing nucleation sites and achieving an immediate filler effect. NanoLS may also contribute to compressive strength through its reaction with the aluminate phase that resulted in the higher volume of the hydration products. Added limestone was shown to favor the replacement of monosulphate by monocarbonate ($C_3A•CaCO_3•11H_2O$) and hemicarbonate ($C_3A•0.5CaCO_3•12H_2O$), with a consequence of suppressing the conversion of monosulphate [18, 39-41]. The stabilization of the voluminous ettringite instead of monosulphate gives rise to an

increase in the total volume of hydration products [19-21, 41], and this can result in a lowering of porosity and an increase in the compressive strength [41, 42].

6.3.2.2 Rapid chloride permeability

The rapid chloride ion permeability measured after 28 days of curing for all three mixes is shown in Figure 6.4. The total charge passed in all three mixes was less than 500 coulombs and assessed to be 'very low' according to ASTM C1202. Moreover, SFSCC with a total of 55% cementitious replacement exhibited 33% lower RCPT value than SCC with 40% cementitious replacement. Chlorides usually penetrate into concrete by diffusion along water paths or open pores. Resistance to chloride ion penetration is significantly improved due to the formation of a less porous, denser microstructure and a discontinuous pore system through the filler effect of MK and a pozzolanic reaction with CH [43, 44]. Tricalcium aluminate (C_3A) also can react with some of the chlorides to form stable chlorocomplexes [44, 45]. Several researchers have observed that less free chloride is consequently available to initiate the corrosion process [46]. The presence of FA and MK led to an increase in the amount of C_3A due to the higher amount of alumina (Table 6.1) and an increase in C-S-H content formed from the pozzolanic reaction. Therefore, the studied SCC and SFSCC mixes had a strong chloride-binding capability and consequent low chloride ion permeability.

The addition of 1% nanoLS to the SFSCC mix caused little difference in the RCPT value. Although, as discussed previously, the presence of small nanoLS particles can beneficially change pore-size distribution and lead to a denser microstructure with lower permeability, the presence of calcium carbonate may increase chloride penetration due to a higher level of OH^- ions present in the pore fluid [47, 48] and a lower chloride-binding capability (calcium carbonate consumes

aluminate phase) of the concrete. Further study is needed on the chemistry of the SFSCC both with and without using nanoLS.

6.3.2.3 Rapid freezing-thawing test

Freezing and thawing tests were evaluated by examining the changes in mass and relative dynamic modulus (RDM) of elasticity, with the results presented in Figures 6.5-6.7. Each value shown in Figures 6.5 and 6.6 is the average of the results from four prisms.

During freezing-thawing cycles, weight gain indicates cracking formation and water absorption, and the weight loss is caused by surface scaling. As can be seen in Figure 6.5, repeated freeze-thaw cycles had a larger influence on the weight change of SCC samples. The weight of the SCC samples first increased, implying absorption of water due to cracking formation. After 90 cycles, the SCC reached a weight gain of 1.08% and started to lose weight, suggesting a considerable amount of surface scaling. After 210 cycles, the mass of surfacing scaling exceeded the mass of absorbed water and the SCC samples exhibited a net weight loss of up to 1.06% at 300 cycles. Figure 6.7 shows the appearance of exposed aggregate as a result of surface scaling of the SCC.

SFSCC and SFSCC with 1% nanoLS shared a similar shift in weight from increasing to decreasing, but occurring at a later time (150 cycles) and on a much smaller scale. SFSCC mixtures exhibited a small amount of weight gain throughout the testing period. It can also be seen from Figure 6.7 that SFSCC mixtures exhibited a much smaller surface-scaling problem and that the additional 15% MK replacement significantly improved the surface appearance of concrete after repeated freezing-thawing cycles. A 1% nanoLS addition resulted in little difference in the weight change of SFSCC samples (Figure 6.5), and produced less surface damage (Figure 6.7).

As can be seen in Figure 6.6, there were similar changes in the RDM values of all three of the mixes studied. SFSCC without nanoLS exhibited the highest RDM reduction throughout the test,

but it still displayed a RDM of 90.3% after 300 cycles. SFSCC with 1% nanoLS addition displayed the lowest RDM reduction, and its RDM after 300 cycles was 91.7%. There was a sharp decrease in RDM for SCC between 90 and 120 cycles, corresponding to the turning point in weight change shown in Figure 6.5 when the weight of SCC began to decrease; this sharp decrease in RDM could be caused by surface scaling.

6.3.2.4 Free-Drying Shrinkage

The average cumulative mass and length change measured from the three prisms of each concrete mix are plotted in Figures 6.8 and 6.9. In general, weight loss and free-drying shrinkage of the concrete increased rapidly with time during in the first 14 days of drying and at a lesser rate after 28 days.

There is a considerable distinction in the shrinkage behavior between the SCC and SFSCC samples. The weight loss and free-drying shrinkage of SFSCC with and without nanoLS were significantly lower than those of SCC; this may be attributed to the effects of MK, since MK replacement for cement could alter capillary porosity and pore structure due to filler effect and greater volume of hydration products produced by pozzolanic reaction. Addition of 1% nanoLS slightly reduced the weight loss and free-drying shrinkage of SFSCC.

6.4 Conclusions

This study examined the fresh and hardened properties of self-consolidating concrete incorporating 40% of fly ash replacement for cement and semi-flowable self-consolidating concrete incorporating 40% of fly ash and 15% metakaolin replacement for cement, both with and without addition of 1% nano-limestone. The following conclusions can be drawn:

1. A SCC mixture with 40% FA replacement displayed good workability and adequate compressive strength, i.e., 19.4 MPa at 7 days and 33 MPa at 28 days.

2. A SFSCC mixture with 40% FA and 15% MK replacement displayed good flowability and shape-holding ability. The replacement of 15% MK for cement also improved compressive strength and freezing-thawing resistance, and also reduced chloride penetration and free-drying shrinkage.
3. Adding a small quantity (1% by weight of cementitious materials) of nanoLS to the SFSCC mix further increased the compressive strength and resistance freezing-thawing at both 7 and 28 days. It also slightly reduced chloride penetration and free-drying shrinkage of the concrete.

6.5 Acknowledgement

The authors would like to acknowledge the Oak Ridge Associated Universities (ORAU) - Tennessee Valley Authority (TVA), USA, for sponsoring the present study (Grant No. 7-22976).

6.6 References

[1] K. Wang, S. Shah and T. Voigt, "Self-consolidating Concrete for Slip-form Construction: Properties and Test Methods," in Proceedings of the International Conference on Microstructure Related Durability of Cementitious Composites, Nanjing, China, October 2008.

[2] K. Wang, S. Shah, G. Lu and J. Grove, "Self-consolidating Concrete for Slip-form Construction: Mix Design Method and Application," in Proceedings of the 2nd International Symposium on Design, Performance and Use of Self-consolidating Concrete, Beijing, China, June 2009.

[3] K. Wang, S. P. Shah, J. Grove, P. Taylor, P. Wiegand, B. Steffes, G. Lomboy, Z. Quanji, L. Gang and N. Tregger, "Self-Consolidating Concrete—Applications for Slip-Form Paving: Phase II," 2011.

[4] B. Pekmezci, T. Voigt, K. Wang and S. Shah, "Low compaction energy concrete for improved slip-form casting of concrete pavements," ACI Materials Journal, vol. 104, pp. 251-258, 2007.

[5] N. Tregger, T. Voigt, K. Wang and S. Shah, "Improving the slip-form process via material manipulation," in Advances in Construction Materials, C. Grosse, Ed., New York, Springer Berlin Heidelberg, 2007, pp. 539-546.

[6] B. Sabir, S. Wild and J. Bai, "Metakaolin and calcined clays as pozzolans for concrete: a review," Cement and Concrete Composites, vol. 23, no. 6, p. 441–454, 2001.

[7] J. M. Justice and K. E. Kurtis, "Influence of Metakaolin Surface Area on Properties of Cement-Based Materials," Journal of Materials in Civil Engineering, vol. 19, pp. 762-771, 2007.

[8] N. Garg and K. Wang, "Comparing the performance of different commercial clays in fly ash-modified mortars," Journal of Sustainable Cement-Based Materials, vol. 1, pp. 111-125, 2012.

[9] B. Sabir, S. Wild and J. Bai, "Metakaolin and calcined clays as pozzolans for concrete: a review," Cement and Concrete Composites, vol. 23, pp. 441-454, 2001.

[10] A. A. Hassan, M. Lachemi and K. M. Hossain, "Effect of metakaolin and silica fume on the durability of self-consolidating concrete," Cement & Concrete Composites 34 (2012), vol. 34, p. 801–807, 2012.

[11] O. Karahan, K. M. Hossain, E. Ozbay, M. Lachemi and E. Sancak, "Effect of Metakaolin Content on the Properties Self-Consolidating Lightweight Concrete," Construction and Building Materials, vol. 31, p. 320–325, 2012.

[12] A. R. Jayapalan, B. Y. Lee and K. E. Kurtis, "Can nanotechnology be 'green'? Comparing efficacy of nano and microparticles in cementitious materials," Cement & Concrete Composites, vol. 36, pp. 16-24, 2013.

[13] L. Singh, S. Karade, S. Bhattacharyya, M. Yousuf and S. Ahalawat, "Beneficial role of nanosilica in cement based materials – A review," Construction and Building Materials, vol. 47, p. 1069–1077, 2013.

[14] X. Liu, L. Chen, A. Liu and X. Wang, "Effect of Nano-CaCO3 on Properties of Cement Paste," Energy Procedia, vol. 16, p. 991 – 996, 2012.

[15] F. Sanchez and K. Sobolev, "Nanotechnology in concrete – A review," Construction and Building Materials, vol. 24, p. 2060–2071, 2010.

[16] M. Nehdi, M. Pardhanb and S. Koshowski, "Durability of self-consolidating concrete incorporating high-volume replacement composite cements," Cement and Concrete Research, vol. 34, p. 2103–2112, 2004.

[17] I. Campillo, J. Dolado and A. Porro, "High Performance Nanostructured Mateirals for Construction," in Nanotechnology in Construction, P. Bartos, Ed., Cambridge, Royal Society of Chemistry, 2004, pp. 215-227.

[18] G. Kakali, S. Tsivilis, E. Aggeli and M. Bati, "Hydration products of C3A, C3S and Portland cement in the presence of CaCO3," Cement and Concrete Research, vol. 30, pp. 1073-1077, 2000.

[19] K. D. Weerdt, M. B. Haha, G. L. Saout, K. Kjellsen, H. Justnes and B. Lothenbach, "Hydration mechanisms of ternary Portland cements containing limestone powder and fly ash," Cement and Concrete Research, vol. 41, pp. 279-291, 2011.

[20] T. Matschei, B. Lothenbach and F. Glasser, "The role of calcium carbonate in cement hydration," Cement and Concrete Research, vol. 37, pp. 551-558, 2007.

[21] B. Lothenbach, G. L. Saout, E. Gallucci and K. Scrivener, "Influence of limestone on the hydration of Portland cements," Cement and Concrete Research, vol. 38, p. 848–860, 2008.

[22] ASTM C192/C192M, "Standard Practice for Making and Curing Concrete Test Specimens in the Laboratory," ASTM International, pp. 1-8, 2012.

[23] ASTM C1611/C1611M-09b, "Standard test method for slump flow of self-consolidating concrete," ASTM International, pp. 1-6, 2009.

[24] ASTM C1621/C1621M, "Standard Test Method for Passing Ability of Self-Consolidating Concrete by J-Ring," ASTM International, pp. 1-5, 2009.

[25] ASTM C39, "Standard Test Method for Compressive Strength of Cylindrical Concrete Specimens," ASTM International, pp. 1-7, 2012.

[26] ASTM C 157, "Standard Test Method for Length Change of Hardened Hydraulic-Cement Mortar and Concrete," ASTM International, pp. 1-7, 2008.

[27] ASTM C 1202, "Standard Test Method for Electrical Indication of Concrete's Ability to Resist Chloride Ion Penetration," ASTM International, pp. 1-7, 2012.

[28] ASTM C 666, "Standard Test Method for Resistance of Concrete to Rapid Freezing and Thawing," ASTM International, pp. 1-6, 2008.

[29] K. G. Babu, "Early Strength Behavior of Fly Ash Concretes," Cement and Concrete Research, vol. 24, pp. 277-284, 1994.

[30] N. Garg, K. Wang and S. W. Martin, "A Raman spectroscopic study of the evolution of sulfates and hydroxides in cement–fly ash pastes," Cement and Concrete Research, vol. 53, pp. 91-103, 2013.

[31] Y. Zhang, W. Sun and H. Yan, "Hydration of high-volume fly ash cement pastes," Cement and Concrete Composites, vol. 22, pp. 445-452, 2000.

[32] J. Kostuch, G. Walters and T. Jones, "High performance concrete incorporating metakaolin-a review," in Concrete 2000, London, 1993.

[33] C.-S. Poon, S. K. L Lam, Y.-L. Wong and R. Wong, "Rate of pozzolanic reaction of metakaolin in high-performance cement pastes," Cement and Concrete Research, vol. 31, pp. 1301-1306, 2001.

[34] M. Zhang and V. Malhotra, "Characteristics of a thermally activated alumino-silicate pozzolanic material and its use in concrete," Cement and Concrete Research, vol. 25, pp. 1713-1725, 1995.

[35] E.-H. Kadri, S. Kenai, K. Ezziane, R. Siddique and G. D. Schutter, "Influence of metakaolin and silica fume on the heat of hydration and compressive strength development of mortar," Applied Clay Science 53 (2011) 704–708, vol. 53, pp. 704-708, 2011.

[36] K. A. Melo and A. M. Carneiro, "Effect of Metakaolin's finesses and content in self-consolidating concrete," Construction and Building Materials, vol. 24, pp. 1529-1535, 2010.

[37] V. Kannana and K. Ganesan, "Chloride and chemical resistance of self-compacting concrete containing rice husk ash and metakaolin," Construction and Building Materials, vol. 51, pp. 225-234, 2014.

[38] S. Wild, J. Khatib and A. Jones, "Relative strength, pozzolanic activity and cement hydration in superplasticized metakaolin concrete," Cement and Concrete Research, vol. 26, pp. 1537-1544, 1996.

[39] A. Barker and H. Cory, "The early hydration of limestone-filled cements," in Proc Blended Cements in Construction, Sheffield, UK, 1991.

[40] W. Klemm and L. Adams, "An investigation of the formation of carboaluminates," in Proc Carbonate Additions to Cement, Philadelphia, PA, 1990.

[41] M. Zajac, A. Rossberg, G. L. Saout and B. Lothenbach, "Influence of limestone and anhydrite on the hydration of Portland cements," Cement & Concrete Composites, vol. 46, p. 99–108, 2014.

[42] D. Damidot, B. Lothenbach, D. Herfort and F. Glasser, "Thermodynamics and cement science," Cement and Concrete Research, vol. 41, pp. 679-695, 2011.

[43] V. Kannan and K. Ganesan, "Chloride and chemical resistance of self-compacting concrete containing rice husk ash and metakaolin," Construction and Building Materials, vol. 51, p. 225–234, 2014.

[44] M. Uysal, K. Yilmaz and M. Ipek, "The effect of mineral admixtures on mechanical properties, chloride ion permeability and impermeability of self-compacting concrete," Construction and Building Materials, vol. 27, p. 263–270, 2012.

[45] P. Dinakar, K. Babu and M. Santhanam, "Durability properties of high volume fly ash self-compacting concretes," Cement and Concrete Composites, vol. 30, p. 880–886, 2008.

[46] N. Koulombi, G. Batis and C. Malami, "Progress in the understanding and prevention of corrosion," J. Costa and A. Mercer, Eds., London, The institute of materials, 1993, p. 619.

[47] M. Ghrici, S. Kenai and M. Said-Mansour, "Mechanical properties and durability of mortar and concrete containing natural pozzolana and limestone blended cements," Cement and Concrete Composites, vol. 29, p. 542–549, 2007.

[48] V. Bonavetti, H. Donza, V. Rahhal and E. Irassar, "Influence of initial curing on the properties of concrete containing limestone blended cement," Cement and Concrete Research, vol. 30, p. 703–708, 2000.

Tables:

Table 6.1 Chemical composition of cementitious materials (mass %).

Chemical composition	PC	FA	MK
SiO_2	20.20	46.00	53.00
Al_2O_3	4.70	17.80	43.80
Fe_2O_3	3.30	18.20	0.43
SO_3	3.30	2.59	0.03
CaO	62.90	8.40	0.02
MgO	2.70	0.95	0.03
Eq. Na_2O	0.54	2.01	0.35
P_2O_5	-	0.11	-
TiO_2	-	0.93	-
SrO	-	0.03	-
BaO	-	0.05	-
LOI	1.10	1.49	-
Physical Properties			
Specific gravity	3.15	2.51	2.56
Blaine fineness (m^2/kg)	391	310	13000

Table 6.2 Concrete mixture proportions.

Concrete Mix	w/cm	PC (kg/m^3)	FA (kg/m^3)	MK (kg/m^3)	nanoLS (kg/m^3)	Aggregate (kg/m^3)		HRWR (ml/m^3)	AEA (ml/m^3)
						Coarse	Fine		
SCC	0.36	321	214	-	-	850	784	3584	1070
SFSCC	0.36	241	214	80	-	850	784	2782	1070
SFSCC+1% nanoLS	0.36	241	214	80	5.35	850	784	2998	1070

Table 6.3 Fresh Properties of Concrete Mixes.

	Slump flow (mm)	**J-ring flow (mm)**	**Slump (mm)**	**Slump spread (mm)**	**Air Content (%)**
SCC	692	686	-	-	6.8
SFSCC	-	-	216	305	7.0
SFSCC+1% nanoLS	-	-	203	305	6.7

Figures:

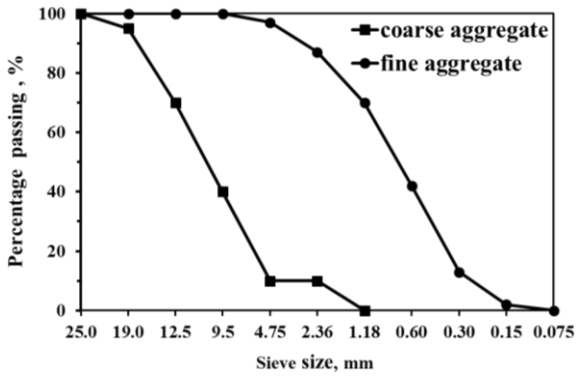

Figure 6.1. Gradation curves of coarse and fine aggregate.

(a) SCC (b) SFSCC (c) SFSCC + 1% nanoLS

Figure 6.2. Slump tests for three mixes.

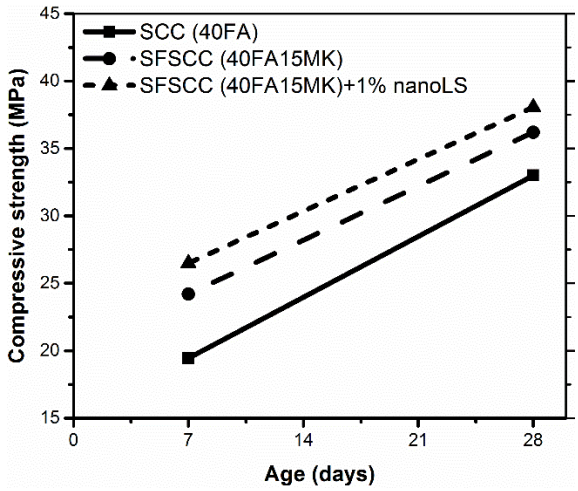

Figure 6.3. Compressive strength development of SCC and SFSCC mixtures.

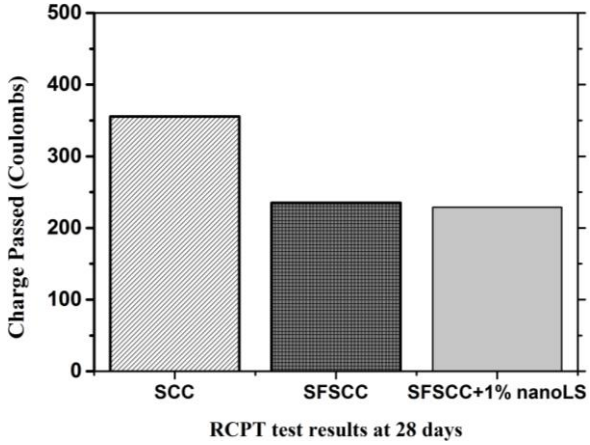

Figure 6.4. RCPT test results at 28 days.

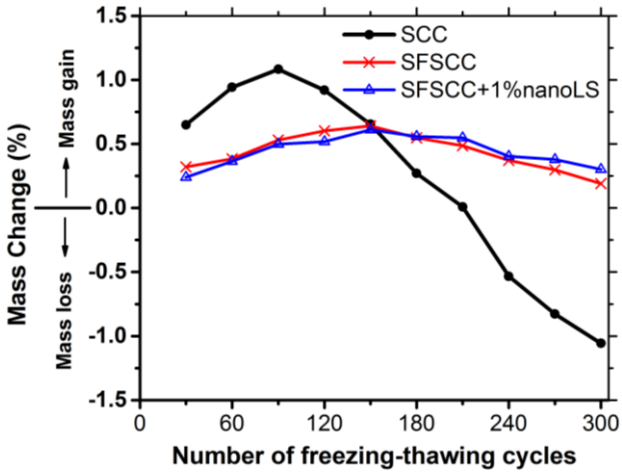

Figure 6.5. Weight change (%) of freezing- thawing samples.

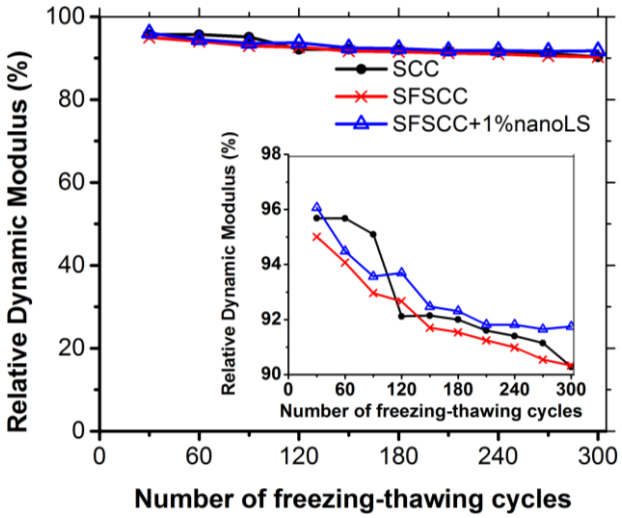

Figure 6.6. RDM (%) of freezing- thawing samples.

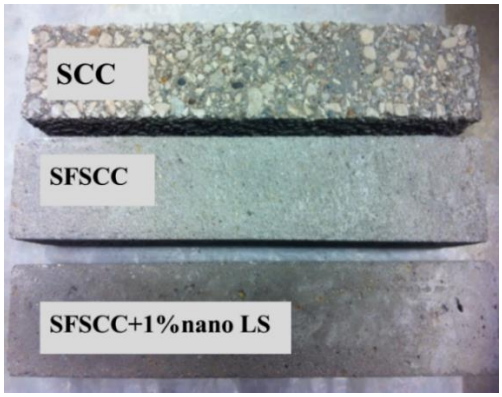

Figure 6.7. Appearance of samples after 300 rapid freezing-thawing cycles.

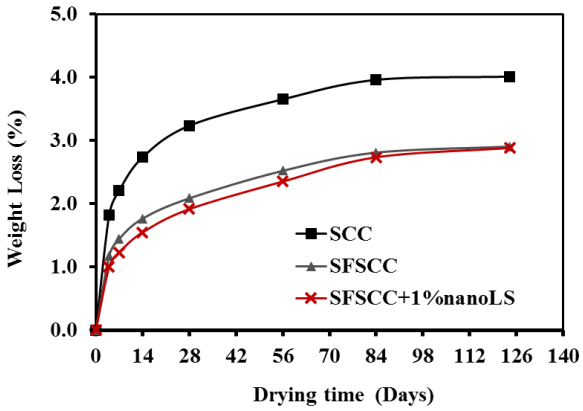

Figure 6.8. Weight loss of concrete samples in free-drying shrinkage test.

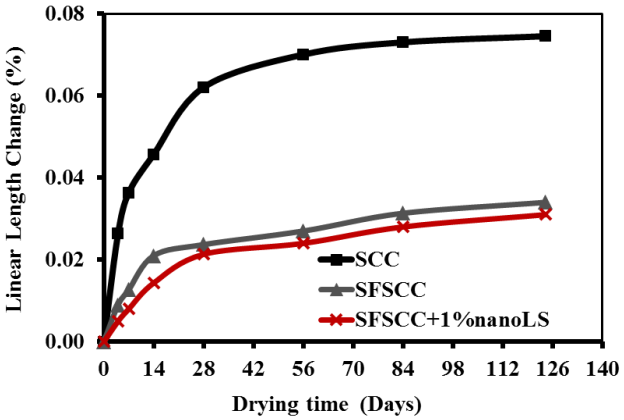

Figure 6.9. Linear length loss of concrete samples in free-drying shrinkage test.

CHAPTER 7. GENERAL CONCLUSION

This dissertation focused on effects of nanomaterials on the hydration and properties of cement-based materials. The nanomaterials studied include nano-limestone, nano-silica, and nano-clay, and the cementitious materials studied are combinations of ordinary portland cement (OPC), fly ash (FA) and metakaolin (MK). The basic concept underlying this study is that, when used together, the deficiencies of each material will be compensated for by advantages of one or more of the others, and in-common advantages of these three materials will be further enhanced.

The main findings and future perspective are presented below.

7.1 Main findings

7.1.1 Effects of nanoparticles on cement hydration kinetics

Early hydration kinetics (first 24 hrs.) of cement pastes with varying types and amounts of nanomaterials addition have been characterized:

1) The addition of all the three nanomaterials studied had an obvious hydration-accelerating effect; the maximum heat flow increased while the time to reach silicate and aluminate reaction peaks decreased.

2) For pastes with nano-limestone and nano-silica addition, the hydration-accelerating effect increased with the addition level.

3) Addition of nano-clay accelerates the consumption of sodium sulphate and the reaction of the aluminate phase, resulting in an earlier and more intense aluminate hydration peak. A 0.5% nano-clay addition had a greater acceleration effect than did a 1.0% nano-clay addition.

4) Both initial and final setting happened during the acceleration period and the addition of nanomaterials reduced the initial and final set times. The extent to which the set times were reduced correlated well with the capability of nanomaterials to accelerate silicate phase hydration.

7.1.2 Effects of nanoparticles on the rheology of cement pastes

Rheology behavior of cement pastes with varying types and amounts of nanomaterials addition have been characterized:

1) Before the acceleration period of hydration (60 min), the viscosity and yield stress of cement pastes with 0.5% and 1.0% nano-limestone addition changed little with time, but addition of 1.5% nano-limestone decreased viscosity without significantly changing yield stress during this period.

2) Addition of nano-silica gradually increased viscosity of cement pastes. There was a significant increase in yield stress with a nano-silica addition level as well as with increased hydration time.

3) The nano-clay studied had a considerable effect on the rheological behavior of cement pastes. Significantly higher shear stress was required to initiate the flow.

4) Non-Binghman (shear stress decreases as the shear rate increases) behavior was observed in many mixtures, especially those tested 120 min after mixing.

7.1.3 Effects of nanoparticles on hydration and microstructure development (1-28 days)

1) Chemical shrinkage and thermogravimetric analysis (TGA) results indicated that FA replacement for cement accelerated cement hydration while having a dilution effect. From 7 to 28 days, fly ash started to react and consume calcium hydroxide. When 1% nanomaterials were added to the cement or cement-fly ash paste, the amounts of both CH-water and H-water increased, indicating that the nanomaterials accelerated cement hydration. This acceleration effect resulting from nanomaterial additions was more profound for the OPCFA pastes.

2) For the cement pastes, nanomaterial addition generally increased chemical shrinkage values, which confirmed the hydration acceleration effects of nanomaterials. However, for the cement-fly

ash paste, only nano-silica addition increased chemical shrinkage of the paste at all ages tested. At 28 days, the nano-limestone and nano-clay additions actually reduced chemical shrinkage value of the pastes. This implied that in these pastes, the permeation of water was inhibited.

3) XRD and TGA results indicated that a new hydration product, calcium hemicarboaluminate hydrate (Hc), was formed in the nanolimestone modified pastes, and this hydration also involved consumption of calcium hydroxide. In the presence of fly ash, the reaction between nano-limestone and the aluminate phases was amplified at 28 days, probably due to the additional alumina provided by the late fly ash reaction.

4) All nanomaterial additions increased the specific surface area and total volume of pores with sizes ranging from 2 nm to 100 nm of the early age cement hydration cementitious pastes (7 days). The results indicate that nanomaterial additions effectively accelerated early age cement hydration. At 28 days, addition of nano-silica continued to increase the specific surface area and the amount of gel pores, especially in the fly ash blended paste. However, addition of nano-limestone reduced the specific surface area and the total amount of pores (2-100 nm) at 28 days, especially in the portland cement paste.

5) Two major volumes of pores were observed in the differential pore size distribution curves of pastes without nanoparticles at the age of 7 days: one was in the pore size range of 3-4 nm (nano-sized gel pores) and the other in the pore size range of 50-60 nm (relatively large capillary pores). The peaks in the pore size range of 50-60 nm all disappeared as 1% nanomaterial was added to these pastes, regardless the nanomaterial type and paste composition. This clearly evidenced that nanomaterial additions refined pore structures of the early age pastes. An additional signature pore peak located around 18 nm was observed in the nano-silica modified and 28-days fly ash blended pastes.

7.1.4 Effects of nanoparticles on strength and durability

1) Regardless the types of nanomaterials, 1% nanomaterial addition improve the compressive strength of both cement and cement-fly ash pastes at all ages studied (up to 28 days). Among three nanomaterials studied, NS appeared to be the most effective one in the strength development, possibly due to its smallest particle size and highest reactivity.

2) A SFSCC mixture with 40% FA and 15% MK replacement displayed good flowability and shape-holding ability. The replacement of 15% MK for cement also improved compressive strength and freezing-thawing resistance, and also reduced chloride penetration and free-drying shrinkage. Adding a small quantity (1% by weight of cementitious materials) of nano-limestone to the SFSCC mix further increased the compressive strength and resistance freezing-thawing at both 7 and 28 days. It also slightly reduced chloride penetration and free-drying shrinkage of the concrete.

3) Additions of nano-silica generally increased the total shrinkage of cement pastes. However, addition of nano-limestone sometimes reduced drying shrinkage, especially for the later age cement pastes. Nanomaterial additions and extended curing increased reversible drying shrinkage, which suggests that the volume of gel (2-10 nm) pores appeared more closely related to reversible shrinkages. However, for OPC pastes, reversible shrinkage was the major portion of the total shrinkage, especially for the pastes at 28 days. For OPCFAMK pastes, irreversible shrinkage was the major portion of the total shrinkage, especially for the pastes at 28 days. For OPCFA pastes, reversible and irreversible shrinkage was the same for the paste with no nanomaterials at 7 days, and extended curing from 7 to 28 days increased irreversible shrinkage of the paste. Additions of nanomaterials primarily increased the irreversible shrinkage at 7 days but extended curing from 7

to 28 days typically reduced the difference between irreversible and reversible shrinkage of the pastes.

4) The shrinkage in each relative humidity range was found to be dependent on the volume of pores evaporate in the corresponding RH range and the resistance of the paste to deformation, especially at 7 days. The volume of gel (2-10) nm pores appeared more closely related to reversible shrinkages. That is, as the volume of the pores with sizes of 2-10 nm increased, the irreversible shrinkage intensified.

7.2 Further study

The long-term goal of this research is to obtain a better understanding of the mechanisms of the interactions in a PC – SCM - nanomaterial system and to gain an insight into processing - microstructure - property relationships of such systems.

7.2.1 Dispersion of nanoparticles by ultrasonication and surfactant in cement-based systems

It is important to obtain well-dispersed, stable nanoparticles in aqueous suspension, especially for in-situ use. Moreover, various types of chemical admixtures (such as water reducing agent and retarder) are often used during mixing to satisfy different needs regarding the fresh properties of concrete mixtures. These chemical admixtures are themselves surfactants which can influence the dispersion state of nanoparticles.

Therefore, it is suggested to investigate the effects of ultrasonication protocols and surfactant types on the dispersion quality and stability of nanoparticles in cement-based systems and then to quantitatively tied the degree of dispersion to the early-age properties (such as rheology and set times) of fly ash–cement-metakaolin pastes.

To fully characterize properties of a suspension, three levels of investigations are needed: (1) investigation of the system at a molecular level, including the examinations of the structure of the

solid/liquid interface, namely the structure of the electrical double layer (for charge stabilized suspensions), adsorption of dispersing agents, and conformation of the adsorbed layers (e.g., the adsorbed layer thickness); (2) investigation of the state of suspension on standing, namely flocculation rates, flocculation points with sterically stabilized systems, spontaneity of dispersion on dilution, and Ostwald ripening or crystal growth. All these phenomena require accurate determination of the particle size distribution as a function of storage time; and (3) Investigation of the bulk properties of the suspension, such as the amount and rate of sedimentation.

7.2.2 Growth of C-S-H on nanoparticle surfaces

It is generally accepted that C-S-H is forming by a heterogeneous process and that the species are available everywhere in the pore solution. Nanoparticles can accelerate cement hydration, providing additional nucleation sites for the precipitation and growth of new regions of C-S-H gel.

Most of the studied used kinetic data such as isothermal calorimetry or consumption of the main clinker phases to study the acceleration effect. It will be interesting to gain microscopic observations of the amount and morphology development of C-S-H on the surfaces of cement grains and nanoparticles. Studies on how the important parameters (such as surface properties, chemical composition, and particles size) affect the accelerating effect of nanoparticles will bring new insights regarding the nucleation and growth mechanism of C-S-H.

7.2.3 Reduction of drying shrinkage

The addition of nanomaterials studied generally increased total drying shrinkage of cementitious pastes. Two strategies for reducing shrinkage can be proposed: one is to use shrinkage reducing admixtures and another is to change the pore size distribution of cement based materials.

7.2.4 A complete pore structure analysis by water vapor adsorption

Properties, including viscous flow, drying shrinkage, and cohesion, are controlled by mechanisms that operate at the nanoscale, which includes solid and the smallest pores. The present study investigated the pore structure of cement-SCM-nanomaterial pastes by nitrogen adsorption in the 2-100 nm range and related the results to the drying shrinkage behavior.

On the other hand, deterioration of concrete associated with ingress of chemicals from the environment are closely related to the permeability and ion transport which are largely controlled by the capillary porosity. Pore structure analysis by water vapor adsorption becomes vitally important when only a part of the pore system of the adsorbent is accessible to nitrogen, and especially when the researcher is interested in the movement of water into and out of the pore system and its behavior in the pores.

7.2.5 Properties of concrete

The present study focused on the effects of nanoparticles on the properties of cementitious pastes. It is implicated that the pore solution chemistry changed in the presence of nanoparticles, especially in the presence of supplementary cementitious materials. Further study on the hardened properties of cement-based concretes (such as are alkaline-silica reaction, corrosion) are of vital importance.

APPENDIX A. STATISTICS ON INDEPENDENT SAMPLES

For thermogravimetric analysis (TGA), compressive strength, and nitrogen adsorption tests, two independent samples of the ordinary portland cement (OPC) were studied. Mean and standard deviation are calculated.

A-1 TGA, compressive strength, and nitrogen adsorption results of OPC from two independent samples

Time (days)	Sample	CH (%)	H (%)	Compressive strength (MPa)[1]	BET specific surface area (m^2/g)
3	OPC-1	16.06	14.98	27.6	-
3	OPC-2	16.35	15.18	30.0	-
7	OPC-1	18.47	16.79	32.8	50.58
7	OPC-2	18.79	16.98	35.1	52.04
28	OPC-1	21.06	20.23	41.6	68.06
28	OPC-2	21.44	20.41	45.0	70.01

A-2 CH (%) calculated from thermogravimetric analysis

Time (days)	Number of independent experiments	Mean	Standard deviation
3	2	16.20	0.14
7	2	18.63	0.16
28	2	21.2	0.19

[1] Average of three replicates from one sample.

A-3 H (%) calculated from thermogravimetric analysis

Time (days)	Number of independent experiments	Mean	Standard deviation
3	2	15.08	0.10
7	2	16.89	0.09
28	2	20.32	0.09

A-4 Compressive strength

Time (days)	Number of independent experiments	Mean	Standard deviation
3	2	28.8	1.2
7	2	33.9	1.1
28	2	43.3	1.7

A-5 BET specific surface area calculate from nitrogen adsorption

Time (days)	Number of independent experiments	Mean	Standard deviation
7	2	51.31	0.73
28	2	68.03	0.98

APPENDIX B. VARIABILITY IN REPLICATES

To reduce measurement error, replicates were used in this study. The data from isothermal calorimetry, chemical shrinkage, and drying shrinkage tests are reported here.

B-1 Isothermal calorimetry

For isothermal calorimetry test, two replicates were tested for each mix. The results of ordinary portland cement (OPC) paste are shown in Figure B.1. The average absolute difference between replicate specimens is 2.5 x 10^{-5} W/g (cement) for measurements conducted between 1 and 24 hrs. For all mixes tested, the average absolute difference between replicate specimens is no more than 2.5 x 10^{-5} W/g (cement). The average of the two replicates are reported in the paper.

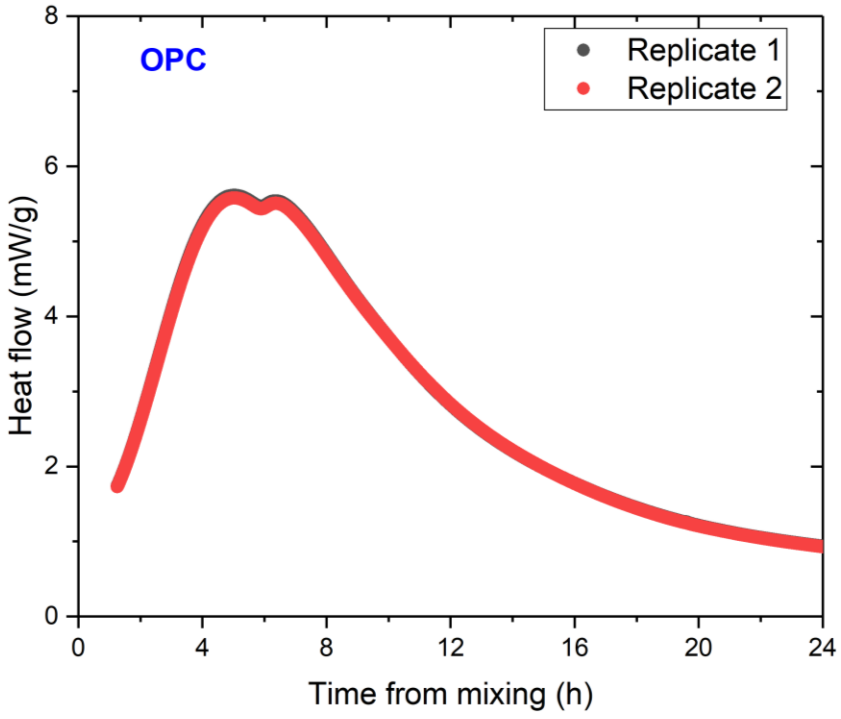

Figure B.0.1. Isothermal calorimetry results of OPC paste on two replicates.

B-2 Chemical shrinkage

For chemical shrinkage test, three replicates were tested for each mix. The results of ordinary portland cement (OPC) paste are shown in Figure B.2. The standard deviation is no larger than 0.13 $cm^3/100g_{cement}$ between 7 and 28 days. For all mixes studied, the average standard deviation is no larger than 0.20 $cm^3/100g_{cement}$ between 7 and 28 days.

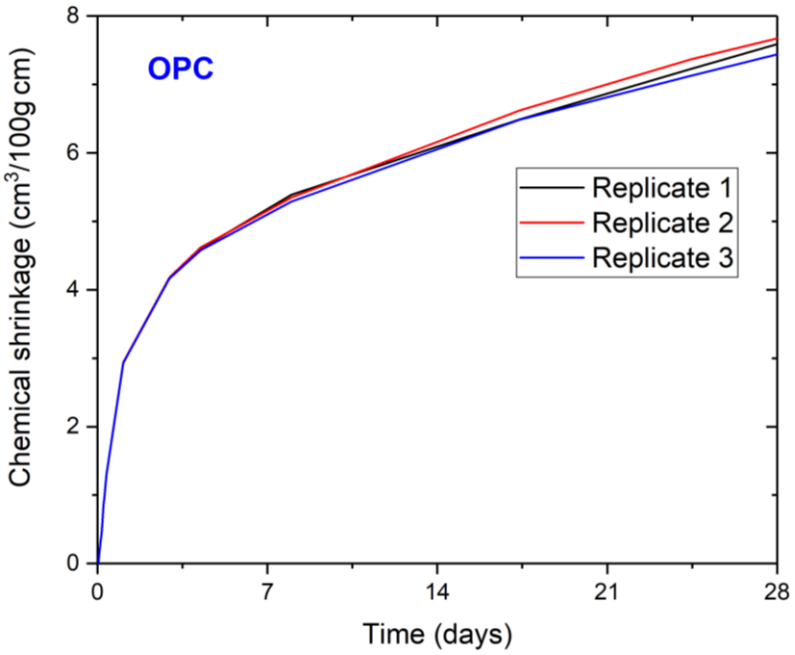

Figure B.0.2. Chemical shrinkage results of OPC paste on three replicates.

B-3 Drying shrinkage

For drying shrinkage test, three replicates were tested for each mix. The results of ordinary portland cement (OPC) paste curing for 7 days are shown in Figure B.3. The standard deviation is no larger than 0.01% during the drying and rewetting period. For all mixes studied, the average standard deviation is no larger than 0.03% during the drying and rewetting period.

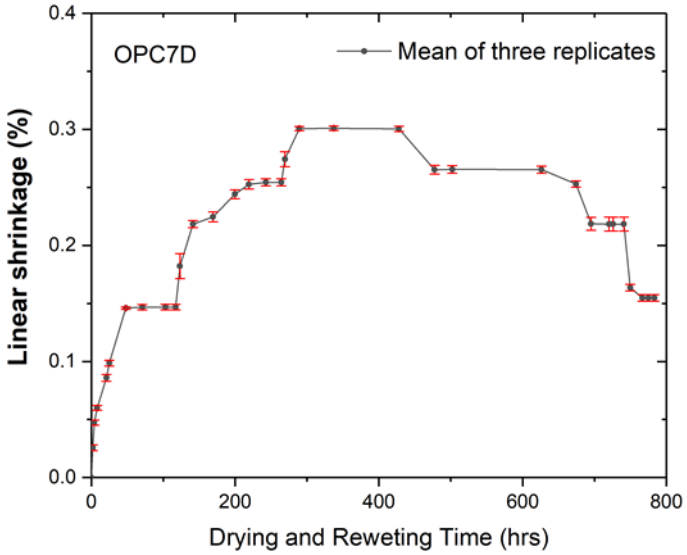

Figure B.0.3. Drying shrinkage results of 7-day cured OPC paste on three replicates with error bars.